Diss. ETH No. 20667

Studying the Performance of a Commercial Plasma Air Purifier: Prospects and Limitations

A dissertation submitted to
ETH ZURICH

for the degree of
Doctor of Sciences

presented by

STEFAN SCHMID

Diplom als Chemiker FH, Fachhochschule beider Basel, Switzerland
Master of Science in Chemistry, University of Basel, Switzerland

born March 2, 1982
citizen of Seon (AG), Switzerland

accepted on the recommendation of

Prof. Dr. Renato Zenobi, examiner
Prof. Dr. Urs Baltensperger, co-examiner
Dr. Andreas Gerecke, co-examiner

2012

Dedicated to my dear family
and in Memory of my Sister Miriam Schmid

I. DISCLAIMER

I hereby declare that this dissertation represents the result of my own original work, and it has not been submitted to any other institution for another degree or qualification. I also declare that it contains no material written by another person without proper citation in the text.

Stefan Schmid Date

II. Acknowledgements

It all began back in 1998 when I started my apprenticeship in chemistry at Hoffmann-La Roche. Almost fourteen years later I am finishing my thesis in analytical chemistry in the group of Professor Renato Zenobi. I would like to gratefully and sincerely thank him for giving me the chance of doing my doctoral degree in his research group. I really appreciated the freedom that he gave me to investigate new research topics, his guidance through my rather unique research topic, and allowing me to present my research on various scientific conferences.

Special thanks goes to Matthias Jecklin who taught me how things work at ETH and about all of the pieces of equipment available in our laboratories. He was a great coach and it was a pleasure to work with him.

Many thanks to Lukas Meier with whom I spent the last two years in the same office at ETH. We often had fruitful and interesting scientific discussions. Lukas always helped me to improve my English and he was a great companion whenever we were doing any extreme sports.

Stefanie Mädler, Robert Nieckarz and my emergency twin brother: Bartosz Koprowski are gratefully acknowledged for their help with correcting my thesis.

I thank Chrisoph Bärtschi for his excellent work in constructing many parts of the designed bench setup system as well as custom designed parts to interface many analytic devices.

I owe a special thanks to my family for always supporting me, encouraging me when I needed it and often invited me for dinner on Sunday. At this point I also thank my flat mate Matthias Kull for interesting discussion outside of the field of chemistry.

I would like to acknowledge all of my co-workers that have contributed to my published papers.

Special thanks goes to Pavel Urban who was a real pleasure to work with. I had never experienced such a stable capillary electrophoresis system before I met him.

Brigitte Bräm is thankfully acknowledged for her support, being happy and for helping me whenever she could.

Stefanie Mädler, Stephan Fagerer, Konstantine Barylyuk for having an unforgettable trip through the canyons in the United States.
Thanks go also to Christian Berchtold who tried to help everyone. Our joint path eventually ends after we first met in the apprenticeship.

Eventually, I would like to thank all of the members of the Zenobi group: Fan Chen who always tried to teach me Chinese (sadly I could only remember few things), Volker Neu who taught me how to exercise in the gym properly, Fanny Widjaja who had the great patience to teach me how to dance, Dragana Cubrilovic who often went along with me to Werdinsel, Johannes Stadler and Simon Weidmann are kindly acknowledged for helping me whenever I had a computer problem or when I simply needed a piece of advice, and Carolin Blum for organizing lots of social events and caring about the group.

III. Publications

Schmid, S.; Seiler, C., Gerecke, A. C.; Hächler, H.; Hilbi, H.; Frey, J.; Weidmann, S.; Meier, L.; Berchtold C.; Zenobi, R., Studying the Degradation Processes of non-Volatile Organic Compounds in a Commercial Plasma Air Purifier, submitted to *J Hazard Mater*.

Berchtold, C.; Müller, V.; Meier L.; **Schmid S.**; Zenobi, R., Desorption Electrospray Ionization for the detection of chlorpropham on potato peel, manuscript in preparation.

Meier, L.; Berchtold, C.; **Schmid**, **S.;** Zenobi R., Sensitive detection of drug vapors using an ion funnel interface for secondary electrospray ionization mass spectrometry, *J. Mass. Spectrom*., **2012**, 47, (5), 555.

Cvetković, B. Z.; Puigmartí-Luis, J.; Schaffhauser, D.; Ryll, T.; **Schmid, S.**; Dittrich P. S., Confined synthesis andintegration of functional materials in sub-nanoliter Microreactors, submitted to *ACS Nano*.

Meier, L.; Berchtold, C.; Martinez, P.; **Schmid**, **S.;** Zenobi R., Examining Breath Profiles using Secondary electrospray ionization mass spectrometry assisted by an ion funnel, submitted to *J. Mass. Spectrom.*

Berchtold, C.; **Schmid, S.**; Meier, L.; Zenobi, R., In situ detection of γ-hydroxybutyrate and γ-butyrolactone in drinks by secondary electron spray ionization, submitted to *Analyst Methods*.

Schmid, S.; Meier, L.; Berchtold, C.; Zenobi, R., Online Monitoring of Molecular Processes in a Plasma Air Purifying System. *Environ. Sci. Technol.* **2012**, *46*, (7), 4067-4073.

Meier, L.; Berchtold, C.; **Schmid, S.**; Zenobi, R., Extractive Electrospray Ionization Mass Spectrometry Enhanced Sensitivity Using an Ion Funnel. Anal. Chem**. 2012**, *84*, (4), 2076-2080.

Schmid, S.; Jecklin, M. C.; Zenobi, R., Electrosonic spray ionization—An ideal interface for high-flow liquid chromatography applications. *J. Chromatogr. A* **2011**, *23*, (1), 3704-3710.

Meier, L.; **Schmid, S.**; Berchtold, C.; Zenobi, R., Contribution of liquid-phase and gas-phase ionization in extractive electrospray ionization mass spectrometry of primary amines. *J. Mass. Spectrom*. **2011**, *17*, (4), 345-351.

Schmid, S.; Jecklin, M. C.; Urban, P.; Amantonico, A.; Zenobi R., Miniature flowing atmospheric-pressure afterglow ion source for facile interfacing of CE with MS. Electrophoresis **2010**, *31*, (21), 3597-3605.

Schmid, S.; Jecklin, M. C.; Zenobi, R., Degradation of volatile organic compounds in a non-thermal plasma air purifier. Chemosphere **2010**, *79*, (2) 124-130.

Mai, T. D.; **Schmid, S**.; Müller, B.; Hauser, P. C., Capillary electrophoresis with contactless conductivity detection coupled to a sequential injection analysis manifold for extended automated monitoring applications. Anal. Chim. Acta **2010**, *665*, (1) 1-6.

IV. Conference Contributions

Schmid, S.; Seiler, C., Gerecke, A. C.; Hächler, H.; Hilbi, H.; Frey, J.; Weidmann, S.; Meier, L.; Berchtold C.; Zenobi, R., The functionality of a commercially available plasma air purifier. *19th IMSC Conference on Mass Spectrometry and Allied Topics,* Kyoto, Japan, September 15-21, 2012.

Schmid, S.; Meier, L.; Berchtold, C.; Zenobi, R., Molecular Processes in an Atmospheric Pressure Non-Thermal Plasma Based Air Purier. *Fall Meeting of the Swiss Chemical Society*, Lausanne, Switzerland, September 9, 2011.

Schmid, S.; Meier, L.; Berchtold, C.; Zenobi, R., Molecular processes in an alternating current driven plasma air purifier. *59th ASMS Conference on Mass Spectrometry and Allied Topics*, Denver, Colorado, USA, June 5-9, 2011.

Schmid, S.; Meier, L.; Berchtold, C.; Zenobi, R., Discovering the degradation mechanism of a plasma driven air purifier. *ANAKON 2011*, Zurich, Switzerland, March 22-25, 2011.

Schmid, S.; Jecklin, M. C.; Urban, P.; Amantonico, A.; Zenobi, R., Miniature flowing atmospheric-pressure afterglow ion source for robust coupling of capillary electrophoresis with mass spectrometry. *Fall Meeting of the Swiss Chemical Society*, Zurich, Switzerland, September 9, 2010.

Schmid, S.; Jecklin, M. C.; Urban, P.; Amantonico, A.; Zenobi, R., Robust capillary electrophoresis–mass spectrometry interface using a miniature flowing atmospheric-pressure afterglow ion source. *58th ASMS Conference on Mass Spectrometry and Allied Topics*, Salt Lake City, Utah, USA, May 23-27, 2010.

Schmid, S.; Schwarz, R.; Zenobi, R., Analysis of Plasma Degraded Biomacromolecules in a Plasma Air Purifier. *Fall Meeting of the Swiss Chemical Society*, Lausanne, Switzerland, September 4, 2009.

Schmid, S.; Schwarz R.; Zenobi, R., Analysis of Plasma Degraded Biomacromolecules in an Air Purifier. *Analytical Chemistry Symposium: Analyze that*, Zürich, Switzerland, Mai 13, 2009.

Schmid, S.; Schwarz R.; Zenobi, R., Untersuchung der Zersetzung von Biomakromolekülen durch einen Plasmafilter. *ANAKON 2009*, Berlin, Germany, March 17-20, 2009.

V. Table of Contents

Summary

Today, people often spend the majority of the day indoors. Good indoor air quality is therefore of paramount importance. Unfortunately, facility management often reduces the air turnover rate to keep air conditioning costs minimal. The consequence is poor indoor air quality. While outdoors the amount of air pollutants such as bacteria and viruses is reduced by chemical reactions, they can thrive when protected from sunlight and active species in an indoor environment. Therefore, it is very important to clean indoor air thoroughly. A novel approach is to use non-thermal plasma-based air purifiers. The manufacturer of a commercially available plasma air purifier speculates that electromagnetic processes are responsible for the flue gas degradation in their system. Harmful compounds are proposed to be fragmented to non-toxic low molecular weight compounds. In this thesis, degradation mechanisms and efficiencies of this commercial plasma air purifier are investigated. In order to simulate realistic conditions in common ventilation systems, the plasma air purifier was incorporated in a test bench setup system. To keep the number of possible degradation products manageable, a selection of volatile organic compounds were studied in the beginning. The observed results clearly showed that oxidation processes are the main cause for degradation. Degradation efficiencies of the plasma air purifier of less than 12% were found for all volatile compounds studied. The investigation of cyclohexene showed several by-products such as adipaldehyde, which indicated reactions with hydroxyl radicals as well as ozone. However, further study showed that ozonolysis cannot be the dominating process for the degradation of cyclohexene. A set of different amines was studied online by directly coupling the exhaust of the plasma air purifier with a homemade helium plasma ionization source and a mass spectrometer. Surprisingly, only high molecular weight products of the studied amines were found. The formation of ionic sandwich clusters involving the positively charged amines and nitrate resulted in crowded mass spectra. Hydroxyl radicals seemed to be responsible for side chain oxidation of the amines, which was confirmed by repeating the experiments using deuterated amine standards. Non-volatile molecules showed a different behavior in the plasma air purifier. The higher the

molecular weights of the molecules studied the higher the observed removal efficiency of the plasma air purifier. Bioparticles were removed with close to 100% efficiency, whereas for volatile organic compounds degradation efficiencies of only ~10% were found. However, the removal of bioparticles was mainly caused by deposition onto the copper electrodes of the plasma air purifier instead of chemical degradation. It is assumed that electrostatic precipitation is the dominating processes responsible for the observed reduction in the amounts of particles. We conclude that in its current state the plasma air purifier cannot be recommended for use as an all-round air purification system. Nevertheless, the technology of plasma based air purifiers is interesting and its combination with catalytic material seems very promising, especially for less volatile compounds. In order to remove bioparticles from indoor air, corona discharge-based precipitators offer high trapping efficiencies while using only little amounts of power. A combination of both technologies is believed to offer an ideal all-round air purification system in the future.

Zusammenfassung

Heutzutage verbringen Menschen oft die Mehrheit des Tages in Gebäuden. Gute Luftqualität ist deshalb von enormer Wichtigkeit. Leider wird durch das Gebäudemanagement die Luftumwälzrate oft verringert, um die Klimatisierungskosten tief zu halten. Die Konsequenz daraus ist eine schlechte Luftqualität. Während im Freien Luftschadstoffe wie Bakterien und Viren durch chemische Reaktionen reduziert werden, gedeihen sie in Innenräumen weil sie von Sonnenlicht und aktiven Spezien geschützt sind. Deshalb ist, es von höchster Priorität, Innenluft gründlich zu reinigen. Ein neuartiges Vorgehen ist dazu nicht-thermische, plasmabasierende Luftreiniger zu verwenden. Der Hersteller eines kommerziell erhältlichen Plasmaluftreinigers spekuliert, dass elektromagnetische Prozesse verantwortlich für die Schadstoffreduzierung in ihrem System sind. Schädliche Verbindungen sollen zu ungiftigen kleinen Molekülen abgebaut werden. In dieser Dissertation wurden die Abbaumechansimen und Effizienzen eines kommerziellen Plasmaluftreinigers untersucht. Um realistische Bedingungen wie in herkömmlichen Ventilationssystemen zu simulieren, wurde der Plasmaluftreiniger in ein Laborversuchssystem integriert. Damit die Zahl der möglichen Abbauprodukte überschaubar zu halten war, wurde zu Beginn eine Auswahl von flüchtigen organischen Verbindungen studiert. Die beobachteten Resultate zeigen klar, dass unter anderem oxidative Prozesse für den beobachteten Abbau verantwortlich sind. Abbaueffizienzen des Plasmaluftreinigers von weniger als 12% wurden für die flüchtigen organischen Verbindungen gefunden. Die Untersuchung von Cyclohexen zeigte verschiedene Nebenprodukte wie Adipaldehyd, was auf Reaktionen mit Hydroxyl-Radikale sowie Ozon hindeutete. Weiterführende Studien zeigten hingegen, dass die Ozonolyse nicht der dominierende Abbauprozess für Cyclohexen sein konnte. Verschiedene Aminen wurde mittels einer direkten Verbindung der Plasmaluftreinigerabluft über eine selber hergestellte Helium-Plasma-Ionisierungsquelle mit dem Massenspektrometer verbunden und online studiert. Überraschenderweise wurden nur hochmolekulare Abbauprodukte der untersuchten Amine gefunden. Die Bildung von ionischen Sandwich-Clustern, welche durch positiv geladene Amine und

negativ geladene Nitrat-Moleküle entstanden sind, manifestierte sich in schwer zu interpretierbaren Massenspektren mit zahlreichen Signalen. Hydroxyl-Radikale scheinen für die Seitenkettenoxidationen verantwortlich zu sein, was durch Wiederholung der Experimente mit einem deuterierten Amin bestätigt wurde. Nichtflüchtige Moleküle zeigten im Plasmaluftreiniger ein unterschiedliches Verhalten. Je höher das Molekulargewicht der untersuchten Verbindung war, desto höher war auch die beobachtete Abbaueffizienz des Plasmaluftreinigers. Biopartikel wurden mit einer Abbaueffizienz von nahezu 100% abgebaut, wobei für flüchtige organische Verbindungen Abbaueffizienzen von nur ~ 10% beobachtet wurden. Der Abbau der Biopartikeln wird hauptsächlich durch Ablagerungen auf den Kupferelektroden des Plasmaluftreinigers verursacht und nicht durch Abbauprozesse. Es wird angenommen, dass hauptsächlich elektrostatische Ablagerungen für den beobachteten Abbau in der Menge der Partikel verantwortlich sind. Fasst man alle erhaltenen Resultate zusammen, wird die Schlussfolgerung gezogen, dass der Plasmaluftreiniger in seiner momentanen Form nicht als universelles Luftreinigungsgerät empfohlen werden kann. Nichtsdestotrotz ist die Technologie eines plasmabasierenden Luftreinigungssystems interessant. Die Kombination eines solchen Systems mit katalytischem Material scheint, vor allem für nichtflüchtige Verbindungen, erfolgsversprechend zu sein. Um Biopartikel aus der Gebäudeluft zu entfernen, scheint ein Koronaentladung basierender Abscheider die richtige Lösung zu sein, da er hohe Effizienzen bei kleinem Stromverbrauch aufweist. Eine Kombination dieser beiden Technologien scheint eine ideale Lösung für ein zukünftiges universelles Luftreinigungssystem zu sein.

Chapter 1

Introduction and Background

This chapter contains a general introduction to plasma-based air purification systems. The introduction is followed by the motivation and the organization of this thesis.

In addition to security and health issues, saving energy has become a major interest to both the general public and the economy in recent years. However, it is often difficult to save energy without sacrificing quality of life. Good thermal insulation of buildings, as well as humidity and temperature control, results in smaller turnover rates with the outdoor air, and thus in poorer indoor air quality. Within buildings, airborne pathogens, such as bacteria, viruses and volatile organic compounds, are protected from sunlight, ozone, hydroxyl radicals, and other active species which are responsible for their degradation in the open atmosphere.[1-6] The large majority of infectious diseases that are caused by airborne pathogens are exclusively spread indoors.[3] This takes a toll on the quality of a community's health and on the economy, especially since many people spend at least 80% of their time indoors.[7-10] Indoor air pollution is among the top five environmental risks to public health, and it is suggested to ventilate buildings and rooms several times a day with clean outdoor air. Infections in naturally ventilated (by opening doors and windows) facilities built pre-1950 were 11%, whereas with mechanical ventilation in modern facilities the infections increased to 33%.[11] However, opening doors and windows is not always desirable or possible, due to weather conditions or energy saving issues. Therefore, air cleaning systems have become increasingly important. One way to clean air is to use high efficiency particulate air (HEPA) filters. Unfortunately, these filters have two major drawbacks:

(1) HEPA filters cause high pressure drops in heating, ventilating, and air conditioning systems, resulting in higher energy consumption to power stronger fans.

(2) Due to the passive nature of such HEPA filters, living bacteria and viruses are deposited on the filters, where they can survive or even reproduce and migrate through the filter. Therefore, regular replacement is essential.

Novel alternatives to HEPA filters are purifiers based on non-thermal plasmas. None of the disadvantages mentioned above are observed in such plasma air purifier (PAP). PAPs consume little power and are designed to decompose air contaminants to small non-toxic compounds. However, incomplete oxidation may lead to toxic by-products, which obstructs a broad application of PAPs as

universal air cleaning devices at the moment. This thesis focuses on studying the fate of flue gasses in a commercially available PAP using mass spectrometry (MS) and related analytical methods. The studied compounds vary from volatile organic compounds (VOCs) to high mass proteins and bioparticles.

1.1 Nonequilibrium Plasma

Low temperature plasmas are divided into non-thermal and thermal plasmas. In this work, we only focus on non-thermal or nonequilibrium plasmas, where electrons have a much higher energy or temperature than the passing neutral gas particles. A plasma generally consists of positively and negatively charged particles, e.g. electrons and ions. Overall, such plasmas are quasi-neutral, since the numbers of positively charged carriers are practically equal to the negatively charged ones. The density of charged particles is low compared to neutral particles. In the applied electric field, smaller charged particles are accelerated to higher extent between collisions than larger ones. Electrons therefore have a higher kinetic energy than heavier ions, while the bulk of the gas (neutral particles) is not directly affected by the electric field. This is generally true for low pressures and high electric fields. In a collision between particles, this kinetic energy gets consumed by the collision partners in these plasmas. A nonequilibrum plasma is often also called cold plasma. However, if the pressure in the plasma is higher, more collisions occur, energy gets transported to neutral molecules, and the gas heats up. Such plasmas are in equilibrium and are often referred to as hot plasma.

The biggest advantages of using cold plasmas compared to thermal plasmas are the rather low power consumption as well as the fact that only cold plasmas allow the excitation of a small fraction of the gas atoms or molecules to the desired energy level without affecting the bulk gas. [12-16] Non-thermal plasmas are well suited for the decomposition of lower concentrations of flue gasses (< 1000 ppm VOC) with a flow rate of 100 $Nm^3\ h^{-1}$ ($Nm^3\ h^{-1}$ = normal meters cubed per hour at 0°C and 1.013 10^5 Pa). The lower the air flow rate to be treated, the higher the possible VOC concentration which can be handled. VOC decomposition is a very important application of non-thermal plasmas as VOCs

can be extracted from water by air-stripping. However, for some VOCs, very large amounts of energy are used to obtain complete destruction.[17]

1.2 Plasma reactors

There are different ways to generate nonequilibrium plasmas due to their pressure range and electrode geometry. In this part, three important characteristics of nonequilibrium discharges are introduced.

(1) Glow discharge
(2) Corona discharge
(3) Silent Discharge or Dielectric-barrier discharge (DBD)

(1) Glow discharges generate luminous plasma as the electron energy is high enough to excite the gas molecules generating visible light, which is typical for each gas. Glow discharge is widely used for lighting devices. It usually occurs between two flat electrodes at low pressure using direct current (DC) with high voltage. Its big advantage is the relatively low voltage and power consumption. In analytical chemistry, it is mostly used as a secondary ionization source in different modifications, since it generates a fairly homogenous discharge consuming only little amounts of auxiliary gas due to the low pressure needed.[18]

(2) The physical process of corona discharges is dominated by an axial DC field. The discharges take place on a time scale of sub-nano-seconds. Therefore, applying an alternating current (AC) voltage with a frequency of 50 Hz has hardly any measurable impact on physical processes that take place and hence such discharges can be treated as they would be a DC corona discharge plasma. This is especially important for the theoretical formalism.[17, 18] A corona discharge is usually generated from sharp points, sharp wires or edges. **Fig.1.1** illustrates such inhomogeneous electrode geometry on the example of a corona discharge from a sharp point and a plane electrode. Ionization in a DC corona occurs only when the electrical field strength is above the average value. Outside this region, no ionizing collisions take place. At high voltages, the corona discharge turns into a glow discharge when it becomes visible to the eyes. The

visible glow discharge is usually described with the active radius or visible radius of a corona discharge. Within this active volume, most of the corona initiated chemistry is taking place. One problem of

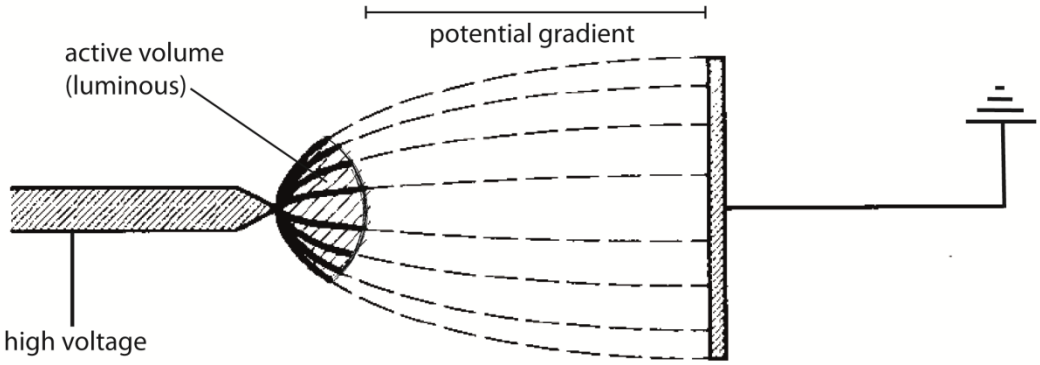

Fig. 1.1: Inhomogeneous corona discharge at atmospheric pressure. High voltage is applied to a SS needle in front of a grounded metal plate. A corona discharge is formed from a sharp point and a plane electrode. Adapted from Eliasson and Kogelschatz,[12] with kind permission of the Institute of Electrical and Electronics Engineers.

using DC voltage to produce a corona discharge is that sparks can bridge the gap between electrode and counter electrode when the applied voltage is too high. This does not happen when using AC since the voltage amplitudes applied can be far above the static breakdown voltage. The active region of a corona discharge plasma (small volume) is small and not very well suited to produce large quantities of chemical species and is therefore not ideal for industrial production. However, corona discharge finds its applications in electrostatic precipitators, copying machines, high-speed printout devices, dry-ore separation systems, radiation detectors, surface treatment of polymers and recently also large scale application in the treatment of flue gases.[12, 17, 18]

(3) In 1857, Siemens introduced the idea of producing ozone with a special electrical discharge. Today, this type of plasma reactor is called silent discharge or DBD.[19] The DBD combines the large active volume of the glow discharge with the high pressure tolerance of the corona discharge. Therefore, it is well suited for industrial plasma chemistry applications. The key element in a DBD is the dielectric, where charges are accumulated on the inner walls during

ionization. The electrical field generated from these charges interrupts the current flow after a specific time, which depends on the properties of the dielectric material, the geometry of the plasma reactor, the helping gas, and the pressure. These discharges are sometimes also called “microdischarges”.

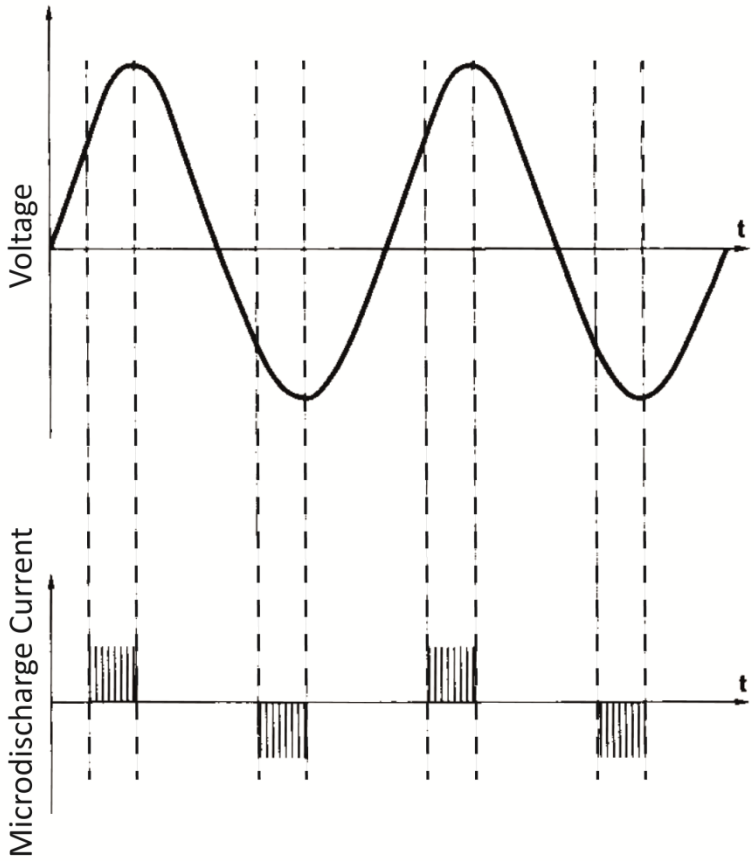

Fig. 1.2: Applied sinusoidal voltage to a DBD and the resulting bursts of microdischarges. Adapted from Eliasson and Kogelschatz,[12] with kind permission of the Institute of Electrical and Electronics Engineers.

Using a sinusoidal voltage, discharges are usually generated shortly before the maximum and minimum of the amplitude (breakdown of the gas), which is schematically shown in **fig. 1.2**. This is the case when the potential drop exceeds the ignition voltage at the discharge gap. The DBD is a very well suited source to produce energetic electrons, which is beneficial for plasma-chemical efficiency.

A special type of a DBD is the dielectric packed bed reactor,[20] which is also sometimes called ferroelectric packed bed reactor. The dielectric material is often chosen as a reactive catalyst, which should improve the complete oxidation of flue gases. Such reactors are frequently studied in the flue gas treatment.[21]

1.3 Non-thermal plasma in the flue gas treatment

Holzer *et al.* presented a DBD plasma using heterogenic catalytic material for enhanced oxidation of VOCs.[15, 16, 22] They described in their work in-plasma catalysis reactors, where the catalytic material is directly placed into the active plasma zone, and post-plasma catalysis reactors, where the catalytic material is placed after the active plasma zone. [22] The non-thermal plasma technology appears to be not well suited for cleaning flue gas, since the desired total oxidation is usually not achieved. This leads to the formation of partly oxidized, possibly harmful by-products. They attempted to overcome this problem using a combination of heterogeneous catalysts and non-thermal plasma. In a later study, they could show that in porous catalyst grains an enhanced amount of short-lived oxidants exists enhancing the total oxidation of the studied VOCs.[15] However, due to CO_2 poisoning, the activity of the catalytic material was dramatically reduced within few hours of plasma treatment. Furthermore, Holzer *et al.*[22] concluded that non-thermal plasma does not usually allow both, sufficient degradation of the incoming molecules to the desired reaction products (e.g. CO_2 and H_2O) and high conversion. They further showed the inactivation of their heterogeneous catalytic material γ-Al_2O_3, as well as the decomposition of the long living ozone. Another conclusion was that ozone plays a major role in the post-plasma treatment mode, since it decomposes catalytically on the γ-Al_2O_3 surface leading to the formation of atomic oxygen as oxidizing species. Furthermore, the role of ozone in the in-plasma treatment mode proved to be much more complex. In both treatment modes, they observed CO_2 poisoning of the catalyst. [15]

D. E. Tevault[23] used a DBD reactor to treat an air-methane mixture. He found that nitrogen oxides play the key role in the removal of ozone in nitrogen-containing plasmas. Using his plasma reactor, full decomposition of methane was not achieved. He observed a significant problem of plasma air purification devices as those produce a considerable amount of CO even when operating them in pure air. To overcome this problem working in humid air enhanced the CO_2 and reduced the CO production.

In the group of Kiwi-Minsker, Ch. Subrahmanyam and M. Magureanu studied several catalytic DBD reactors for the decomposition of VOCs.[24-29] They

could improve the performance of their reactor significantly by using sintered metal fibers (SMF) modified with Mn oxide. Total oxidation could only be achieved with a rather high input energy of 760 J L^{-1} for a concentration of 250 ppm isopropanol, whereas complete destruction was observed with less energy (235 J L^{-1}). However, complete destruction resulted in a lot of oxidized by-products. Moreover, they observed no direct correlation between the efficiency of their reactor and its produced ozone. They concluded that the catalytic decomposition of ozone on the catalyst surface might form short lived atomic oxygen, which is a very strong oxidizing species. The production of atomic oxygen on their MnOx/SMF catalyst is also thought to be the reason for the enhanced performance of their DBD reactor.[29] In another interesting work,their DBD reactor geometry was optimized using trichloroethylene as a model compound. They found that a smaller discharge gap increases the removal efficiency. For 3 mm they observed complete destruction with an input energy of 480 J L^{-1}, whereas with a discharge gap of 5 mm only a conversion of 97% was achieved with the same amount of input energy. Using their MnOx/SMF catalyst they could significantly enhance the selectivity towards CO_2. They observed that the higher the input energy the higher o the selectivity towards CO_2.[27]

Futamura *et al.*[20, 21, 30, 31] studied special packed bead reactors for the decomposition of butane and benzene. In their earlier work they studied a ferroelectric packed-bead plasma reactor and its chemical processes. Decomposition was found to be much faster in a complete nitrogen atmosphere than in air. The key factor for the decomposition of butane was considered to be the energy transfer of the hot electrons to butane. Furthermore, water was found to help to enhance the decomposition efficiency of butane.[30] Futamura *et al.*[31] showed improved decomposition of benzene in air using a silent discharge reactor equipped different catalysts (MnO_2 and TiO_2). They also concluded that the strong oxidizing species formed in the plasma improved the decomposition. Only one year later Futamura *et al.*[21] presented a plasma-driven catalyst (PDC) reactor, once again using the decomposition ofbenzene as a model. They successfully decomposed a concentration of 110 ppm benzene using a specific input energy of 130 J L^{-1}. They also confirmed that UV light, which usually comes

from nitrogen when working in air, is not a controlling factor in plasma based air cleaning devices.

A very interesting comparison of five different non-thermal plasma reactors was published in the same year by the same authors. The five different plasma reactors are a pulsed corona reactor, a DBD reactor, a surface discharge reactor, a catalytic packed-bed reactor and a PCD reactor (cf. **fig. 1.3**).

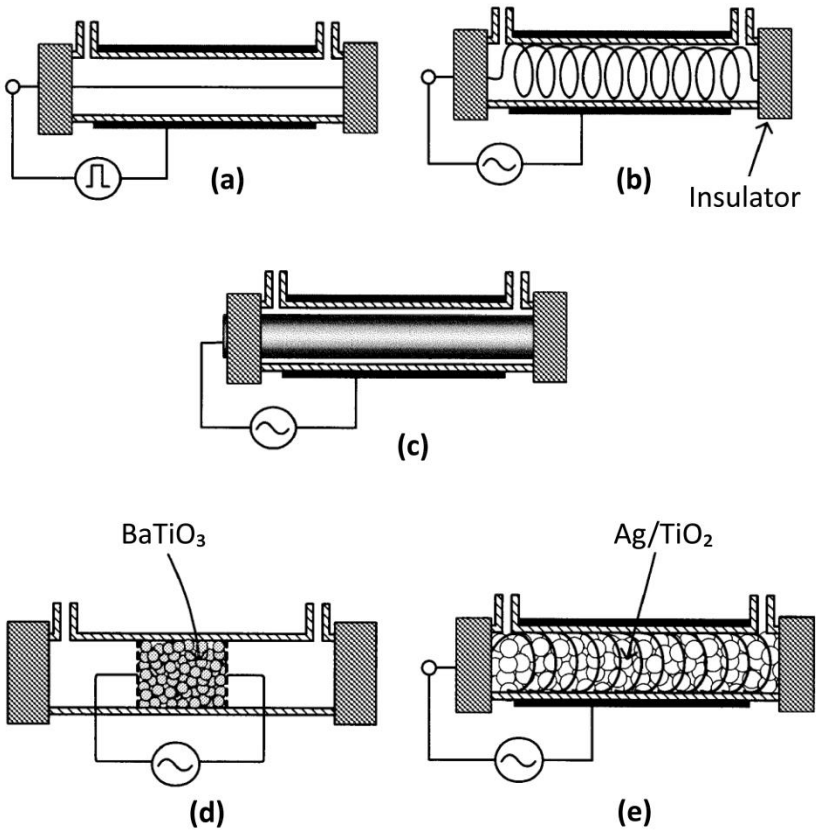

Fig. 1.3: Schematic overview about five different types of plasma reactors used in flue gas treatment. (a) Pulsed corona reactor, (b) surface discharge reactor, (c) DBD reactor, (d) packed-bed reactor and PDC reactor. Adapted from Hyun-Ha Kim,[20] with kind permission of the Institute of Electrical and Electronics Engineers.

To get a non-thermal PAP that is capable of performing well in flue gas treatment, it needs both low overall energy consumption and must not lead to too many by-products. In the ideal case only H_2O and CO_2 are generated. Hyun-Ha Kim *et al.*[20] studied the decomposition of benzene in plasma reactors at dry and humid conditions. For the non-catalytic plasma reactors (DBD, pulsed corona and surface discharge reactor) an enhanced destruction efficiency of benzene was observed under humid conditions. In contrast to this observation a decrease in conversion efficiency was observed for catalytic plasma reactors

(packed bed and PCD reactor). Similar decomposition behavior has been found for the non-catalytic plasma reactors, which let them conclude that the plasma reactor type is not crucial. However, they found a considerably higher amount of aerosols when using the pulsed corona reactor compared to the others. On the other hand, close to no aerosol production was found with the catalytic plasma reactor. The worst carbon balance was found for the surface corona discharge and for the pulsed corona discharge reactor. This observation is supported by the fact that these two reactors also had the highest amount of aerosols formed. Kim *et al.* conclude that the PDC reactor was superior to all the other tested non-thermal plasma reactors for the decomposition of benzene.[20]

Mok and Nam[32] used a dielectric packed-bed reactor combined with post catalytic treatment to oxidize nitrogen oxide to nitrogen dioxide. The dielectric packed-bed reactor particularly for the ozone generation was used, whereas the catalyst helped to improve the oxidation reaction.

Ayrault *et al.*[33] presented a DBD reactor using a honeycomb monolith supported platinum-based catalyst for the oxidation of low concentrations of 2-heptanone. Complete decomposition of 2-heptanone was observed and the presence of water vapor enhanced the CO_2 selectivity. Moreover, the ozone concentration could be reduced strongly in the presence of water vapor. A small disadvantage was a slight drop in the decomposition efficiency of 2-hetanone and the observed polymeric by-products when applying lower voltages.

Morvovà *et al.*[34] tested a completely different approach using a spontaneously-pulsing DC corona discharge coupled with a heterogeneous catalyst on various sources of exhaust. Their final degradation product is a powder with a fractal structure on the microscopic level. In contrast to all the other publications they did not focus on total oxidation. They noticed that the low mass powder is completely insoluble in water and was mainly an amorphous condensate of amino acids. They could identify the following amino acids in the powder: alanine, serine, glycine, aspartic acid, lysine, arginine, methionine and histidine.

Oda *et al.*[35] gave a review about the progress of the non-thermal plasma technology in flue gas treatment. In this article the authors noted that small scale non-thermal plasma reactors are receiving much more attention than large scale

reactors. One reason for this observation could be that small scale non-thermal plasma reactors are much easier to study. In their work 1000 ppm trichloroethylene (TCE) was decomposed using zeolite and vanadium oxide as catalyst and showed that the initial adsorption was 80 and 50%, respectively. They observed non satisfactory total decomposition performance using zeolite due to desorption processes. However, vanadium oxide showed higher total decomposition (>99%) of TCE when applying an input energy of 0.27 W. In some cases even the by-product concentration was enhanced when inserting a catalyst into the active plasma zone. Therefore, it is quite difficult to elucidate which part of the decomposition efficiency was coming from the non-thermal plasma and which part was just coming from absorption. Both lead to a reduction of the flue gas in the exhaust of the studied non-thermal plasma reactor.

To sum up all the presented methods, it is obvious that non-thermal plasma is often assisted with a catalyst for better oxidation, however, there are also some disadvantages to keep in mind. Catalysts need to be replaced from time to time due to carbon poisoning and are often not as reactive in humid conditions as they are in dry conditions. Furthermore, catalysts can absorb a part of the flue gas which could decrease its activity as well as wrongly lead to a higher degree of observed decomposition efficiency.

1.4 Chemistry in the nonequilibrium plasma

In nonequilibrium plasma two points are of great importance: the physics of the discharge and the chemical reactions in the plasma. Since the arrangement of the electrodes in the PAP, used in this work is fixed, we are interested in the chemical reactions in the plasma. In nonequilibrium plasma chemistry the electrical discharges deliver the energy (usually from electrons) to initiate chemical reactions. It is important that the energy transfer between electron and reaction partner is efficient in a plasma reactor. **Fig. 1.4** shows a current pulse of 10 ns initiated by a single microdischarge in air. The energy of such a microdischarge is transferred into N_2 and O_2. Various excited levels of N_2 and O_2 dissociate and eventually result in the formation of ozone and various nitrogen oxides. After around 50 ns the main chemical processes are taking place as most of the charge carriers have disappeared.

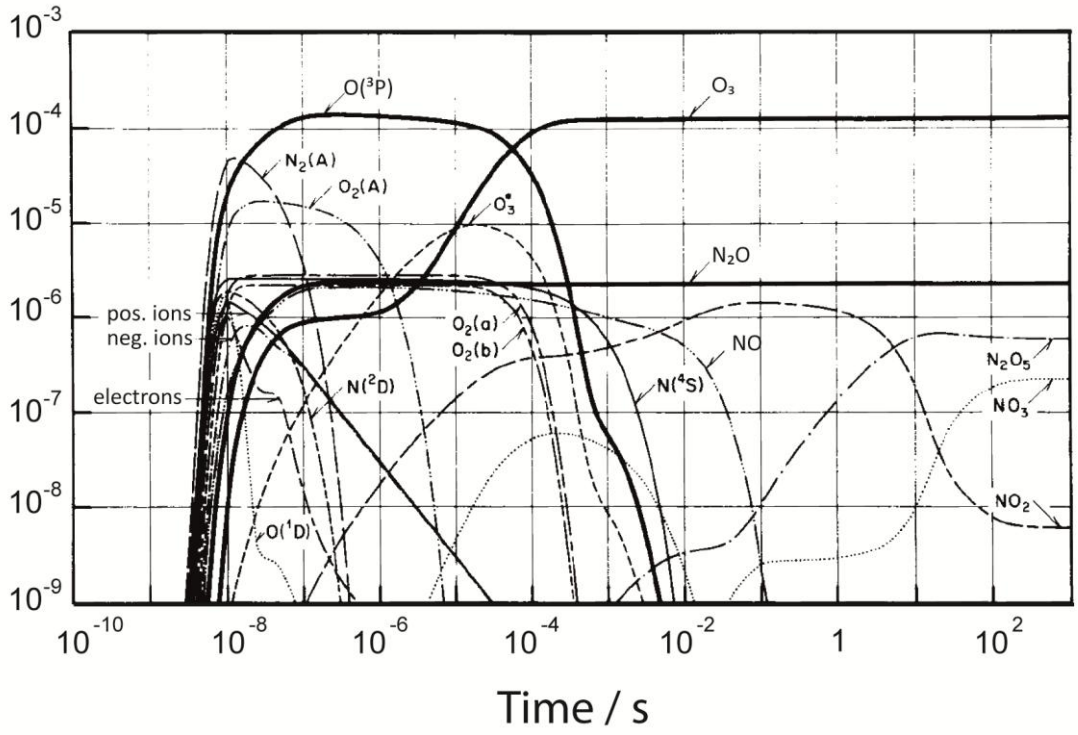

Fig. 1.4: Microdischarge initiated chemical reactions initiated by plasma in air (20% O_2 and 80% N_2**).** Adapted from Eliasson and Kogelschatz,[12] with kind permission of the Institute of Electrical and Electronics Engineers.

In **fig. 1.5** a schematic of what happens in the plasma is shown. Hot electrons (e) excite the neutral species (A) to excited species (A*). During this process positive and negative ions are formed (I). A* and e react further to new species (B) and (C). The ultimate goal of all non-thermal plasma reactors is to get

as much A* as possible to initiate new reactions using as little input energy as necessary. Formula (1) and (2) show how these reactions would look like. Reaction (1) initiates reaction (2) and is the limiting factor for the production of (B) and (C). The end products (B, C) and its reaction velocities depend on the pressure, temperature, the reaction and the rate coefficients for electronic reactions.

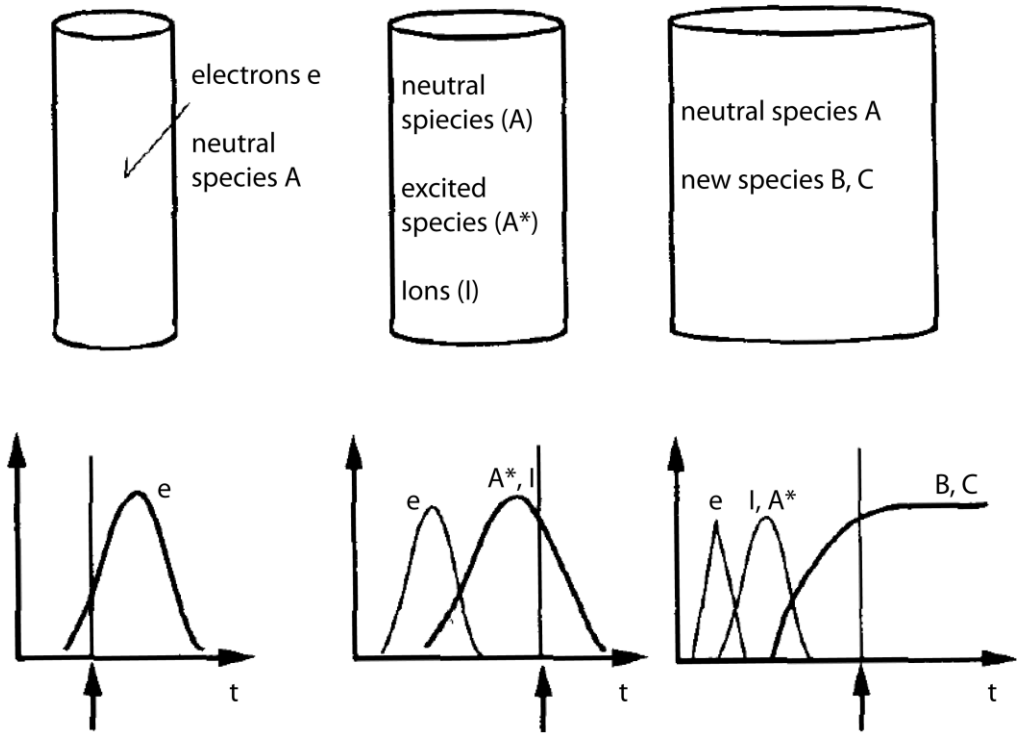

Fig. 1.5: Three different time dependent processes in a plasma showing the different species generated. Adapted from Eliasson and Kogelschatz,[36] with kind permission of the Institute of Electrical and Electronics Engineers.

$$e + A \rightarrow A^* + e \tag{1.1}$$

$$A + A^* \rightarrow B + C \tag{1.2}$$

Table 1.1 presents the known main chemical reactions occurring in plasma. A and B present atoms, A_2 and B_2 gas molecules, M a temporary collision partner and e stands for an electron.

Table 1.1: The main reaction types that occur in a plasma reactor are illustrated. A and B stand for atoms, A_2 and B_2 stand for molecules and M stand for a temporary reaction partner.

The Main Plasma Reactions

Electron/Molecular Reactions			
Excitation	$e + A_2$	→	$A_2^* + e$
Dissociation	$e + A_2$	→	$2A + e$
Attachment	$e + A_2$	→	A_2^-
Dissociative attachment	$A_2^* + e$	→	$A^- + A$
Ionization	$A_2^* + e$	→	$A_2^+ + 2e$
Dissociative ionization	$A_2^* + e$	→	$A^- + A + e$
Recombination	$A_2^* + e$	→	A_2
Detachment	$A_2^* + e$	→	$A_2 + 2e$
Atomic/Molecular Reactions			
Penning Dissociation	$M^* + A_2$	→	$2A + \mathrm{M}$
Penning Ionization	$M^* + A_2$	→	$A_2^+ M + e$
Charge Transfer	$A^\pm + B$	→	$B^\pm + A$
Ion Recombination	$A^- + B^+$	→	AB
Neutral Recombination	$A + B + M$	→	AB + M
Decomposition			
Electronic	$e + AB$	→	$A + B + e$
Atomic	$A^* + B_2$	→	$AB + B$
Synthesis			
Electronic	$e + A$	→	$A^* + e$
	$A^* + B$	→	AB
Atomic	$A + B$	→	AB

Summing up, the chemistry taking place in the plasma is mainly initiated by hot electrons. These electrons excite neutral reaction partners (gas molecules such as O_2 or N_2) to higher energetic levels and these can initiate other reactions. Ozone is a long living reactive species generated in the plasma. It can either react directly in the gas-phase or indirectly when it first reacts with a third reactant

(e.g. H_2O) to form a more reactive species like atomic oxygen or OH radicals. Since water is initially present (as humidity and since it is a product of the total oxidation) in the flue gas treatment, these radicals play a key role in the removal process.

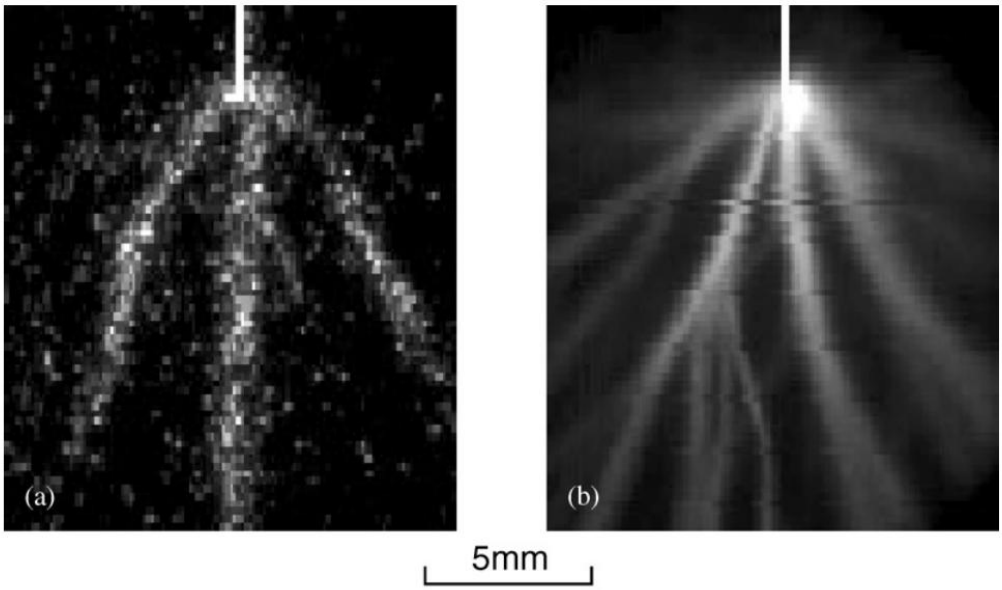

Fig. 1.6: (a) Shows the laser induced fluorescence of the OH radicals distribution (white dots) from a positive pulse discharge in nitrogen containing 2.4% water. (b) Photo of a spontaneous positive discharge. Adapted from Oda,[35] with kind permission of Elsevier.

F**ig. 1.6** shows a photo, as well as the OH radical distribution, of a positive pulse discharge plasma in nitrogen containing 2.4% water. Oda[35] used laser-induced fluorescence (LIF) in his work to obtain the OH distribution. It clearly proves that OH radicals are formed in a non-thermal plasma under humid conditions. Hammer[17] reported that for high radical formation rates the energy requirement is on the order of 20 to 100 eV, depending strongly on the gas to be treated. This means that the plasma should deliver at least this amount of energy to electrons so that they can collide with neutral molecules and excite them to higher energy levels and initiate chemical reactions.

1.5 Objectives and Organization of the Thesis

The goal of this work was to investigate the chemical processes of a commercially available PAP based on pulsed (50 Hz) corona plasma discharge using a rather low input energy. This PAP was designed to be maintenance free. Hence, no catalytic stage was incorporated. Moreover, it offers the advantage of not imposing a pressure drop in a ventilation system in contrast to HEPA filters. The mentioned PAP is designed to decompose aerolized bacteria and viruses as well as environmental toxins. The supplier of the system claims that it decomposes everything that is flying through it to small non-toxic degradation products, but in reality it was not exactly clear what happened to the molecules passing through the PAP. Since incomplete oxidation could induce toxic by-products formation, it is of great importance to study the fate of such flue gases in the PAP. In a first step, a ventilation system was designed to incorporate the PAP. Rather high flow rates (>3000 L min^{-1} or an air flow velocity through the ventilation system of 3 m s^{-1}) made sampling challenging.

A short introduction into the materials and methods used in this thesis is given in **Chapter 2**.

In order to understand the chemical processes in the PAP it was decided to study VOCs as the first compounds, which is commonly used as in a Non-thermal plasma reactors with and without catalysts. Choosing VOCs as compounds to study offered a rather easy model system which helped to elucidate the dominating degradation processes in the PAP. **Chapter 3** deals in detail with the fate of a specific set of VOCs using polar and non-polar adsorption tubes to take samples from the PAP exhaust. Subsequent GC-MS analysis allowed for the identification of a fairly wide range of degradation products.

Calculations, combined with the measured ozone concentration inside of the PAP showed that oxidation of cyclohexene due to ozone cannot be the main degradation pathway. In order to get a better idea of what reactions are taking place, a smaller version of the PAP was placed in front of our mass spectrometer. The exhaust was ionized using a glow discharge ion source. Another approach with the regular PAP was to use a resistor based VOC online sensor to study the degradation of the VOC. Measurements with different VOC concentrations could

help to quantify the degraded amount of VOC using the PAP. **Chapter 4** summarizes all the data obtained in this project.

Chapter 5 introduces an ion source, which is based on a DC voltage helium glow discharge plasma. This ion source was used as a secondary ion source in chapters 4, 5 and 6 and is especially useful, when gases with high flow rates need to be ionized. In capillary electrophoresis (CE) experiments this ion source showed extraordinary robustness, even though high nitrogen gas flow rates were used for nebulization of the CE effluent. This nebulizer gas helped to transfer the analytes from the liquid phase to the gas phase before they were ionized by the glow discharge plasma. Since the front plate of the presented ion source is grounded, using it as a secondary ionization source is rather simple as well as more secure in terms of safety issues compared to other secondary ionization sources based on AC voltage. This chapter presents a separation of five different analytes using this homemade glow discharge plasma ion source for sheathless coupling of capillary electrophoresis with mass spectrometry. The chapter closes with the observed results and discusses further prospects of using the glow discharge plasma as an ionization source.

In **Chapter 6,** the glow discharge plasma source is incorporated in a newly designed interface. This interface allowed a direct coupling of the PAP exhaust with the mass spectrometer. Therefore, it helped to circumvent the problems observed while using offline sampling. Several amines were used to study the processes in the PAP. A basic experiment was carried out to check the performance of the interface. Afterwards, specifically chosen amines were used to unravel the processes in the PAP. A detailed characterization and interpretation of the observed results is presented. This chapter closes with a general discussion about the characterization and methods how to measure the degradation efficiency of PAPs.

Chapter 7 presents a performance study of the PAP using three different classes of substances. Environmental toxins were studied as representatives for low molecular weight molecules, bovine serum albumin represented high mass proteins, and bacteria from the type *Legionella* and *Bacillus* were studied representing bioparticles. When passing through the plasma air purifier, a reduction in concentration of the compounds/particles studied was found.

Therefore, it was inalienable to perform a detailed mass balance study for the different substance classes. A detailed description of how the mass balances were performed is shown. The observed results are discussed and final conclusions about the mechanism behind the observed degradation of the studied PAP are presented. **Chapter 6** and **7** present some observed chemical processes in the PAP. **Chapter 7** unravels the processes of the observed degradations efficiencies and shows the risk that an incomplete or missing mass balance can bear.

In **Chapter 8,** the same sonic spray ionization source that was used to nebulize all compounds in our mockup to study the PAP is presented. This nebulization source was the ideal source to guide all analytes into the gas phase. If high voltage is applied to this ionization source a technique called electrosonic spray ionization (ESSI), a hybrid of electrospray and sonic spray ionization, is obtained. The performance of ESSI was compared with pneumatically-assisted electrospray ionization by coupling both sources to a high performance liquid chromatography system. Much interest in the use of these sources for high flow applications has been generated in recent years. The two sources performance was evaluated using a chromatographic separation of a test mixture containing five peptides these two sources, which allows for the direct comparison, in the context of both low and high sample flow velocities. The chapter ends with a short outlook of potential areas where the ESSI source could be of interest.

The thesis closes with **Chapter 9**, which contains a general conclusions and future prospects of PAPs. The bibliography at the end of this thesis contains all the references used in this work.

Chapter 2

Experimental Methods

This chapter gives a short introduction into mass spectrometry as well as an overview of the most important experimental methods used in this work. After a short description of the commercially available PAP, the flowing atmospheric afterglow ion source is introduced. The chapter closes with the introduction of two ionization methods, of which the sonic spray ionization source was used for the nebulization of the compounds studied in our mockup system.

2.1 Mass spectrometry as analytical tool

Mass spectrometry (MS) allows measuring the mass-to-charge ratio of charged molecules and helps to identify the chemical structure of unknown compounds as well as their elemental composition. In contrast to nuclear magnetic resonance or infrared analysis of compounds, MS consumes the analyte molecules. However, the sample amount required for MS analysis is very little (in the µg range) and the technique can therefore be regarded as quasi non-destructive.

In 1886, Eugen Goldstein laid the basis for the invention of MS with his discovery of the positively charged anode rays he called canal rays. These rays could pass in opposite direction as expected through the holes of the perforated cathode he used.[37] In 1889, Wilhelm Wien constructed an apparatus capable of separating canal rays by their mass-to-charge ratio using parallel magnetic and electric fields. Nine years later, he further established that canal rays carry a positive charge. [38] In 1912, Joseph John Thomson designed the first mass spectrometer working at reduced pressure, which he called "parabola spectrograph". Even though the first instruments in MS were similar to a spectroscope, one should not make the mistake of calling mass spectrometry "mass spectroscopy" as some mass spectrometrists could get upset when this issue is mixed up.[39] In the beginning of the 20th century Arthur Jeffrey Dumpster and Francis William Aston modernized MS. Dumpster used an electron ionization source coupled with a sector-shaped magnet and Aston could focus the ion velocity with his system.[40]

A mass spectrometer consists of five parts: Sample introduction, ion source, mass analyzer, detector and readout system. The mass analyzer, as well as the detector, and sometimes the ion source, are under high vacuum. From the beginning of MS until now, mass spectrometers have changed tremendously. Many different ionization sources have been introduced: Electron ionization (EI),[41, 42] atmospheric pressure chemical ionization (APCI),[43] glow discharge ionization,[44-46] matrix-assisted laser desorption ionization (MALDI),[47-49] electrospray ionization (ESI),[50, 51] and many more which are described in detail by Edmond de Hoffmann and Vincent Stroobant.[40] In this chapter, three specific ionization sources used in this thesis are described in more detail.

2.1.1 The flowing atmospheric pressure afterglow ion source

In 2008, Andrade *et al.*[52] invented a DC helium driven flowing afterglow atmospheric pressure glow discharge (FA-APGD) ionization source. In this thesis, the term flowing atmospheric pressure afterglow (FAPA) is used to describe this ionization source since it better emphasizes the generated active species as opposed to how the plasma is produced. This source offers simplicity in design and high sensitivity for a wide range of organic compounds. **Fig. 2.1** shows the schematic of a FAPA ionization source as well as a photograph of an APGD between the cathode and anode. After being transported outside of the ion source, ions and the excited species can react with the analyte compounds. These reactions lead to ions that do not have to flow through the discharge chamber. Mass spectra obtained from a FAPA ionization source are very similar to those obtained using atmospheric chemical pressure ionization (APCI) sources. A background spectrum of the ionizing species generated by the FAPA ionization source showed strong signal intensity of water clusters in a fashion similar to what has been observed with APCI sources. The strongest water cluster signal is observed at *m/z* = 37 which corresponds to the protonated water dimer $(H_2O)_2H^+$. Charge transfer might play a significant role in the ionization pathways of this ionization source.

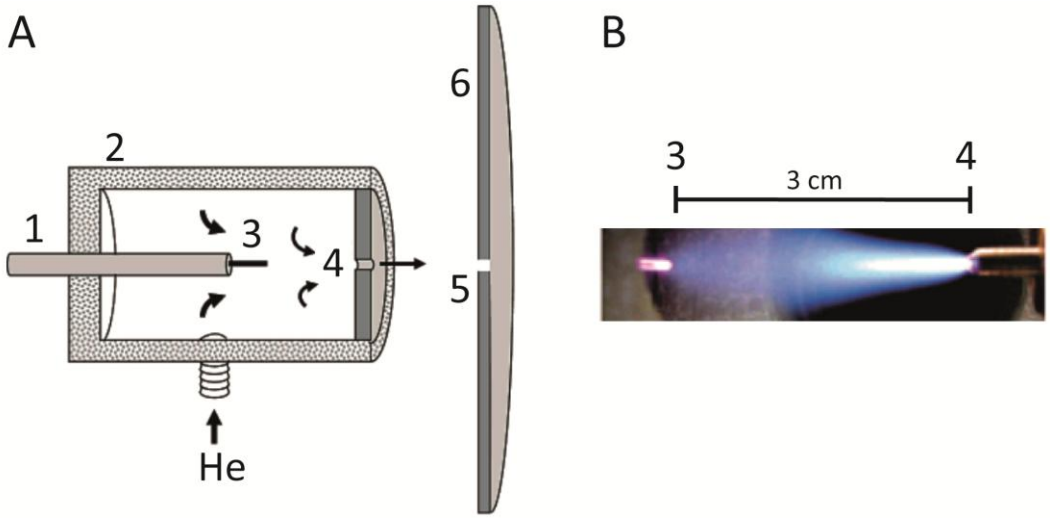

Figure 2.1: (A) Schematic view of a FAPA ionization source: 1, steel mount; 2, Teflon body; 3, tungsten cathode; 4, anode; 5, sample ionization region; 6, mass spectrometer front plate. (B) Photograph of a typical APGD with a pin cathode (3) and a rod anode (4). The gap between the electrodes was set to 3 cm. Adapted from Andrade *et al.*[52] with kind permission of the American Chemical Society.

A drawback of the FAPA ionization source is the fact that high-purity helium (99.999%) is needed to run it properly, otherwise impurities could interfere with the analyte molecules. The FAPA ionization source is suitable for solid[53-55] as well as for liquid[52] samples.

There are two main advantages to using a FAPA ionization source compared to similar DBD helium plasmas such the low temperature plasma (LTP) ion source, introduced by Harper *et al.*[56] in 2008: (1) safety and ease of interfacing to an MS are greatly enhanced since the ground of the FAPA ionization source is always connected to the front plate. This means that it is even possible to touch it without harm and there are no disturbances of the electrical field in front of the MS cone. (2)The produced plasma torch is not easily disturbed, in contrast to the LTP source, and is therefore well suited for interfacing with a MS. Even when very high nebulization gas velocities are used this source showed a very stable total ion current (TIC).

2.1.2 Sonic spray ionization

In 1994 Hirabayashi *et al.*[57] introduced the sonic spray ionization (SSI) source. The construction of this ionization source is rather simple (*cf*. **fig. 2.2**) as no heating of the nebulization gas is needed as well as no electric field has to be applied in contrast to electrospray ionization. Charged droplets are produced at

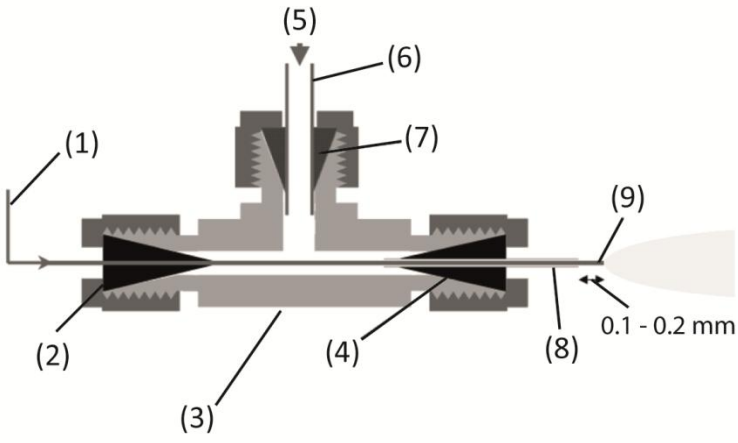

Fig. 2.2: schematic of the homebuilt SSI source. 1, sample flow rate Sample (~250µL min^{-1}); 2, graphite ferrule (0.2 mm ID); 3, Swagelok® T-element (1/16" stainless steel (SS)); 4, PTFE ferrule (0.4 mm ID); 5, N_2 (p ~8-12*10^5 Pa); 6, SS tubing (5.0 cm); 7, SS ferrule (1/16"); 8, fused silica (FS) capillary (L =2.5 cm, 0.25 mm ID, 0.38 mm OD); 9, FS capillary (L ~50 cm, 0.075 mm ID, 0.15 mm OD). Adapted from Takats *et al.*[58], with kind permission of the American Chemical Society.

atmospheric pressure by a gas flow coaxial to the fused silica (FS) capillary coating the sample (*cf*. **fig.2.2**). Using nebulization velocities at the speed of sound (Mach 1) the SSI source is capable of most efficiently guiding solubilized molecules into the gas phase. The signal intensity reached its maximum with these nebulization velocities.

Two models of how gas phase ions can be formed from liquids are known, the ion evaporation model (introduced by Iribarne and Thomsen[59]) and the charge residue model (introduced by Dole *et al*.[60]). While studying the SSI source in 2002 Dames *et al.*[61] observed that ion formation is independent of the ionization source used. However, the charged droplet formation is characteristic for each ion source and therefore largely determines the ion generation efficiency of the SSI source. SSI can be performed with high reproducibility for a wide range of compounds. Even thermally labile compounds can be ionized, since no heating of the nebulization gas is needed.[61, 62] A comparison of the SSI source with an atmospheric chemical ionization (APCI) source showed even superior sensitivity for the SSI source.[63] Although the SSI source became commercially available in the beginning of 2000, only a few researchers used it as an ionization source. Nevertheless, this source was suited ideally to nebulize the compounds studied here and guide them into the gas phase. Moreover, since a motorized syringe pump was used to feed the SSI source, it was possible to exactly nebulize a defined amount of analyte within a specific time. This allowed for a high reproducibility of the experiments.

2.1.3 Electrosonic spray Ionization

The electrosonic spray ionization (ESSI) source is a modification of the SSI source. The only difference to the SSI source is that high voltage (3 to 5 kV) is applied to the FS sample capillary. As usually, a syringe is used to deliver the sample, while the SS needle is connected to a high voltage power supply. This rather novel ionization technique was introduced by Takats *et al.*[64] studying ion molecule reactions in the gas phase at atmospheric pressure. Touboul *et al.*[65] investigated the deprotonation reactions of multiply charged proteins at atmospheric pressure using ESSI-MS. On the other hand, Jecklin *et al.*[66] did a comparison of ESI, nanoESI and ESSI to determine protein-ligand interactions

using mass spectrometry. They could all show that the ESSI source is very well suited for these kinds of applications. **Chapter 9** will show that ESSI is not limited to low sample flow rates only. On the contrary, the ESSI source offers a lot of different advantages in high flow rate applications.

After the introduced sample gets ionized by the ionization source, gas phase ions are separated according to their physical properties. Mass analyzers separate ions according to their mass-to-charge ratio. Several mass analyzers exist: electric sector, magnetic sector, quadrupole, ion trap, time-of-flight, Fourier transform ion cyclotron resonance and recently also the orbitrap was analyzer was introduced.[40] Each mass analyzer has its own advantages and limitations. Mass analyzers can be divided into two classes according how the mass-to-charge ratio is measured. Ions can be transmitted simultaneously or only a certain mass-to-charge ratio passes at a given time.

After the ions have passed the mass analyzer they are detected and transformed into an electrical signal, which is usually recorded and visualized using a personal computer. Electron multipliers are commonly used detectors. They incorporated a dynode where ion impact events are converted to an electrical signal. One of these detectors is the Faraday cup. The Faraday cup can reach an amplification of up to 10^7. Another detector which is based on the continuously electron multiplying is the microchannel plate (MCP). Several plates together can reach an amplification of 10^8.

MS is often coupled to separation methods such as gas chromatography (GC), liquid chromatography (LC), or capillary electrophoresis (CE) in order to analyze samples with complex matrices. All the mentioned separation techniques in combination with MS were used in this thesis. Interfacing LC and CE with the MS presents a challenging task and this thesis shows some new designs how to interface MS with such separation methods.

2.2 The plasma air purifier

Fig. 2.3 shows the design of the PAP used in this thesis. It has an inner diameter of 160 mm, a length of 180 mm and an overall weight of 10.5 kg. The material of construction for the four electrodes is copper, which has been coated

with chromium. The copper electrodes have a special shape to maximize corona discharges (lots of sharp edges and tips). All other plates are made of poly-(methyl-methacrylate) (PMMA). Spacers as well as the case for all the plates are made of polyvinyl chloride (PVC). The four electrodes are connected to a freely adjustable high voltage power supply (230 V, 50Hz). An operating voltage of 6.1 kV was recommended from the supplier. Copper electrodes 1 and 4 are connected to the ground and the copper electrodes 2 and 3 to the high voltage (*cf.* **fig. 2.3**). The plasma is generated in normal air without any auxiliary gas. Air flow velocities through the PAP from 0.3 to 3.0 m s^{-1} (320 L min^{-1} to 3200 L min^{-1}) can be handled according to the manufacturer.

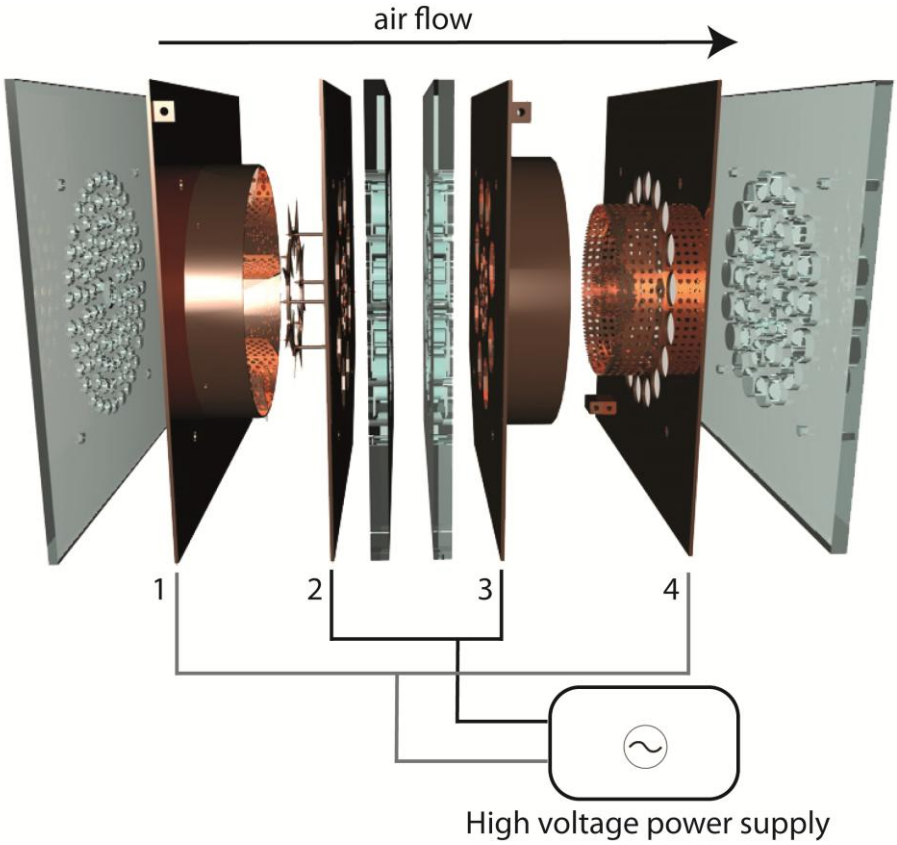

Figure 2.3: Schematic of the PAP: From left to right. poly-(methyl-methacrylate) plate, two copper electrodes, two poly-(methyl-methacrylate) middle plates, two copper plates, poly-(methyl-methacrylate) back plate.

2.3 Chromatography as method of separation

In the late 1800s chromatography was invented by Russian botanist Michail Semjenowitch Tswett. Today the term is used to describe various separation techniques. In most cases sample mixtures are dissolved in a solvent (the mobile phase) which transports the sample through a stationary-phase

medium. According to physical and chemical properties, compounds contained in the sample travel through the stationary medium at different speeds and get separated. Today, chromatography is e.g. used to separate complex mixtures or to purify samples of interest for better analytical characterization. Gas chromatography, high performance liquid chromatography and capillary electrophoresis will be explained below in more detail as these techniques found their application in this thesis.

2.3.1 Gas chromatography

In the 1950s gas chromatography (GC) was first introduced, by A.T. James and A.J.P. Martin.[67] Today, GC finds its applications in most industry areas such as environmental, food, pharmaceutical, forensic and many more sciences. In GC, a gaseous mixture is separated with help of an inert mobile phase (gas) and a stationary phase (usually liquid). **Fig. 2.4** shows the schematic of a normal gas chromatograph, which consists of five parts: 1, an inert gas carrier; 2, an injection port; 3, a column; 4, a detector and 5, the data acquisition.

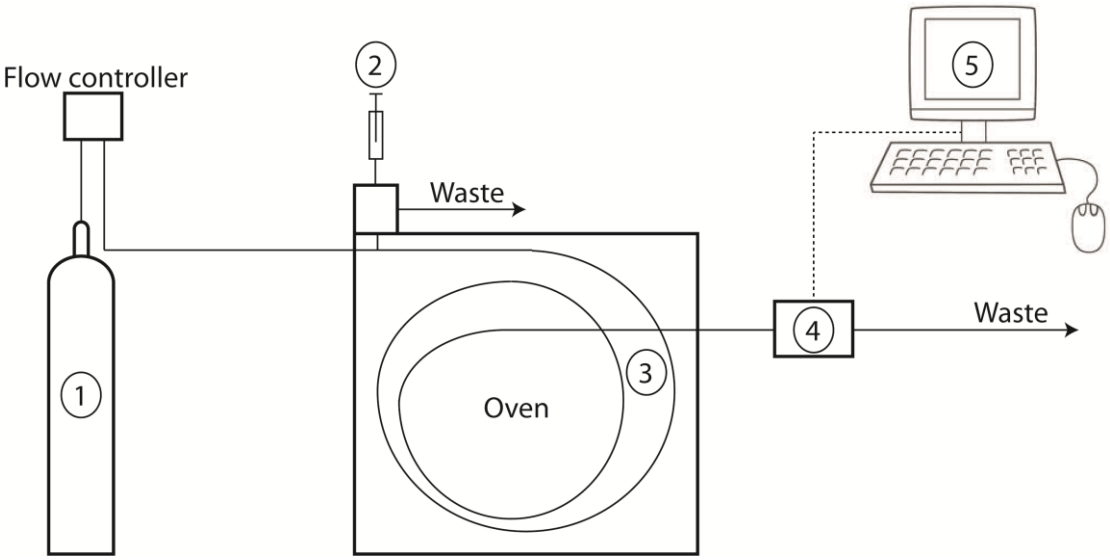

Figure 2.4: Schematic of a gas chromatograph. 1, carrier gas; 2, injection port; 3, column; 4, detector and 5, Data acquisition.

The carrier gas (1) is chosen depending on the application and the type of detector used. Helium is the carrier gas most commonly used due to safety reasons and its good performance. Hydrogen, nitrogen and air are other carrier

gases, which are used in GC. The gas purity is of paramount importance in order to obtain appropriate sensitivity and selectivity. However, analytical grade helium is rather expensive and one might choose cheaper quality as long as the separation is not influenced.

The injection port (2) is responsible for the introduction of the sample into the carrier gas. In most cases split injectors are in industry. Here, samples are dissolved in an appropriate solvent so that sample signals can be separated from solvent signals. Afterwards, the diluted sample is vaporized and only a small fraction of it is allowed to enter the capillary column, the remaining part is usually split to the waste. For thermally labile compounds on column injectors are used. Here, the sample is injected directly into the column without vaporization. However, difficult handling of the syringes and possible contamination of the capillary inlet are the reason this technique is used only in rare occasions. A more wildly used technique is the headspace technique. It allows analyzing volatile organic compounds in difficult samples such as viscous liquid or sludge. The samples are placed in an enclosed vial and the vapor space is then injected into the gas chromatograph.

The heart of the GC is the column (3), which is located in an oven. The temperature of the oven is precisely controlled and determines the time sample needs to pass through the column. The column separates the components in the sample mixture. Today, capillary columns are the columns of choice offering high-resolved separation of complex mixtures. Wall-coated open tubular and porous layer open tubular columns are commonly used in GC. The inner wall of such a capillary is coated either with a viscous liquid material (wall-coated open tube) or with a solid porous material. Due to the length of up to 50 m GC offers numbers of theoretical plates of above 10^5. The temperature of the oven is usually optimized for the separation of a complex sample mixture.

A huge variety of detectors (4) exist to interface a gas chromatographs with: Thermal Conductive detectors (TDC), electron capture detectors (ECD), flame ionization detectors (FID), mass selective detectors (MSD) and many more. After the FID the MSD is the most frequently used detector in industry. The FID is a rather simple detector burning organic compounds in a hydrogen-air flame generating ions that are converted into an electrical signal.[68]

Today, data acquisition is done by a personal computer (5). Using an MSD detector equipped with an electron ionization source allows for the use of libraries containing data of millions of compounds to compare and identify signals analyzed in GC-MS experiments. As the sample to be analyzed needs to be vaporized, GC is usually the first choice to analyze volatile organic compounds (VOCs).

2.3.2 High performance liquid chromatography

High performance liquid chromatography (HPLC) has been developed in the late 1960s, when pumps became available delivering a sufficient flow rate withstanding a high back pressures generated by the separation column. HPLC and its related techniques such as ultra-high performance liquid chromatography (UHPLC) are the most widely used separation techniques in analytic chemistry and biochemistry. In contrary to GC, it is not necessary to vaporize the analytical sample. HPLC helps to identify, quantify and purify individual components of a complex sample mixture such as measuring vitamin D levels in serum. **Fig. 2.5** shows the schematic design of a conventional HPLC system. The pump moves the mobile phase and the sample components through the analytical column. Injection is accomplished by using a special loop injection valve for high accuracy of the amount injected. The different components of the

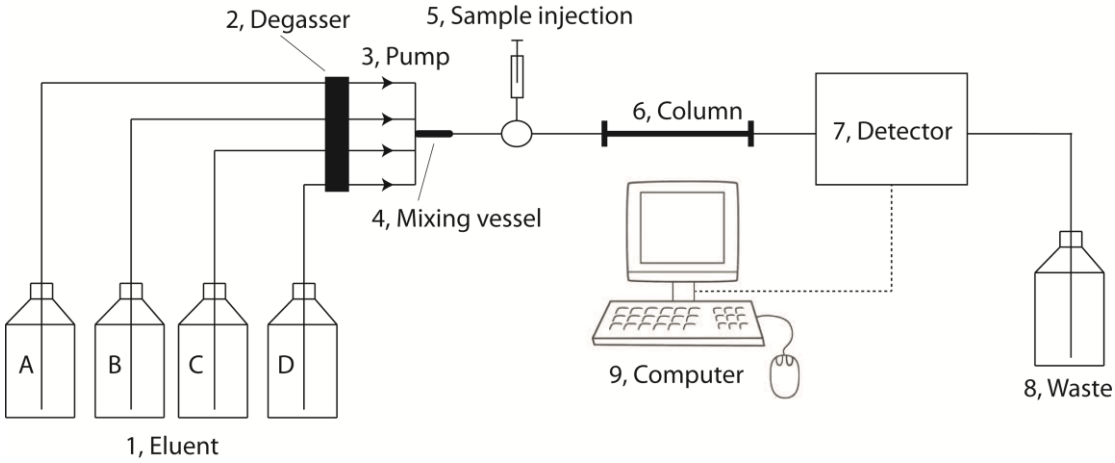

Figure 2.5: Schematic of a conventional HPLC system: 1, solvent reservoirs A-D; 2, degasser; 3, high-pressure pump; 4, mixing vessel; 5, sample injection; 6, analytical column; 7, detector; 8, solvent waste; 9, Data acquisition.

sample interact in the column with the stationary phase. Hence, they move through the column with different velocities and a time resolved separation of the components is obtained. A detector records the signals and sends the data to a computer. There are several types of HPLC among them: The reversed-phase HPLC and the normal-phase HPLC. Normal-phase HPLC uses a silica-based stationary phase. Heptane, methanol and ethanol are solvents commonly used in normal-phase HPLC. As water reduces the separation efficiency of normal-phase HPLC, dried solvents have to be used. Today, normal-phase HPLC finds it application especially for enantiomer separation of racemic mixtures. This requires the use of enantioselective material. This kind of chromatography is often carried out in special laboratories, which makes this separation technique rather expensive. Reversed-phase HPLC uses a non-polar stationary phase. Here, silica-based columns are modified with different alkyl groups to make them non-polar. The retention time of an analyte is longer for less polar components as those interact stronger with the stationary phase. The retention time is the time a component needs from injector to detector. To reduce the retention time of a component one can increase solvent polarity in the eluent. On the other hand, by adding more water to the eluent the retention time of a component is increased.

Both isocratic solvent flows and gradient flow can be used in HPLC. Using isocratic elution, the ratio of solvents is not changed during the analysis only a single solvent system is used. On the other hand, the polarity of the mobile phase is changed continuously during the separation using gradient flow experiments. Using a solvent gradient flow helps to reduce analytical separation times of complex mixtures. In the most modern analytical separation methods solvent gradient flow is used.[68]

Modern HPLCs use photodiode array (PDA detectors) as well as a mass spectrometers. Quantification of the components in a sample mixture is usually done with a PDA detector, whereas identification is done by a mass spectrometer.

2.3.3 Capillary electrophoresis

In 1960s, capillary electrophoresis (CE), also known as capillary zone electrophoresis (CZE) was introduced as a high-efficiency separation technique.

It was designed to separate ionic species by their electrophoretic migration velocity (v_p). The electrophoretic mobility (μ_p) is proportional to the charge (q) and inversely proportional to the frictional forces of the ionic components. The friction force depends on the viscosity (η) of the buffer and the hydrodynamic radius of the ions as shown in formulae (2.1) and (2.2).

$$v_p = \mu_p E \tag{2.1}$$

$$\mu_{p=} \frac{q}{6\pi\eta r} \tag{2.2}$$

The instrumentation of a capillary electrophoresis system is relatively simple (see **fig. 2.6)**. Electrophoretic separation is typically performed using fused silica capillaries with an ID of 10 to 75 µm, an OD of 375 µm and a length of 50 to 100 cm. The fused silica capillary is usually conditioned by flushing it with 0.1 M hydrochloric acid, followed by water, a 0.1 M sodium hydroxide solution, water and eventually the buffer solution. The sample can either be introduced hydrodynamically, by overpressure, or electrophoretically by placing the capillary inlet into the sample vial. After the sample introduction the capillary is placed back into the buffer reservoir and electric field (E) is applied. Due to the electric field buffer the sample immigrates through the capillary according to their electrophoretic mobility. Voltages up to 30 kV are used in CE. The various migration velocities of components cause a separation. Components are detected time resolved by the detector. The signal is sent to a computer where it is displayed. The output is called electropherogramm. When an electric field is applied to a fused silica capillary a volumetric flow occurs. This flow is called electroosmotic flow (EOF). Neutral analytes cannot be separated with conventional CE and will migrate with the EOF. In contrast to GC and HPLC, CE does not need expensive separation columns. Conditions are changed by changing the buffer. Chiral separation can be achieved by changing the buffer solution too. Neutral components, on the other hand, can be separated using a sodium dodecyl sulfate buffer forming micelles. The neutral components stick to the micelles and can be separated. Sensitive detection of the separated analytes is difficult, as only very little sample amounts can be analyzed at a given time. UV/VIS detectors are commonly used in commercial CE systems, although they

have approximately a 100 times lower detection limit compared to HPLC.[68] Mass spectrometry seems to be very suitable for interfacing with CE. Unfortunately, interfacing CE with MS has to deal with high buffer concentrations and unstable electrospray. An alternative for a sheathless CE-MS interface is presented in **Chapter 5.** This novel interface offers a very robust method to interface CE with MS incorporating a miniaturized flowing atmospheric pressure afterglow ionization source.

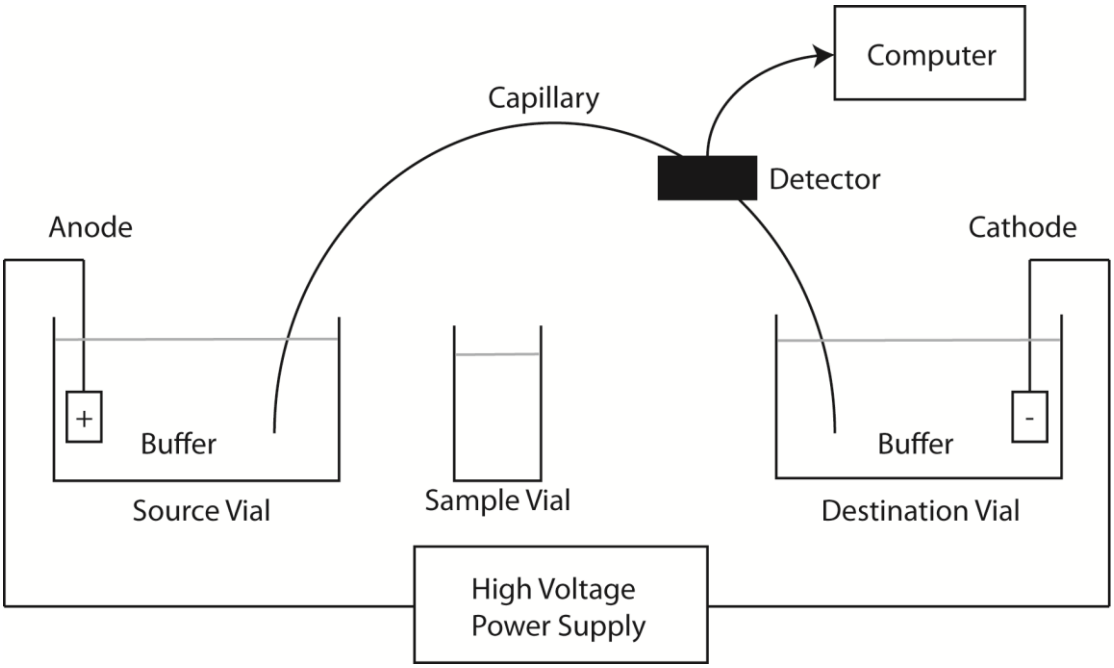

Figure 2.6: Schematic illustration of a capillary electrophoresis system. The main components are the two electrolyte reservoirs, sample container, high voltage power supply, capillary and detector.

2.4 Sampling methods

2.4.1 Solid sorbent sampling

Tubes containing solid sorbents are used to chemically adsorb contaminants in the air by drawing a small airflow through it. This sampling technique is commonly used to collect VOCs as well as semi volatile organic compounds including polycyclic aromatic hydrocarbons (PAHs). There are numerous customized sorbent types available, which are each optimized for a particular chemical class. It is important to know the exact flow rate of the aspirated air, as it needed in order to being able to calculate the concentrations of the contaminants. After the adsorption, the sample tube is closed and analyzed

in an analytical chemistry laboratory. Desorption of the air contaminants is usually done by extraction with a low volatility solvent. For nonpolar sorbent material carbon disulfide is used and for polar sorbent material methanol is often used. This method is an offline sampling method, which was used to sample contaminants in **Chapter 4** and **7**.

2.4.2 Impinger sampling

One way to sample airborne contaminants can be sampled using liquid impingers. Contaminants are usually dissolved into an aqueous solution as sample air is bubbled through water. Impinger sampling was historically used for workplace monitoring of contaminants. Although many alternative methods exist for ambient/indoor air monitoring, impinger sampling is still used in industry. An impinger was used to sample bovine serum albumin in **Chapter 7**.

2.4.3 Online sampling

Several attempts to circumvent offline sampling were done in this thesis (see **Chapter 3** and **6**). As it is not known what kind of products should be expected in the exhaust of the PAP. Highly reactive degradation products could be formed passing through the PAP. These could react with the sorbent material of the solid sorbet sampling. This would result in the problem, that those products cannot be desorbed anymore in an extraction step. Directly interfacing the PAP exhaust with a mass spectrometer is thought to circumvent this problem.

Chapter 3

Degradation of volatile organic compounds in a non-thermal plasma air purifier

This chapter is adapted from:

Schmid, S.; Jecklin, M. C.; Zenobi, R., Degradation of volatile organic compounds in a non-thermal plasma air purifier. Chemosphere **2010**, *79*, (2) 124-130.

3.1 Abstract

The degradation of volatile organic compounds in a commercially available non-thermal plasma based air purifying system was investigated. Several studies exist that interrogate the degradation of VOCs in closed air systems using a non-thermal plasma combined with a heterogeneous catalyst. For the first time, however, our study was performed under realistic conditions (normal indoor air, 297.5 K and 12.5 g m^{-3} water content) on an open system, in the absence of an auxiliary catalyst, and using standard operating air flow rates (up to 320 L min^{-1}). Cyclohexene, benzene, toluene, ethylbenzene and the xylene isomers were nebulized and guided through the plasma air purifier. The degradation products were trapped by activated charcoal tubes or silica gel tubes, and analyzed using gas chromatography mass spectrometry. Degradation efficiencies of 11±1.6% for cyclohexene, < 2% for benzene, 11±2.4% for toluene, 3±1% for ethylbenzene, 2±1% for σ-xylene, and 3±0.4% for m-/ρ-xylene were found. A fairly wide range of degradation products could be identified. On both trapping media, various oxidized species such as alcohols, aldehydes, ketones and one epoxide were observed. The formation of adipaldehyde from nebulized cyclohexene clearly indicates an ozonolysis reaction. Other degradation products observed suggests reactions with OH radicals. We propose that mostly ozone and OH radicals are responsible for the degradation of organic molecules in the plasma air purifier.

3.2 Introduction

Volatile organic compounds (VOCs) present in emission gases have received increased attention in recent years. Contaminated air can contain significant amounts of these components, and in many situations needs to be cleaned/purified since some VOCs are carcinogens, can cause allergic reactions, headaches, eye, nose, and throat irritation, and even concentration problems.[3, 10] Benzene, toluene, ethylbenzene and the xylene isomers (BTEX) are the most cited VOC contaminants in the environment due to emissions from burnt fossil fuel, the semiconductor industry, agricultural effluents, plastics and cleaning products.[69-72] Since in indoor environments, VOCs are protected from sunlight and oxidizing species, and the natural turnover rate is very low, such contaminates can concentrate and become even more problematic.[73-75] Therefore it is a major public health concern to remove VOCs from the air. One very traditional method is the use of activated charcoal to adsorb VOCs.[76] Although this procedure is very effective, activated charcoal is quite an expensive material and has to be regenerated by a thermal process, in which the VOCs are oxidized at around 973-1173 K.[25, 71]

An interesting, novel alternative is the use of a non-thermal plasma (NTP), which can be generated at room temperature, at atmospheric pressure, and without an additional plasma gas. A NTP is a non-equilibrium plasma where free electrons as well as highly excited reactive atoms, ions, and molecules are created mostly from air constituents. Ions and molecules can either fragment and degrade into new, smaller species or lead to the formation of activated chemical species (e.g. $\cdot O$, $\cdot O_2$, $\cdot OH$ radicals, and O_3) which can undergo further reactions with neutrals (e.g. VOCs).[12]

Roland *et al.*[14] oxidized organic air pollutants (toluene, phenol and methyl tert-butyl ether) in an NTP using ferroelectrically and catalytically active materials. They concluded that the oxidation process is mainly due to a direct or indirect reaction of ozone. Other authors have presented the decomposition of toluene in a catalytic reactor with a dielectric barrier discharge at atmospheric pressure.[25, 26] Using MnO_X and CoO_X catalysts, up to 80% efficiency to total oxidation (CO_2 and H_2O) was achieved. Kohno *et al.*[70] used a capillary tube discharge reactor to decompose typical VOCs from the semiconductor industry

with a destruction efficiency of up to 90%. Van Durme *et al.*[74] present several degradation products and possible reaction pathways of toluene in a positive corona discharge reactor. It has recently been shown that it is even possible to achieve complete decomposition of VOCs using thermal plasmas.[77]

The goal of this work was to study a commercially available plasma air purifier (PAP, Askokoro, Switzerland), which is based on an NTP and works with a high AC voltage (3 to 8 kV) at 50 Hz. Such air purifier systems are mainly considered for the purification of indoor air and for destroying VOCs as well as living species such as microorganism or viruses. We investigated how the PAP degrades organic pollutants and which chemical reactions are responsible for the decomposition of the contaminant molecules. To reduce the complexity and to establish the reaction mechanisms operating in the PAP, our studies were carried out with small, volatile, organic molecules, cyclohexene and BTEX. The degradation products of these typical VOCs clearly indicate that oxidative reactions must be responsible for the decomposition.

3.3 Experimental section

3.3.1 Air purifying system.

The experimental setup of the experimental air purifying system is shown in **fig. 3.1a**. The air flow is from left to right and the first component (1) is a HEPA (filter class H13, camfil, Reinfeld, Germany) filter which purifies the air before it enters the system to make sure that no contamination from the outside is collected. Component (2) is the fan (Vortice Lineo 125 V0, VORTICE, Tribiano, Italy) generating an air flow which is continuously adjustable from 0 to 360 $m^3\ h^{-1}$. An interface (3) made of polyvinyl chloride (PVC), connects the fan (inner diameter (ID) 125 mm) to the PAP (ID 150.6 mm). The tube in the middle of the system with the two windows is a 40 cm long PVC tube (5) with an ID of 150.6 mm which contains two inlets: one for the nitrogen gas to operate the nebulizer, and the second one to a motor driven syringe pump which provides the sample solution for the nebulizer. The nebulizer (4) itself is located exactly in the middle of the system to generate the best homogeneous nebulization possible. The two windows allow observing and adjusting the nebulizer spray for

optimizing it. The water content of the incoming air was continuously measured with a hygrometer (Extech 445815, Conrad, Switzerland).

Fig. 3.**1b** shows an exploded view of the PAP. Dimensions and technical specifications are: diameter 160 mm, length 180 mm; overall weight 10.5 kg; materials of construction: nickel, lead, copper, PVC and poly-(methyl-methacrylate); power consumption: 17.3 W (root-mean-square); power supply: 230 V, 50 Hz. An operating voltage of 8 kV was used to maximize the degradation efficiency; the normal recommended operating voltage is 6.1 kV, resulting in much less O_3 production. The plasma is generated in normal air without any auxiliary gas. The air velocity in the system is measured with an anemometer (PCE group, Germany) before and after the PAP. The sampling funnel (C) with an

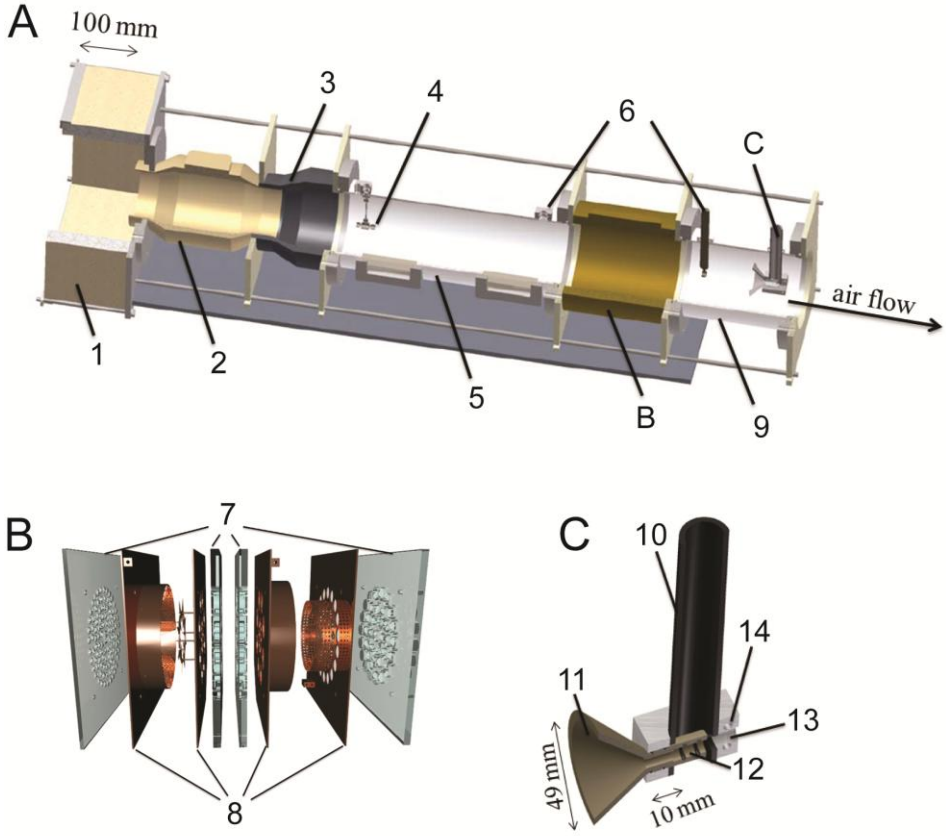

Figure 3.1: (A) Schematic of the air purifying system setup. 1, HEPA filter; 2, Continuously adjustable fan (0 to 360 m3 h-1); 3, polyvinyl chloride (PVC) interface; 4, Nebulizer; 5, 400 mm long PVC tube with two Plexiglas windows; 6, Holes for measuring the air velocity with an anemometer; 7, 200 mm long PVC tube; 9, PVC tube connected with a funnel for the collection of the compounds after the PAP. (B) Exploded view of the PAP (Askokoro, Switzerland). 8, Specially designed copper plates where AC high voltage is applied; 9, Plexiglas spacers. (C) Schematic of the sampling system. 10, PVC holder; 11, poly(tetrafluorethylene) (PTFE) funnel OD 52.5 mm and ID 49 mm; 12, O-ring seals allow the connection with a 6-mm ID PTFE tube; 13, PTFE tube with an ID of 6 mm connected to the sampling tubes; 14, Aluminum block to fix the PTFE funnel with the PVC tube.

ID of 52.5 mm is located exactly in the middle of the 20 cm long tube at the end and will be discussed later. The other end of the sampling device is connected to adsorbing tubes which are coupled to a vacuum pump (DIVAC membrane pump 2.2 L, Wexford, Ireland). The aspirated flow was measured with a flow meter and was varied between 0.1 and 3.5 L min^{-1} by using a pressure reducing valve. An ozone monitor (Model C-30ZK, Ecosensors, Netherlands) was placed after the air outlet of our setup (after No. 9 in **fig. 3.1a**) for ozone detection.

3.3.2 Sample introduction/nebulization

For sample nebulization a system similar to a sonic spray ionization source was constructed.[58] A fused silica capillary with an ID of 150 µm and an outer diameter (OD) of 375 µm was used for sample infusion. The capillary for the nebulizing gas had an ID of 530 µm and an OD of 700 µm. Both capillaries were sealed in a stainless steel T-piece (Swagelok) with polytetrafluoroethylene (PTFE) ferrules. A 1.5875 mm (1/16") SS tubing was used to deliver the nebulizing gas. This home-made nebulizer was fixed in the center of tube (4) (cf. **fig. 3.1a**). Nitrogen was used as nebulizer gas, and the flow rate was varied from 0.45-1.25 L min^{-1}. A syringe pump (model 4400-001, Harvard Apparatus, USA) was used for sample introduction. The settings of the syringe pump were the following: diameter, 14.57 mm; sample flow speed, 5 to 20 µL min^{-1}; target volume 1000 and 250 µL, respectively. The sample nebulization with this technique was found to be very reproducible (stable spray and good area coverage of the PAP) and the sample flow rate as well as the sampling time could simply be adjusted using a syringe pump. The usage of a syringe (1010 LTN 10 mL, HAMILTON, Boeckten, Switzerland) made of glass did not allow high sample flow rates (not higher than 500 µL min^{-1}) due to the high back pressure from the capillary (ID 150 µm). With a 0.2 g L^{-1} solution of brilliant of blue R (Bio-Rad Laboratories, USA) the optimum spray distance was experimentally determined. By spraying the blue dye solution onto a white paper, an optimum distance of 40 cm was found, at which the whole cross section of the PAP was covered.

3.3.3 Sampling approach

The sampling funnel (**fig. 3.1c**) was placed 150 mm behind the PAP and was fixed inside the system by a PVC holder. The funnel (11) was made of PTFE and was connected to the PVC holder (10) inside an aluminum block (14) via an O-ring seal (12) that allows a tight connection with a PTFE tube (13, ID 6 mm, which is exactly the inner diameter of the funnel). This is to avoid any gaps and edges, where sample could accumulate. The other end of this PTFE tube (ID 6 mm) is connected to trapping media in tubes, which are coupled to the high vacuum pump. Two types of adsorbents were used: (i) charcoal type G (750 mg sampling medium and 250 mg control medium) and (ii) silica gel type G sampling tubes (1100 mg sampling medium and 450 mg control medium. The sampling efficiency such sampling tubes can be shown to be nearly 100% using the control layer (0.1 L min^{-1} aspiration flow). Also, the manufacturer guarantees that the pressure drop induced by the sampling tube is less than 3 kPa (Dräger safety AG & Co. KGaA, Germany). Charcoal tubes are often used to collect VOCs and were used throughout in this work.[78] Although activated charcoal types are usually used to collect BTEX,[79] silica gel can also be used to collect possible polar substances formed during the degradation processes in the activated PAP. After each VOC experiment the fan was switched on for around 8 h, usually overnight, to minimize cross contamination.

3.3.4 Materials and Methods

Benzene (> 99.7%, Sigma-Aldrich, Switzerland), toluene (> 99.7%, Fluka, Switzerland), cyclohexene p.a. (Fluka, Switzerland), ethyl benzene p.a., and xylene isomers p.a. (mixture, house stock), chloroform (> 99.7%, Fluka, Switzerland) and carbon disulfide for analysis (Merck, Darmstadt, Germany) were used. The sample flow rate was either 5 µL min^{-1} (corresponding concentration ~$1.5*10^{-7}$ M), 10 µL min^{-1} (~$3.0*10^{-7}$ M), or 15 µL min^{-1} (~$4.5*10^{-7}$ M); a nebulizing gas flow rate of 1.0 L min^{-1} was used during all measurements. To be able to see degradation products 2.0 mL of BTEX as well as cyclohexene were studied in the PAP using a sample flow rate of 5 µL min^{-1}. For every experiment a negative control experiment with the PAP switched off was done.

To evaluate the efficiency of the PAP, two experiments were performed for all compounds: a negative control experiment, and an experiment with activated air purifier. 250 µL of cyclohexene and 500 µL of BTEX, respectively, were nebulized for this purpose. Charcoal type G sampling tubes were used to adsorb the VOCs after the activated PAP as these are optimal for the collection of nonpolar substances. Cumene p. a. (Fluka, Switzerland) was used as an internal standard and was added to the desorption solvent in a ratio of 1 to 5000.

For desorption of the sample from the adsorbents, the tubes were broken very carefully, and the sample layer (750 mg activated charcoal, 1100 mg silica gel, respectively) was transferred into a 3.0 mL glass vial with screw cap. 2.0 mL carbon disulfide (CS_2, cooled at 253 K to avoid boiling of CS_2 before the vial is closed) in case of the charcoal tubes, and chloroform in case of the silica gel tubes were pipetted into the vial, which was closed immediately. The vials were then put into an ultra-sonic bath for 30 min to desorb the trapped compounds. The resulting solution was first centrifuged to get rid of any remaining particles. 200 µL of the clear supernatant were then transferred into vials. 1.0 µL of each sample was afterwards injected into gas chromatography mass spectrometry apparatus (GS-MS) using pulsed splitless injection (100 kPa injection pulse pressure until 0.5 min).

3.3.5 Sample analysis by GC-MS

Analysis of the samples was done with two different GC-MS systems mainly to save time. The first system was an Agilent Technologies 7890A GC coupled with a 5975 inert mass selective detector (Triple-Axis). A capillary column HP-5-MS (30 m x 0.25 mm x 0.25 µm) was used with a He flow of 1.0 mL min^{-1} and a pressure of 50 kPa. The separation was done with a temperature program starting at 308 K, holding this temperature for 10 min, increasing to 473 K with a temperature gradient of 20 K min^{-1} and holding at 473 K for 1.75 min. The total time was thus 20 min. The second system was a HP 6890 GC with a HP 5973 MSD equipped with an Optima-5-MS column (50 m x 0.20 mm x 0.35 µm, Macherey-Nagel, Düren, Germany) and an auto sampler model GERSTEL. The column was used with a He flow of 5.7 mL min^{-1} and a pressure of 194.3 kPa. Separation was achieved using a temperatur program

starting with 323 K, holding this temperature for 5 min, increasing to 473 K with a temperature gradient of 10 K min^{-1}, which allowed measurements within 22 min. The temperature settings for the two systems were the following: inlet 573 K, MS source 503 K, MS Quad 423 K and Aux-2 temperature 553 K.

Both GC-MS systems were equipped with the mass spectral reference library from the National Institute of Standards and Technology (NIST version 2.0a). Only substances with a confidence > 50% for identification via the NIST library were considered for evaluation and discussion of the plasma degradation process. The decomposition efficiencies of BTEX and cyclohexene were measured quantitatively using cumene as internal standard, whereas the degradation products were measured qualitatively and afterwards identified with the NIST database. Limits of detection were not determined but are depending on the instrumentation, in the range of 0.5 to 0.8 µg VOC per sample.[79]

3.4 Results and Discussion

3.4.1 Degradation efficiency of the PAP

First, a mixture of BTEX (1:1:1:1) as well as cyclohexene was measured with and without the PAP activated to obtain information about the degradation efficiency of the plasma air purifier. Three independent experiments of BTEX and cyclohexene were performed. Low compound loadings were used for these quantitative measurements, in order to not saturate the trapping media; this is, however, not optimal for detecting small quantities of degradation products. 50 µL of BTEX and 250 µL cyclohexene respectively delivered with a sample flow rate of 5 µL min^{-1} (were nebulized with 1.0 L min^{-1} nitrogen. The air velocity, monitored with the anemometer after the PAP (B in **fig. 3.1a**), was adjusted to 0.3 m s^{-1}, which corresponds to 16 ppb cyclohexene when a 5 µL min^{-1} infusion rate was used. When turned on, the PAP was operated at a voltage of 8.0 kV. Higher voltages were not used, because breakdown occurs in the PAP and a spark bridges the gap between the two electrodes where the high voltage is applied. The degradation efficiencies of BTEX and cyclohexene are shown in **fig. 3.2**. The efficiency was calculated by normalizing the observed signal area using the internal standard (cumene). The intensity observed for the negative control

experiment was then taken as 100%. The difference compared to the negative control was assigned to degraded analyte. A much higher degradation efficiency of the plasma was observed for cyclohexene and toluene (around 10%) than for the other five substances. Very similar degradation efficiencies were obtained for ethyl benzene and the xylene isomers. Almost no degradation was measured for benzene. This result shows that the attack of radicals only takes place on the side chains of the aromatic compounds, and not directly on a carbon atom in the aromatic system. When considering the low power consumption (17.3 W), the degradation efficiencies are reasonable. However, degradation efficiencies of up to 70-100% using NTP (power consumption between 4 and 8 W) combined with heterogeneous catalysts have been reported.[14, 22, 25, 26, 70, 74] A major drawback of such catalysts is that they can easily become deactivated by impurities and by the accumulation of solid byproducts[77] such that they have to be replaced from time to time. This is not necessary when using the PAP. Moreover, in the references cited above, much lower air flow rates were used compared to our study: Roland *et al.*[14] and Holzer *et al.*[22] worked with an air flow rate of 0.1 L min^{-1}, Subrahmanyam et al.[28, 29] used 0.5 L min^{-1}, Kohno et al.[70] 9 L min^{-1} and Van Durme *et al.*[74] 10 L min^{-1}. In the work presented here an air flow rate of 320 L min^{-1} was used, since this is in the range of the actual air velocity (0.3 to 3 m s^{-1}) in a practical PAP usage scenario. Of course, the dwell time of the analyte molecules in the plasma region is a lot shorter in this case (< 0.6 s compared to, for example, Holzer *et al.*[22] with a dwell time of ~20 s), which also leads to reduced degradation efficiency.

The degradation efficiency of the PAP was measured for two different air flow rates (320 and 640 L min^{-1}). With air flow rates lower than 640 L min^{-1} higher efficiencies could indeed be detected (increase from 8 to 11%). It has been demonstrated that the energy density (power per volume) of a plasma reactor is indirectly proportional to the air flow rate which leads to a decrease in the degradation efficiency.[26] Since 320 L min^{-1} already is at the lower limit of the standard operating flow rates of the PAP suggested by the manufacturer, this flow rate was used throughout all our experiments.

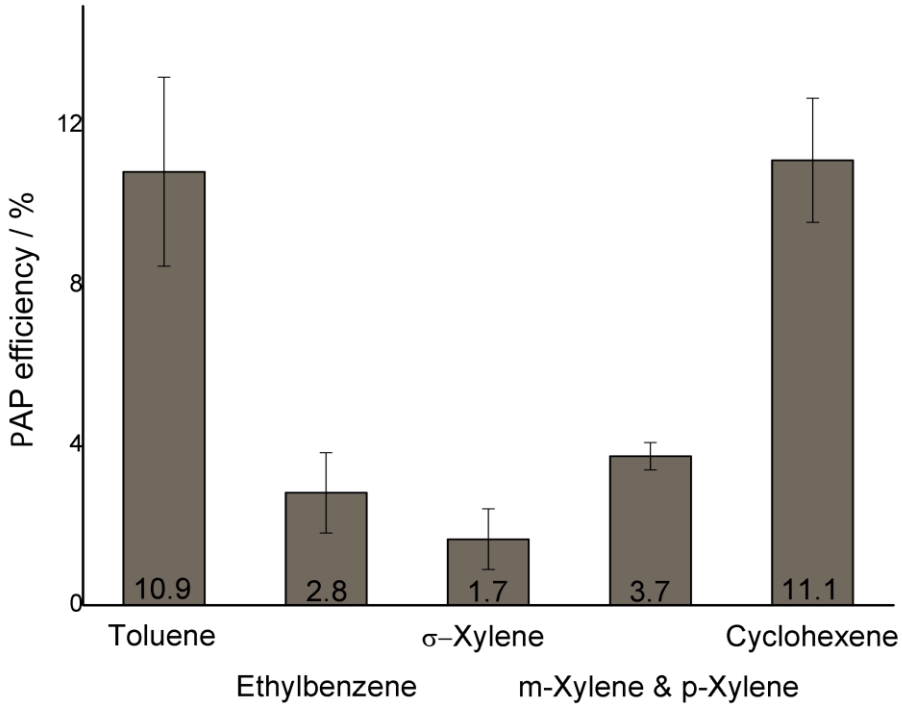

Figure 3.2: Efficiency of the PAP for toluene, ethylbenzene, the xylene isomeres and cyclohexene (n=3). Collection was done on activated charcoal tubes. Carbon disulfide was used for desorption. System settings: 500 µL sample, flow speed, 5 µL min-1; air flow, 320 L min-1; PAP, 8.0 kV 50 Hz. An Agilent GC-MS 7890A system was used for sample analysis.

The degradation efficiency of the PAP was also measured as a function of the analyte concentration ($1.5x10^{-7}$, $3.1x10^{-7}$ and $4.6x10^{-7}$ M). Different sample concentrations were generated by using different sample infusion flow rates (5, 10 and 15 µL min^{-1}), using 250 µL of each VOC. One experiment with activated PAP and one negative control was carried out for each flow rate. As described above, the analyte amount sampled in the negative control was set to 100% and based on this, the degradation efficiency of the PAP was calculated. For cyclohexene, the highest PAP efficiency, 11%, was found at the lowest sample concentration of $1.5x10^{-7}$ M. For a sample concentration of $4.6x10^{-7}$ M a degradation efficiency of only 4% was observed for cyclohexene. We hypothesize that not enough active species are generated to degrade all molecules in the PAP in this short time interval. Increasing the concentration of the VOCs without increasing the concentration of the active species in the PAP should lead to a decreased degradation efficiency. Increasing the applied voltage to increase the efficiency and the amount of active species, however, leads to electrical

breakdown, as mentioned above. With a sample concentration of $1.5x10^{-7}$ M, the limit of detection was nearly reached. Moreover, further decrease of the sample concentration would lead to unfeasibly long sampling times. Furthermore, the main goal of this work is to study the mechanism behind the degradation of the molecules using the PAP.

3.5 Degradation mechanism

For establishing the degradation mechanism, it is very important to identify as many products as possible. Therefore, a much higher load of reactants were used, in order to nearly saturate the trapping media. In our first experiment ethylbenzene was nebulized, in order to check the suitability of our sampling technique. A total volume of 2000 µL was used with a sample flow rate of 5 µL min^{-1}, corresponding to a concentration of $1.3x10^{-7}$ M. Adsorption was achieved using silica gel tubes.

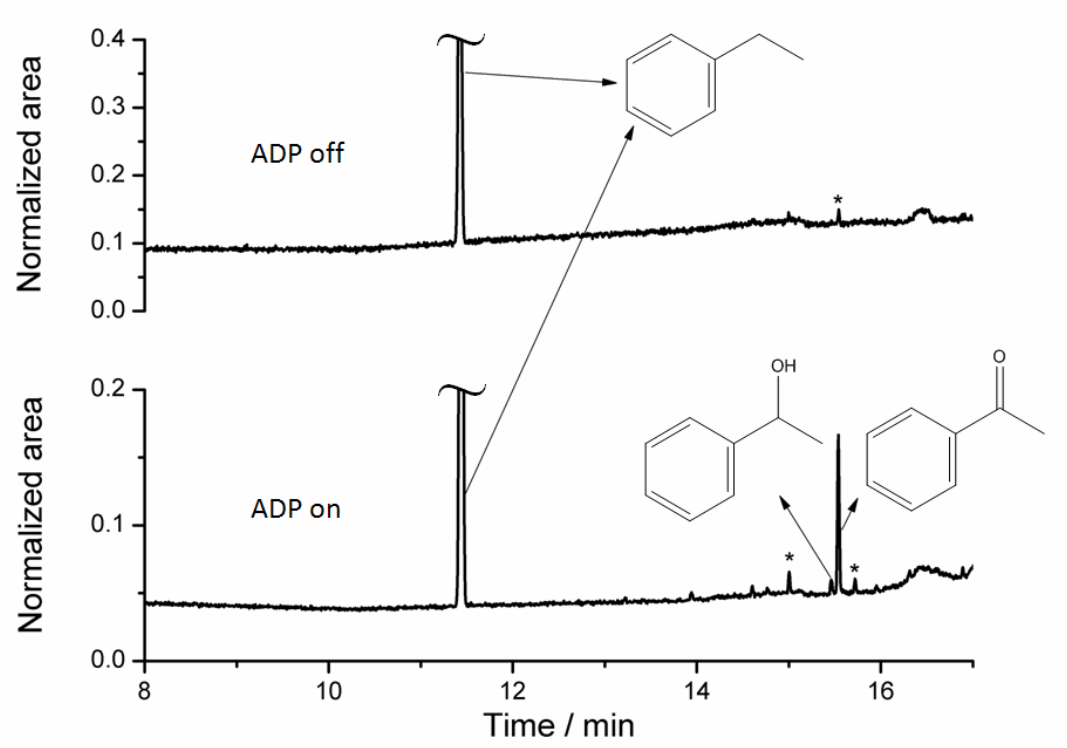

Figure 3.3: GC-MS chromatograms recorded with the Agilent GC-MS 7890A system. Adsorption was done on silicagel tubes and desorption with chloroform. System settings: 2.0 mL ethylbenzene, flow speed, 5 µL min^{-1}; air flow, 320 L min^{-1}; PAP, 8.0 kV 50 Hz. With the PAP activated 1-phenylethanol, acetophenone were identified as degradation products with a confident of more than 50% using NIST library. Signals marked with an asterisk (*) correspond to compounds with < 50% confidence in the NIST library and to impurities.

The GC-MS chromatograms of this experiment with and without activated PAP are shown in **fig. 3.3** substances with a confidence of < 50% in the NIST library and impurities were labeled with an asterisk (*). Two degradation products could be identified for ethylbenzene with a confidence of > 50% using the NIST library: 1-phenylethanol and acetophenone. These two products almost co-elute but are clearly distinguishable by GC-MS and indicate an oxidative process, most likely involving OH radicals. The humidity during our experiments was determined to be in the 10 to 14 g m^{-3} range, i.e., the formation of OH radicals due to reaction of H_2O with exited NO_2 is very probable.[80] Moreover, processes due to collisions of H_2O with electrons, such as dissociative excitation of H_2O or dissociative electron attachment can also lead to OH radical formation.[81, 82] An H-atom abstraction from the C-H bond of the ethyl group induced by OH radicals, followed by further reaction with O_2 catalyzed by NO has been reported to be a possible reaction of ethylbenzene to acetophenone.[83] It is very likely that this reaction occurred in the PAP. Based on the work by Eliasson and Kogelschatz,[12] we assume an electron transfer from the plasma region to the air molecules (which are in a huge excess compared to the analyte), to form reactive species such as $^{\bullet}O$, $^{\bullet}O_2$, O_3, $^{\bullet}OH$, which then react with the analyte molecules.

3.5.1 Cyclohexene – Sampling with activated charcoal tubes

Among all VOCs investigated, the highest degradation (cf. **fig. 3.2**) and also the highest variety of degradations products were observed for cyclohexene. Activated charcoal tubes were used in this experiment to adsorb nonpolar products created by the PAP. The chromatogram of the products from degradation of cyclohexene is shown in **fig. 4a**. One drawback of the sampling method used is that highly volatile substances as well as H_20 and CO_X cannot be detected due to the desorption solvent (CS_2) which itself leads to a huge injection signal. Therefore, information is lost about very low molecular weight degradation products. Again only compounds with a confidence of > 50% were taken into account. Non-degraded cyclohexene is observed after some solvent impurities (peak no. 1 in **fig. 3.4a**). The compounds identified are listed in **table 1**, together with the structures, retention times, and confidences. Surprisingly no major nitrogen containing degradation products were observed.

Although there were some tentative identification, their matches with the NIST library were rather poor, and they fell through our selection criterion. Compound 5 was identified with a high confidence (78.9%) as cyclohex-2-enone, which is also a

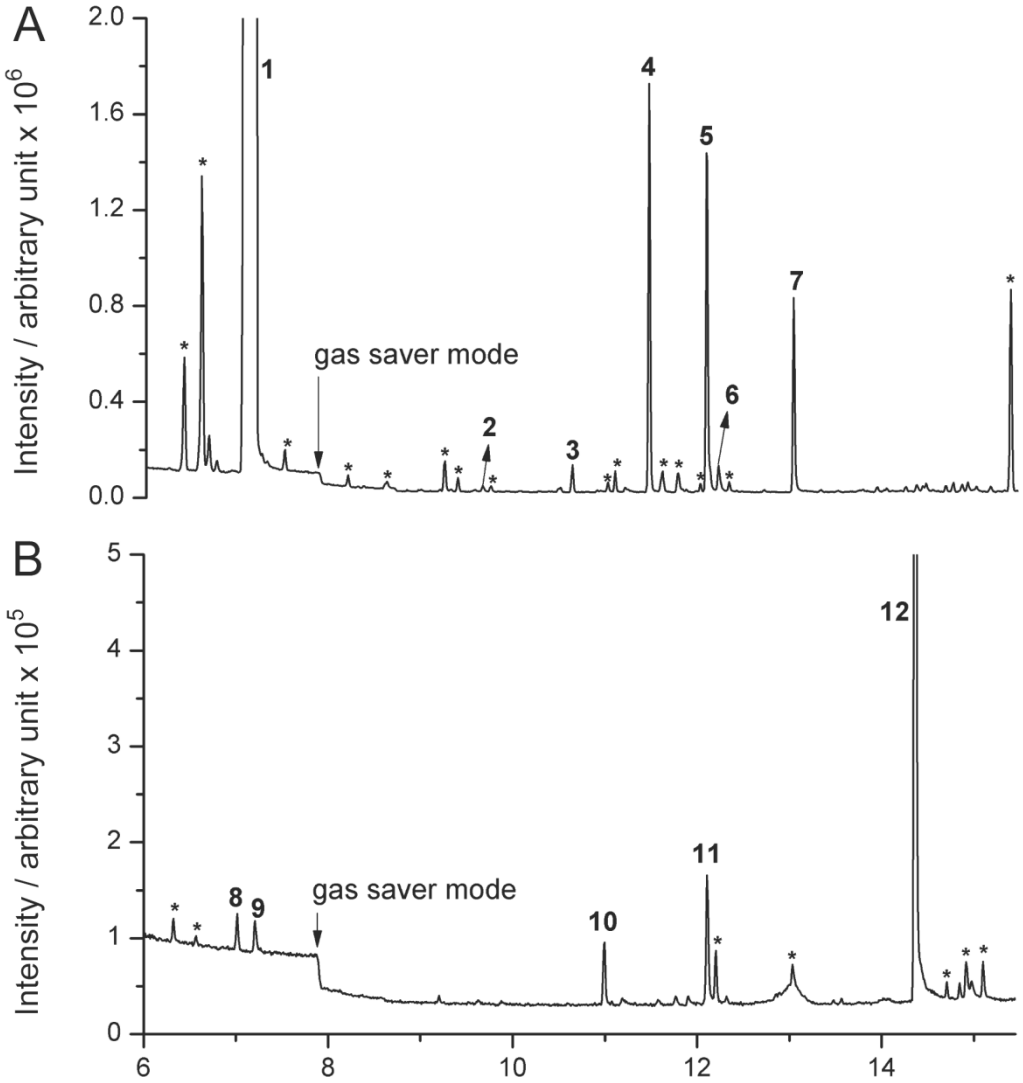

Figure 3.4: Chromatogram of PAP decomposed cyclohexene. Signals marked with an asterisk (*) correspond to compounds with < 50% confidence in the NIST library and to impurities. System settings: 2.000 mL cyclohexene, flow 5 µL min^{-1}; air flow, 320 L min^{-1}; PAP, 8.0 kV 50 Hz. (A) Adsorption was accomplished with charcoal tubes. Carbon disulfide was used for desorption. 1, cyclohexene; 2, cyclopentanone; 3, cyclopentanecarbaldehyde; 4, 7-oxabicyclo[4.1.0]heptane; 5, cyclohex-2-enol; 6, cyclohex-2-enone; 7, 2-methylcyclopentanone. (B) Adsorption was accomplished with silica gel tubes. 8, ethylidenecyclobutane; 9, 6.8-dioxabicyclo[3.2.1]octan-3-ol; 10, cyclopentanecarbaldehyde; 11, 2-ethylbut-3-enal; 12, adipaldehyde.

typical product of a reaction with OH radicals. Compound 4 strongly indicates a reaction with ozone for the formation of oxiranes from ozone reacting with

isoprene, 1,3-butadiene and α-pinene.[84] α-pinene is structurally related to cyclohexene, which suggests this process to be feasible. Furthermore, it is well known that ozone is produced in NTPs in a three-body collision, with the third collision partner being O_2, O_3, O, N_2 or H_2O.[12, 24, 74] Moreover, one of the first NTP reactors was built specifically for generating ozone.[12] According to the literature, this reaction occurs in a few microseconds. However, even during such a short time other competing reactions like the formation of O_2 from O and O_3 are possible. We measured the ozone level in our setup in the exhaust air (after No. 9 in **fig. 3.1a**) using the ozone monitor and found concentrations up to ~1 ppm when a voltage of 8.0 kV was applied. The oxidized species found (cf. **table 3.1**), together with the quite high ozone levels measured clearly support an oxidative reaction mechanism for the PAP.

3.5.2 Cyclohexene – Sampling with silica gel tubes

Silica gel tubes were used with the aim to collect more polar components of the degraded cyclohexene (**fig. 3.4b**). Like in the previous experiments, only the compounds identified with a confidence > 50% are considered (cf. **table 3.2**). All other components are labeled with an asterisk (*). Although only 11% of cyclohexene was degraded, it was not observed in the chromatogram, because it could not be adsorbed on the polar silica gel tubes. Neither cyclohexene nor adipaldehyde could be measured in the negative control. This shows that the degradation of cyclohexene neither occurs during adsorption nor during desorption, as no cyclohexene could be trapped using the silica gel tubes. The observed compounds must be generated by the PAP. Compound 12 (adipaldehyde) is of great interest as it is most likely a reaction product of the thermalized Criegee intermediate with water vapor, which has been described by Aschmann *et al.*[85] Moreover, Hatakeyama *et al.*[86] reported in their work that reaction of ozone with cyclohexene in air creates adipaldehyde as the main product. Conversely, Grosjean *et al.*[87] observed mainly pentanal in the reaction of cyclohexene with ozone in the gas phase. Most of the adipaldehyde produced in their experiments was thought to condense onto aerosol particles. Moreover, in subsequent reactions with OH radicals, they observed butanal, propanal, acetaldehyde and formaldehyde.

Table 3.1: Signals identified with > 50% confidence (according to the NIST library) in the chromatogram shown in Fig. 4 (cyclohexene sampled on activated charcoal tubes after activated PAP), along with their retention time, structure and name, and NIST matching quality.

Signal	Retention time [min]	Structure	NIST Match [%]
1	7.10	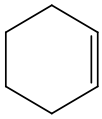 cyclohexene	75
2	9.65	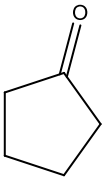 cyclopentaone	54.5
3	10.62	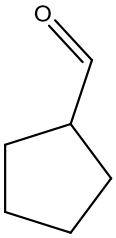 cyclopentanecarbaldehyde	50.2
4	11.45	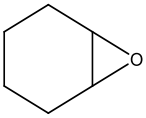 7-oxabicyclo[4.1.0]heptane	76
5	12.07	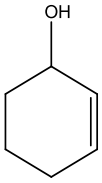 cyclohex-2-enol	78.9
6	12.20	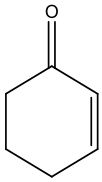 cyclohex-2-enone	77.2
7	13.02	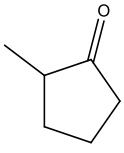 2-methylcyclopentone	52.1

In the work presented here, adipaldehyde was one of the most abundant products observed, whereas the other aldehydes mentioned by Hatakeyama *et al.*[86] and Grosjean *et al.*[87] were not observed. This observation can be due to different reasons: 1) the quite short dwell time of the analyte molecules in the plasma which may prevent the degraded species from undergoing further reaction, 2) the sampling technique which is not optimized for sampling very low molecular weight/high volatility products, or 3) simply the PAP setup with an open air flow, which differs from the controlled gas-phase reactions described in the literature.

A rough mass balance was also calculated by adding up signal areas for all degradation products found in the chromatograms of **fig. 3.4**. When normalizing the result by the cyclohexene signal area, which was taken as 89% (= 100% - 11%, see **fig. 3.2**), we found 2.0% products trapped on activated charcoal tubes (**fig. 3.4a**) and 1.9% on silica gel tubes (**fig. 3.4b**). This contrasts to the overall efficiency of 11% determined for degradation of cyclohexene (**fig. 3.2**). In other words, around 7% of the degradation products are not observed. These may either be too volatile for both adsorbing materials (for example, neither, H_2O nor CO_X can be observed with our analytical method), completely nonvolatile, some compounds may stick to the walls in the ventilation system (c.f. **fig. 3.1a**, especially items 5, 7, 8 and 9), or may be permanently trapped by the adsorbing materials. Nevertheless, around half of all degradation products could be collected and analyzed using adsorbing tubes. Moreover, most of the collected degradation products could be identified using the NIST library database.

Table 3.2: Signals identified with > 50% confidence (according to the NIST library) in the chromatogram shown in Fig. 5 (cyclohexene sampled on silica gel tubes after activated PAP), along with their retention time, structure and name, and NIST matching quality.

Signal	Retention time [min]	Structure	NIST Match [%]
8	7.02	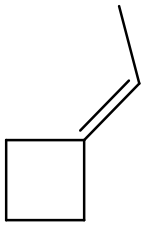 ethylidenecyclobutane	57.7
9	7.21	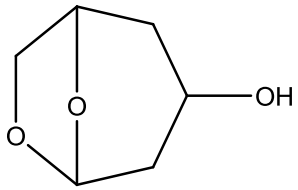 6.8-dioxabicyclo[3.2.1]octan-3-ol	61.2
10	10.99	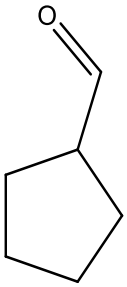 cyclopentanecarbaldehyde	61.8
11	12.11	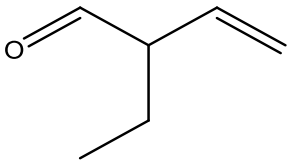 2-ethylbut-3-enal	66.1
12	14.37	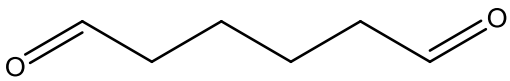 adipaldehyde	53.3

3.6 Conclusions

We investigated the degradation of VOCs in a non-thermal plasma air purifying system operated with realistic parameters. A degradation efficiency of 11% for a single pass was determined for cyclohexene; the lowest measured degradation efficiency was < 1% for benzene. Although much higher efficiencies have been found in model NTP reactors, previous results were often obtained in combination with a catalytic converter, and in all cases for much lower air flow rates. Considering the short residence times (<< 1 s) of the VOCs in the system studied here, the decomposition efficiencies compare favorably with previously reported values. In addition, the chemical degradation mechanism was studied. Our results suggest that oxidative reactions involving ozone and radicals play the dominant role in the degradation of the molecules using a PAP operated at conditions close to those of a standard air handling system. One of the most prominent reaction mechanisms is the ozonolysis reaction as indicated by the presence of adipaldehyde,[85] which was identified to form from degradation of cyclohexene. Another, probably even more important reaction mechanism involves OH radicals, as observed for the degradation products of ethylbenzene and cyclohexene. Atkinson[84] describes OH radicals as the dominating reactive species of the tropospheric removal process. It has also been described that an oxidation of hydrocarbons is OH-initiated and NO_X-catalyzed.[88] In other words, degradation processes similar to tropospheric reactions seem to occur in the PAP. For the first time, a wide range of degradation products could be identified due to the treatment of VOCs in air using a commercially available PAP system.

Chapter 4

Direct coupling of the PAP using mass spectrometry

4.1 Abstract

To discover if ozonolysis could be one of the main degradation pathways occurring in the PAP, ozone concentrations inside the plasma reactor were measured. To circumvent offline sampling using sorption material, several online measuring methods studying the fate of pollutants passing the PAP were tested. Ozone concentrations of 300 ppb were found in the PAP. Kinetic calculations showed that the decomposition of cyclohexene observed in **Chapter 3** cannot be explained by oxidation with ozone only. During our study on the mechanism behind molecular degradation in the PAP, we used a small version of the PAP. This “miniPAP” was found to excite/activate molecules, but does not lead to fragmentation or ionization. The "normal" PAP is capable of ionizing amines, as it generates a much stronger plasma. Four different peptides were studied in the miniPAP by coupling its exhaust directly to the mass spectrometer. Nebulization was accomplished by using a thermospray and the ionization of the miniPAP was achieved with a homemade miniaturized flowing atmospheric pressure afterglow plasma ion source. Using a sensor for VOC it was possible to quantitatively analyze cyclohexene over the range of $1x10^{-7}$ – $5x10^{-7}$ mol L^{-1}. It was also found that the smallest cyclohexene concentration is affected by the PAP when turned on. It seems that a certain amount of cyclohexene is degraded. However, it was not possible to quantify the exact amount as the ozone produced by the PAP interfered with the VOC detector.

4.2 Ozone measurements

The ozone concentration was measured as a function of distance from the PAP using an ozone sensor. The data were extrapolated to estimate the ozone concentration in the PAP. A concentration of 300 ppb ozone was calculated to exist in the PAP. In theory, this ozone concentration would result in only 0.5% cyclohexene degradation, compared to the 11% measured in our previous work. Formula (4.1) was used to calculate the amount of degraded cyclohexene in presence of 300 ppb of ozone. Consequently the result was: 0.5% degradation. However, a cyclohexene degradation of up to 11% with the PAP switched on was observed.

$$[A]_t = [A]_0 * (A_0 - B_0) * \frac{e^{(A_0 - B_0)kt}}{A_0 * e^{(A_0 - B_0)kt} - B_0} \quad (4.1)$$

Where A_0= concentration of cyclohexene at time = 0, B_0= concentration of ozone at time = 0, $[A]_t$= concentration of cyclohexene after a given time, t = time and k(T) = rate constant in L mol^{-1} s^{-1} at 298 K. The formula describes a second-order reaction.

A sample flow rate of 20 µL min^{-1} through the bench setup system resulted in a concentration of 0.989 * 10^6 mol L^{-1} cyclohexene. The time from entering the PAP until the adsorption was calculated to be 9.8 s. All necessary information for the calculation of the kinetic data were found in the NIST web book.[89]This suggests that the main degradation pathway of cyclohexene is not due to ozone alone, at least not for neutral molecules. Ionized molecules will generally react much faster than neutral molecules, i.e., a mechanism of plasma-induced ionization, followed by ozonolysis might be operative.

4.3 Small version of the PAP

One of the most complicated parts of this project was to sample the products after passage through the PAP, since it is not known what exactly will happen to the compounds that are introduced. Offline sampling of a mixture of unknown compounds is extremely difficult as those could react with the sampling material. Therefore, a direct coupling of mass spectrometry with the PAP seems to be an interesting option. Since the analysis of the biomolecules can

be done directly after the PAP, no sample collection step is needed, and the very difficult choice of a sampling medium is circumvented.

To study the degradation mechanism of biomolecules in the plasma, a thermospray nebulization combined with a miniaturized flowing atmospheric-pressure afterglow (miniFAPA) ion source was used. The thermospray (up to 500 °C N_2 desolvation gas) has the advantage of being much more efficient at bringing biomolecules into the gas phase compared to supersonic nebulization where no heating of the nebulizing gas takes place.[57] Although thermal decomposition is a potential risk when using a thermospray for nebulization, adsorption of the introduced sample on the PAP copper plates needs to be avoided as it would lead to cross contamination, and potentially resulting in a false "decrease" of the introduced sample. The better nebulized sample should help to avoid the precipitation of the biomolecules on the surface of the PAP (inefficient nebulization results in droplets, which will stick to the copper plates).

A small version of the PAP (miniPAP) was placed directly in front of our MS system (c.f. **fig. 4.1**) to allow online measurement.

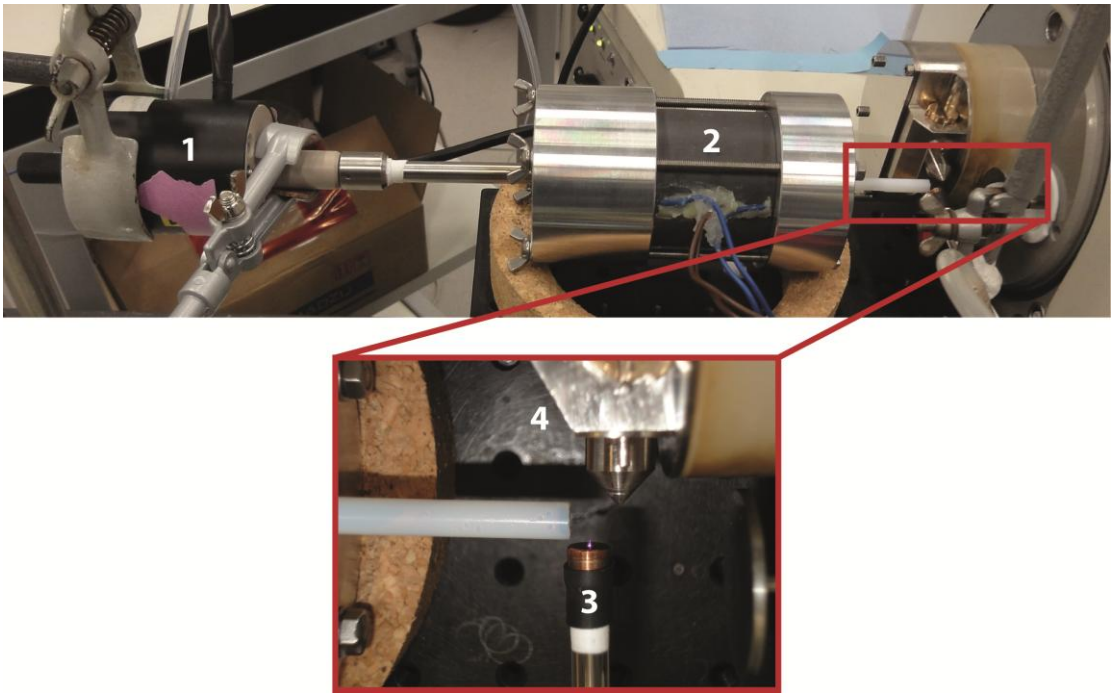

Figure 4.1: System used to study the miniPAP: 1, Thermospray; 2, miniPAP; 3, ionization source (miniFAPA); 4, QToF-MS cone.

To validate the functionality of this setup, trimethylpyridine was nebulized, guided through the miniPAP, and afterwards ionized with a

miniaturized flowing atmospheric pressure afterglow (FAPA). Switching on the mini PAP seemed to enhance the ionization efficiency (c.f. **fig 4.2**). Using a voltage higher than 2 kV was not possible, since a spark bridged the gap of electrodes in the miniPAP and an electrical breakdown occurred. Using only the mini PAP to ionize the trimethylpyridine showed no signal. In contrast, the "normal" PAP was capable of ionizing amines which is shown later in this chapter.

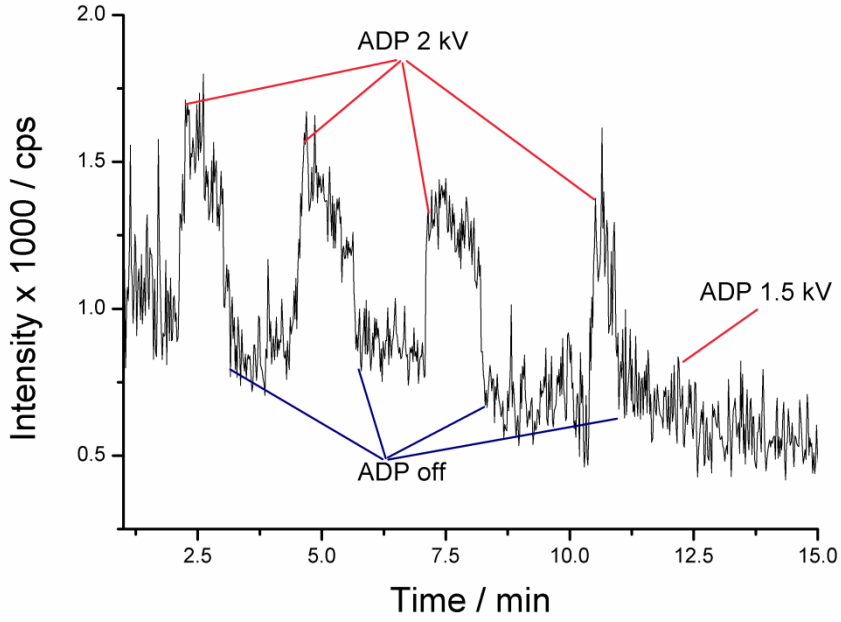

Figure 4.2: Trimethylpyridine (1 ppm in 75% MeOH : 25% H_2O) was sprayed with a sample flow rate of 5 µL min^{-1}. Ionization after the small PAP was accomplished using the miniFAPA ion source.

4.4 Degradation of four peptides by direct coupling of the miniPAP to the MS

The HPLC standard mixture of four peptides used in this work was purchased from Sigma Aldrich (0.5 mg Gly-Tyr (G3502) molecular weight (MW) 238.2, 0.5 mg Val-Tyr-Val (V8376) MW = 379.5, 0.5 mg Met-Enkephalin (M6638) MW = 573.7 and 0.5 mg Leu-Enkephalin (L9133) MW 555.6.

All separation experiments described in this **Chapter** were performed on an HPLC (SHIMADZU Model SCL-10A VP, Duisburg, Germany) equipped with a photo diode array (SPD-M10A VP) detector. The LC effluents were delivered by a LC-10AT VP pump, which was connected to a low pressure mixing valve (FCV-

10AL VP). The samples were loaded with an external manual sample injector (Rheodyne, Whitstable, UK) using a 20 µl loop. Method development was done off-line using the photo diode array (PDA) detector set to 220 nm. A flow rate of 1.0 mL min^{-1} was used, unless otherwise noted. The chromatographic separation of the peptide mix was accomplished with a Waters Symmetry300™ C_4 column (4.6x150mm, 3.5 µm, Waters, Milford, MA, USA) using the following method. Starting with 100% A, holding this ratio for 4 min, decreasing in 7 min to 70% A and finally holding this ratio again for 2 min (A = 5:95 acetonitrile/water containing 0.1% TFA; B= 75:25 acetonitrile/water containing 0.1% TFA). The HPLC was controlled by the CLASS-VP software (version 614_SP1). The outlet of the HPLC system was connected to a thermo spray (623 K), which was able to nebulize the complete solvent flow. The nebulized sample was guided through the mini PAP and afterwards ionized with the miniFAPA ion source. Mass spectrometric analysis was performed with a hybrid quadrupole time-of-flight mass spectrometer (Q-TOF Ultima; Waters/ Micromass Ltd., Manchester, UK) equipped with a Z-spray interface. The instrument was controlled by the MassLynx software (version 4.0). All measurements were performed in positive ion mode. The first experiment was performed with the miniPAP turned off, using a 50 µL min^{-1} peptide stock solution. **Fig. 4.3** clearly shows the four separated peptides. The entire signal area of each peptide was summed up and background subtracted. An identical experiment was performed with the miniPAP turned on (2.0 kV). The entire signal of each peptide was once again summed up and baseline subtracted.

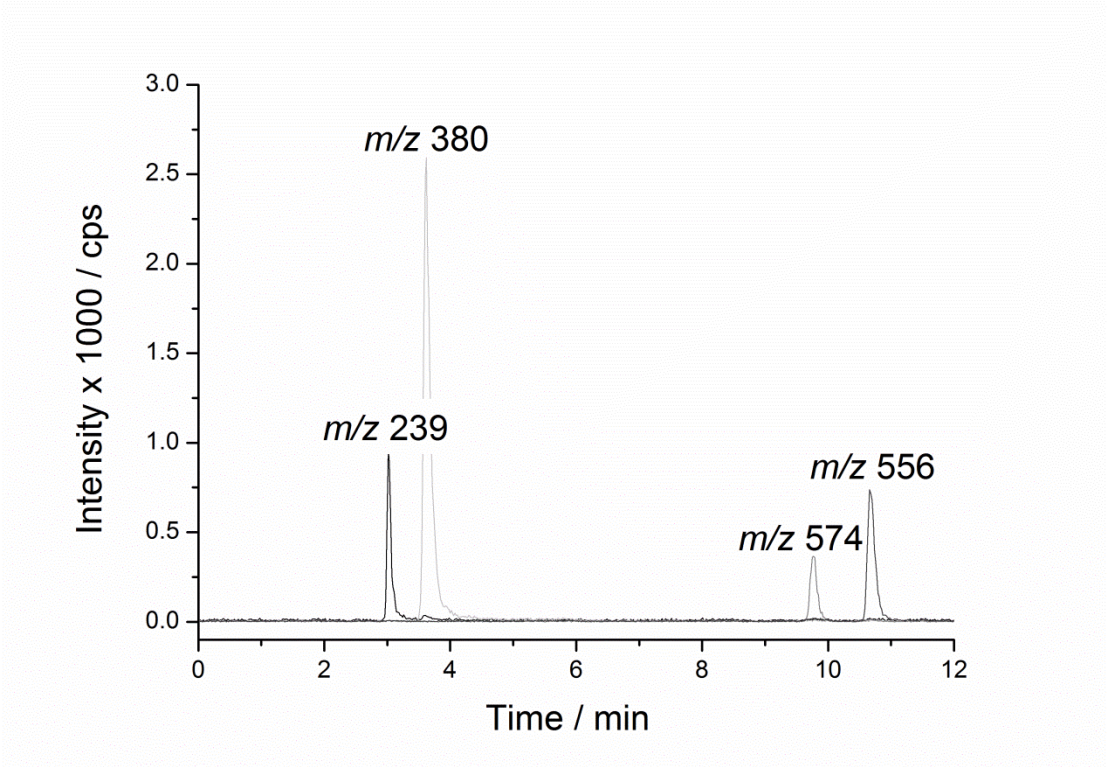

Figure 4.3: Chromatogram of the four separated peptides. 1, Gly-Tyr; 2, Val-Tyr-Val; 3, Met-Enkephalin; 4, Leu-Enkephalin. Injection volume, 20 µL; Flow rate, ~100 µL min^{-1}; Concentration, 50 µg mL^{-1}.

Comparing the results with the PAP switched on and off showed neither a decrease of the signal intensity nor any other new signals within the measured *m/z* range of 50 to 1250. Surprisingly, a small increase of all signal intensites could be observed witch the PAP switched on.

From these results, it can be concluded that the small version of the PAP does not degrade peptides. We assume that the applied voltage of 2.0 kV was not high enough to generate a plasma capable of destroying these biomolecules. However, the higher observed signal intensity shows us that the miniPAP does excite the molecules, making them easier for the miniFAPA to ionize.

4.5 Interfacing the PAP with a portable mini ion trap MS

The idea of this study was to bring a small mass spectrometer to the "big" PAP, which is not movable, for analysis of degradation products. 2-(2-aminoethyl)pyridine (M = 122.12 g mol-1) was nebulized and guided through the PAP (off) which was coupled to a portable handheld MS (Mini 10).[90] No signal could be observed (c.f. **fig. 4.4**). The same experiment was repeated with the

activated PAP (8.0 kV). Ionization of 2-(2-aminoethyl)pyridine could clearly be observed (c.f. **fig. 4.4**).

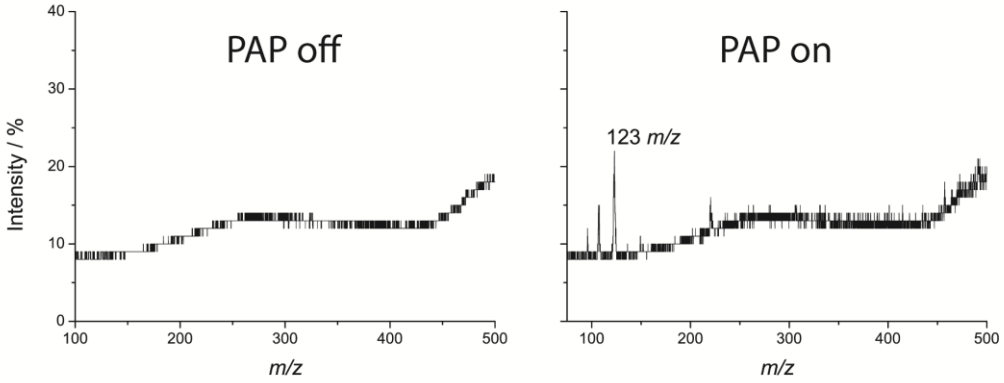

Figure 4.4: On the left mass spectrum of 2-(2-aminoethyl)pyridine, PAP switched off. On the right mass spectrum of 2-(2-Aminoethyl)pyridine, PAP switched on, 8.0 kV.

The experiment clearly shows that the "normal" PAP is able to ionize 2-(2-aminoethyl)pyridine while the mini PAP could not. The PAP was operated with a much higher voltage than the mini PAP, which is a likely explanation of why neither ionization nor degradation was observed using the mini PAP. It seems that the plasma generated in the mini PAP is simply not efficient enough to ionize or degrade any of the introduced compounds.

4.6 VOC measurements, Gas phase kinetics

The idea of this part of the project was (i) to measure VOC directly at various concentrations in our mock-up air purification system with selective sensors, and (ii) to use gas-phase kinetic data to model the observed degradation reactions. Thus the bulk of the work reported here deals with the calibration and characterization of the sensors. Kinetic data were taken from an online library.[91] The gas volume in the PAP was estimated to be 1 L.

The stability of the VOC sensor MiCS-5121 was monitored over a period of 22h, as shown in **fig. 4.5**. The response of the sensor is rather stable, except in the first 5 h where drifts can be observed. As soon as the PAP is switched on the fluctuation of the VOC detector becomes significantly higher, since the VOC sensor exhibits a cross-sensitivity to ozone.

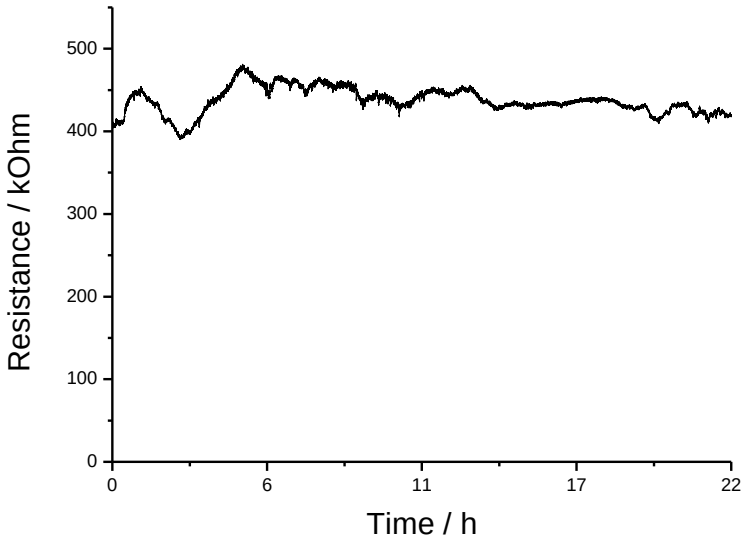

Figure 4.5: Stability of the VOC sensor (MiC-5121) over 22h a time of 22h.

For calibrating the VOC sensor, five different cyclohexene concentrations ($9.89x10^{-8}$, $1.978x1\ 0^{-7}$, $2.967x10^{-7}$, $3.956x10^{-7}$ and $4.945x10^{-7}$ mol L^{-1}) were introduced into our air purification system. The response of the MiCS-5121 sensor to the different VOC concentrations is shown in **fig. 4.6**. A lower resistance corresponds to a higher VOC concentration. A linear calibration was first tried, but a poor coefficient of determination of 0.8507 was obtained. A second-order polynomial fit, could describe the observed data. A coefficient of determination of 0.9960 was found (c.f. **fig. 4.7**). This is much more satisfactory compared to a linear fit, and using this calibration it was possible to quantitatively measure the concentration of cyclohexene online.

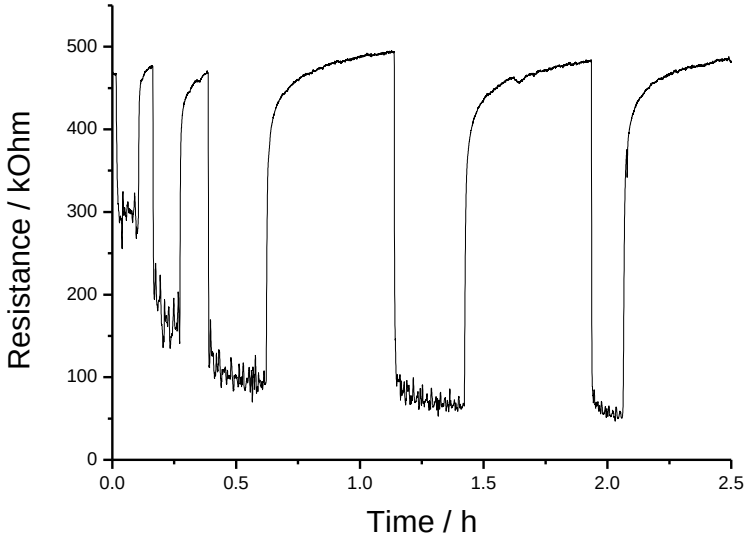

Figure 4.6: Response of the VOC sensor to five different concentrations of cyclohexene ($9.89x10^{-8}$, $1.978x10^{-7}$, $2.967x10^{-7}$, $3.956x10^{-7}$ and $4.945x10^{-7}$ mol L^{-1}). Lowest to highest concentration from left to right. Air flow rate, 0.3 m s^{-1}; nitrogen pressure for nebulization, relative 3 x 10^5 Pa; PAP off; relative humidity, ~ 50%.

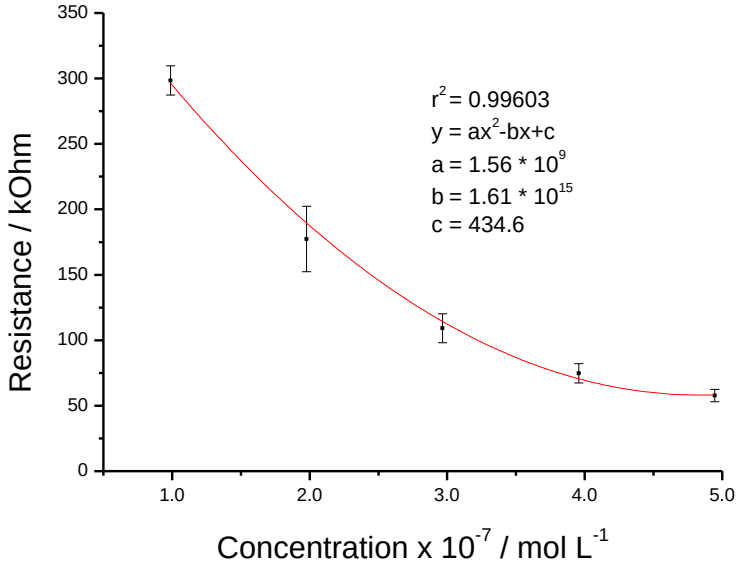

Figure 4.7: Calibration curve for the MiCS-5121 sensor (resistance versus concentration).

In a further experiment the same five concentrations were introduced into our lab-based air purification test bench, using the PAP at an operation voltage of 8 kV. The results are shown in **fig. 4.8**. The background noise of the VOC sensor is much higher when the PAP is switched on, which is most probably

due to the generation of ozone in the plasma. Ozone increases the resistance of the VOC sensor, whereas CO and VOCs reduce the resistance. Resistance is the readout of the MiCS-5121 sensor and a calibration must be done to quantify the introduced VOC. However, the calibration done in the previous experiment without the PAP turned on (c.f. **fig. 4.7)** cannot be used, since the sensor responds strongly to species generated in the plasma. Nevertheless, **fig. 4.8** shows that the relative resistance reduction of the smallest injected concentration (9.89x10-8 mol L^{-1}) of cyclohexene is not as high (31%) as the observed relative resistance reduction (38%) in the experiment with the PAP turned off (c.f. **fig. 4.6**). The background resistance of the activated VOC sensor decreases from 6000 kΩ to 148 kΩ with the PAP turned on (decrease of 97.5%), whereas the resistance with the PAP turned off only decreases from 298 to 58 kΩ (decrease of 80.5%). This shows that small cyclohexene concentrations are affected to a larger extent by the plasma than high cyclohexene concentrations. In other words, a part of the cyclohexene decomposes, which is thought to be always the same amount. This would explain why a stronger influence for smaller concentrations of cyclohexene than for higher concentrations is observed. It is not possible to draw quantitative conclusions about the amount of cyclohexene destroyed. The background noise of the VOC sensor with activated PAP is larger than the highest response of the sensor with the PAP turned off. However, it is very likely that the smallest concentration of cyclohexene is affected by the activated PAP. Two independent experiments (in black and red) were performed; the data are shown in **fig. 4.9**.

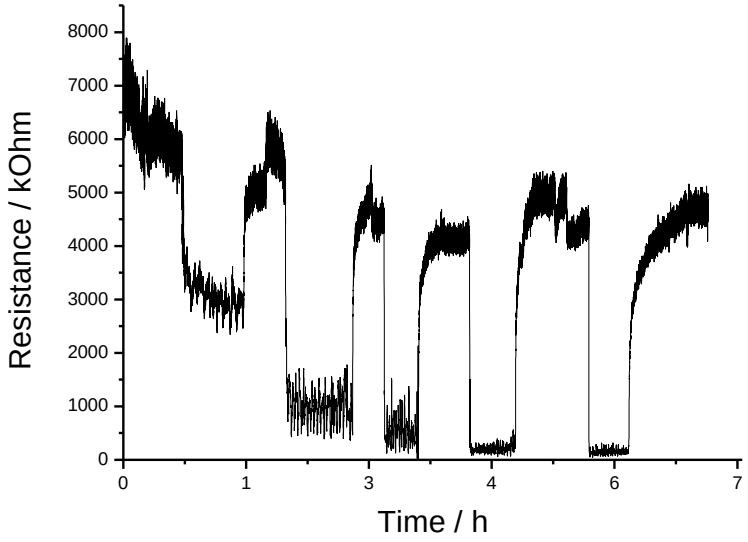

Figure 4.8: VOC sensor response to five different concentrations of cyclohexene ($9.89x10^{-8}$, $1.978x10^{-7}$, $2.967x10^{-7}$, $3.956x10^{-7}$ and $4.945x10^{-7}$ mol L^{-1}). Lowest to highest concentration from left to right. Air flow rate, 0.3 m s^{-1}; nitrogen pressure for nebulization, relative 3 x 10^5 Pa; PAP on, 8 kV; relative humidity, ~ 50%.

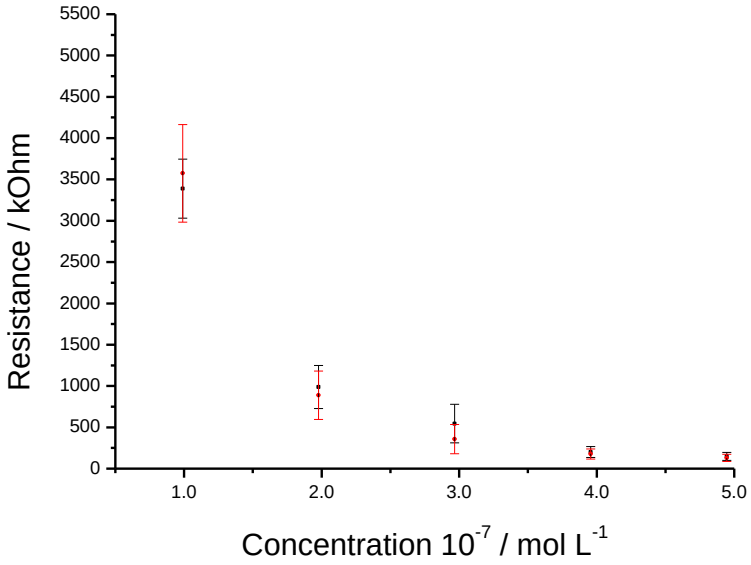

Figure 4.9: Calibration of the MiCS-5121 sensor. Resistance versus introduced concentration. Degradation of the introduced sample probably occurs. Black and red lines stand for the two independent experiments.

4.7 Conclusions

Kinetic calculations have shown that the dominating cyclohexene degradation process cannot be due to oxidation with ozone. It is known that the plasma contains O and OH radicals which react a million times faster with cyclohexene than ozone.

Therefore it can be assumed that most of the degradation occurring in the PAP will come from O and OH radicals.

The further studied miniPAP was not able to ionize the tested amine in contrast to the "normal" PAP. Moreover, it was possible to qualitatively study different VOCs online using a special resistant based sensor. However, as these sensors have a cross reactivity with ozone, quantitative degradations due to the switched on PAP of the studied VOC could not be accomplished.

Coupling of the air purification test bench with the LCQ mass spectrometer that became recently available in our lab seems to be promising. To ionize the generated gas-phase fragments the miniFAPA ionization source will be used. To characterize the species generated in the plasma, a UV/VIS spectrometer could also be used to characterize the species generated in the plasma. O and H radicals have a characteristic excitation wavelength (O 777 nm and H 656 nm) and it should be possible to prove their existence by measuring the UV spectrum of the generated plasma in the PAP.

Chapter 5

Miniature Flowing Atmospheric-pressure Afterglow Ion Source for Facile Interfacing of Capillary Electrophoresis with Mass Spectrometry

This chapter is adapted from:

Schmid, S.; Jecklin, M. C.; Urban, P.; Amantonico, A.; Zenobi R., Miniature flowing atmospheric-pressure afterglow ion source for facile interfacing of CE with MS. Electrophoresis **2010**, *31*, (21), 3597-3605.

5.1 Abstract

We present a miniaturized version of the flowing atmospheric-pressure afterglow (miniFAPA) ion source and use it for sheathless coupling of capillary electrophoresis (CE) with mass spectrometry (MS). The simple design of the CE-miniFAPA-MS interface makes it easy to separate the electric potentials used for CE and for ionization. A pneumatically-assisted nebulization of the CE effluent transfers the analytes from the liquid phase into the gas phase before they are ionized by interacting with reactive species produced by the flowing atmospheric-pressure afterglow. An important advantage of this interface is its high stability during operation: optimization of five different parameters indicated that the interface is not sensitive to minor deviations from the optimum values. Other advantages include ease of construction and maintenance, as well as relatively low cost. Samples with complex matrices, such as yeast extract, soil extract and urine, spiked with the test compounds, were successfully analyzed using the CE-miniFAPA-MS setup.

5.2 Introduction

Analysis of small molecules in complex sample matrices can be challenging. Mass spectrometry (MS) is a potent analytical technique which permits identification of analytes based on their mass-to-charge ratios as well as fragmentation patterns. However, MS often needs to be hyphenated on-line with a separation technique in order to cope with analysis of complex samples and matrices. Capillary electrophoresis (CE) is a versatile separation platform, which generally offers high separation efficiency and can handle nanolitre volumes of samples.

Various on-line interfaces for ion formation in CE-MS, which fulfill the requirements of diverse analytical work regimes, have been introduced to date. These include CE-electrospray ionization (ESI),[92] CE-inductively coupled plasma (ICP) ionization,[93, 94] CE-atmospheric pressure chemical ionization (APCI),[95] and CE-atmospheric pressure photoionization (APPI).[96] The most common CE-MS interfaces are based on the ESI process (for recent reviews see Refs.[97-113]). These are capable of providing excellent sensitivity in analyses even of complex molecules. Moreover, CE-ESI-MS systems are available commercially. There are three main types of CE-ESI-MS interfaces: (i) the sheathless interface, (ii) the sheath-flow interface, and (iii) the liquid junction interface.[110] The sheath-flow design has become especially popular, probably due to its high stability, ease of operation, and flexibility.[97, 109, 110] However, its disadvantage is the dilution of the CE effluent resulting from the relatively high flow rates of the sheath liquid (up to 100× the flow rate of the CE effluent). For this reason, the sensitivity obtained with the sheath-flow interfaces is typically lower than that observed for sheathless interfaces. Irrespective of the presence or absence of sheath liquid, the ESI process requires application of an electric potential between the capillary outlet and the MS inlet cone. Since CE itself needs an electric field for the separation of molecules, implementation of CE-ESI-MS interfaces often requires coupling two power supplies, one for the CE separation and one for the ESI. [107] The present study demonstrates a proof-of-concept of an alternative sheathless CE-MS interface, incorporating a miniature flowing atmospheric-pressure afterglow (miniFAPA) ion source, which enables

decoupling of the separation and ionization voltages and is characterized by relatively stable operation.

The FAPA ion source, also referred to as flowing afterglow atmospheric pressure glow discharge (FA-APGD),[52, 53] is an example of a direct current (DC) plasma source.[18] It operates by the formation of a glow discharge in helium between a pin cathode and plate anode, with voltages between 400 and 500 V and electric currents of roughly 20-25 mA.[55] This ion source was recently introduced by Andrade and co-workers for the analysis of gaseous samples[52] as well as for direct desorption/ionization from solid surfaces.[53] Direct desorption/ionization FAPA-MS has already been used for the analysis of pesticides in fruit,[54] as well as for characterizing polymer samples and plasticizers,[114] but the potential of FAPA in interfacing separation techniques with MS, and the possibility to decouple the electric potentials used for CE and ionization, has not yet been explored.

CE, when used together with MS, can be considered alternative and orthogonal to the classical chromatographic separation techniques routinely used with MS.[99, 105] Nonetheless, hyphenation of CE and MS is still seen to be difficult.[97, 109] The present study uses a downscaled version of the FAPA ion source for hyphenation of capillary electrophoresis with mass spectrometry. We believe that it could be easily adapted to miniature sample preparation and separation systems, including microchips. By way of example, it will be shown that with the simple CE-miniFAPA-MS interface, it is possible to detect several test compounds in unpurified samples containing complex matrices.

5.3 Materials and methods

5.3.1 Materials

Acetic acid, pyridine, 3-methylpyridine, 2,4,6-trimethylpyridine, tripropyl-amine, *p*-chloraniline and *N,N*-dimethylbenzamide were all purchased from Sigma-Aldrich (Buchs, Switzerland). Sodium hydroxide was from Siegfried Handel (Zofingen, Switzerland); ethanol from Scharlau Chemie (Sentmenat, Spain); methanol from Fisher Scientific (Loughborough, UK). Nanopure water (ρ > 18 MΩ cm) was obtained from a NANOpure Diamond system (Skan, Basel, Switzerland).

Urine was collected from a healthy volunteer on the day of the experiment. Soil extract was purchased from Carolina Biological Supply Company (Burlington, NC, USA). A yeast extract was prepared as follows: ~ 1 g of dry yeast (*Saccharomyces cerevisiae*, type I; YSC1; Sigma-Aldrich) was heated with 20 mL of water in a microwave oven at 700 W for the total time of 3 min. All the real samples were filtered with a polyvinylidene fluoride syringe filter (pore size 0.45 µm; Whatman, Clifton, NJ, USA).

5.3.2 Capillary electrophoresis

For the CE separation, a polyimide-coated fused silica capillary manufactured by Polymicro (ID 75 µm, OD. 363 µm, length 58 cm; BGB Analytik, Boeckten, Switzerland) was used. A home-built CE system, used in a previous work,[29] was adapted for the purpose of the present study. When used for the first time, the capillary was flushed with 1 M NaOH using a 1 bar overpressure for 1 h, followed by briefly flushing with water and background electrolyte (BGE). Then, on regular basis (approximately every 2 h), it was flushed for several minutes with 1 M NaOH, water and the BGE. When the capillary was conditioned, the nebulizer gas was switched off and tissue paper was placed at the outlet of the separation capillary to collect the effluent.

5.3.3 CE-MS interface

A schematic of the CE-MS interface is shown in **fig. 5.1A**. Upstream of the interface, a UV imaging detector (ActiPix D100; Paraytec, York, UK) was mounted to provide a UV absorption signal; a 200 nm UV filter was used. The outlet of the CE capillary (~ 10 cm) was coated with silver paint ("Leitsilber 200", Evonik Degussa, Düsseldorf, Germany) (**fig. 5.1B**). The silver paint was applied using a hair-free brush (ITW Texwipe, Mahwah, NJ, USA). The coated outlet section of the CE capillary was inserted into a wider-bore stainless steel capillary mounted inside the T-junction (**fig. 5.1A**). The added stiffness provided by the silver paint ensures the on-axis alignment of the two capillaries. A nebulizer gas (N_2) was used to vaporize the effluent of the CE capillary. A miniature CMOS camera (size: 15 × 22 mm, lens: f = 3.6 mm, 250K (NTSC)) was positioned close to the CE-miniFAPA-MS interface; this enabled real-time monitoring of the interface and

straightforward alignment of the main interface components (a picture taken by the CMOS camera is reproduced in **fig. 5.1C**).

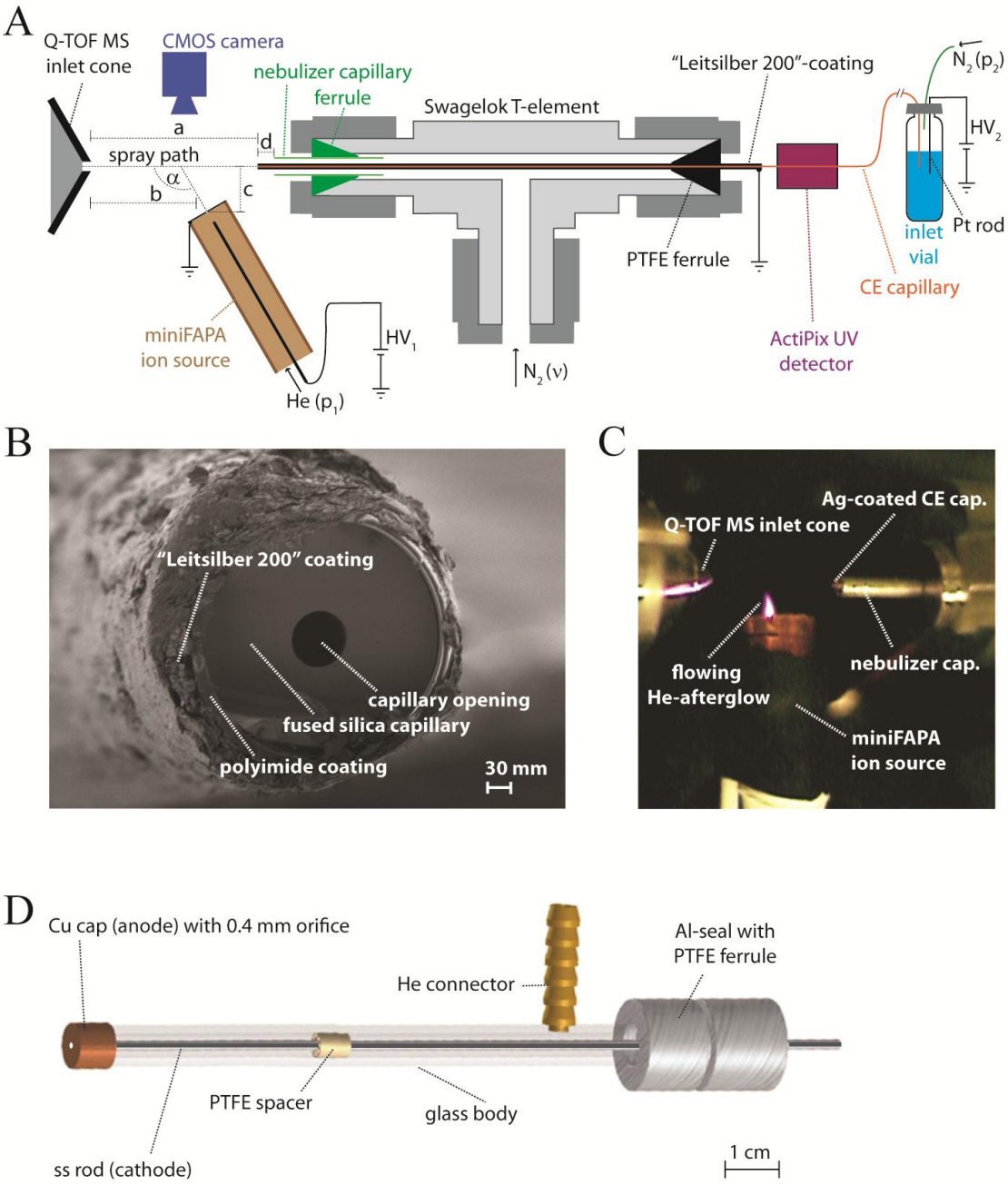

Figure 5.1. Experimental setup used for coupling capillary electrophoresis with mass spectrometry using a miniature flowing atmospheric-pressure afterglow ion source. (A) Schematic showing key components of the setup including (from right to left): CE inlet vial, CE separation capillary, UV detector, nebulizer T-element assembly with the coated section of CE capillary, miniFAPA ion source and MS inlet cone. The main geometrical parameters adjusted during interface optimization are marked as *a*-*d* and α. Figure not drawn to scale. (B) SEM of the CE capillary tip coated with "Leitsilber 200". (C) Picture of the CE-miniFAPA-MS interface recorded by the CMOS camera (*cf.* supporting movie). (D) Schematic of the miniature flowing atmospheric-pressure afterglow ion source (miniFAPA).

5.3.4 Miniature FAPA ion source

The miniFAPA ion source is a redesigned version of the one used in previous work[52, 54] (**fig. 1D**). It consists of a 10 cm long glass tube with an inner diameter of 6 mm. A copper cap (8 mm diameter and 5 mm length) with a central 0.4-mm diameter hole, serving as the anode, was fixed to the front end of the glass body. A stainless steel pin (∅ = 1.1 mm), the cathode, is centered inside the glass body using a polytetrafluoroethylene (PTFE) spacer and fixed with a ferrule in the rear end of the glass body. The PTFE-spacer contains 8 small holes to permit gas to flow through. The source was operated at 15.2 mA and 470-490 V using a power supply (HCN 140-3500, F.u.G. Elektronik, Rosenheim, Germany). A gas connection was glued to the glass body enabling application of helium (99.999%; PanGas, Dagmersellen, Switzerland) at a pressure of ~ 0.4 bar. This resulted in a helium gas flow rate of ~ 1 L min^{-1}. The miniFAPA ion source was positioned such that the outer electrode (the copper cap) faced the spray path, as illustrated in **figs. 5.1A** and **5.1C**.

5.3.5 Mass spectrometry

A hybrid quadrupole time-of-flight mass spectrometer (Q-TOF Ultima; Waters/Micromass, Manchester, UK) was used for mass spectrometric analysis. All measurements were performed in positive ion mode. The cone voltage and RF1 lens voltage were set to 50 V and 60 V, respectively, and the source temperature was kept at 50°C. Calibration of the instrument was performed using cesium iodide (CsI) clusters generated by electrospraying a solution of CsI in water/2-propanol (1:1, v/v) at a concentration of 2 mg mL^{-1}.

5.3.6 Data acquisition and treatment

MS data acquisition was controlled by the MassLynx (v 4.0) software (Waters/Micromass). During the optimization stage, mass spectra were background-subtracted using the Mass Lynx (polynomial order: 4; subtraction below curve: 25.0%; tolerance: 0.01). In the case of urine sample spiked with the test analytes, the mass spectra were further analyzed using MATLAB software (v 7.6.0.324 (R2008a); MathWorks, Natick, MA, USA). All the ASCII files corresponding to a single CE run were automatically loaded and displayed as a

two-dimensional shaded surface using MATLAB (defined by 'migration time' and '*m/z*' axes), in which each point is related to MS signal. Finally, a background subtraction procedure was performed on the data: a 'background spectrum' corresponding to a certain migration time, where no spiked analytes were detected (*e.g.* from the beginning of the CE-MS run), was subtracted arithmetically from each spectrum constituting the 2D graph. UV absorption electropherograms were recorded using the ActiPix D100 software (2008, v 1.0.1120; Paraytec); an exponential filter with a time constant of 0.5 s was applied.

5.4 Results and discussion

5.4.1 Optimization of the interface

During optimization, a mixture of three compounds (3-methylpyridine, *p*−chloraniline and tripropylamine) was continuously infused via the CE capillary by application of an overpressure of 1 bar to the inlet vial. The following parameters were optimized, one at a time, within the technically allowed ranges (see **fig. 5.1A**): length of the spray path (*a*: 5-30 mm), distance from the orifice of the miniFAPA ion source to the orifice of the mass spectrometer (*b*: 0-15 mm), distance from the orifice of the miniFAPA ion source to the spray path (*c* 2.5-20.0 mm), angle measured between the spray path and central axis of the miniFAPA ion source (α: 30-150°), and the nebulizer gas flow (ν: 150-350 L h^{-1}). Based on the results (**fig. 5.2**), we chose the following values to be used in further experiments: a = 15 mm, b = 7.5 mm, c = 2.5 mm, α = 90° and ν = 250 L h^{-1}. The distance d, the protrusion of the CE capillary from the nebulizer capillary, was set to ~ 0.5 mm, based on preliminary tests. In most cases, the trends of the three test compounds were the same. However, some of the parameters are not completely independent from one another. For example, according to **fig. 5.2**, the optimum values for parameters *a* and *c* are 15 and 2.5 mm, respectively. Nonetheless, with these values, the stability of the signal diminished (*cf.* error bars in the bottom panel of **fig. 5.2**). This may be due to an effect of the helium gas coming out of the orifice of the miniFAPA ion source on the nebulized CE effluent; probably this effect is more significant when the miniFAPA ion source is very close to the spray path (c = 2.5 mm). Therefore, in

order to minimize possible deflection of the analyte species near the miniFAPA orifice, we decided to use a value a = 10 mm, instead of 15 mm. Also in the case of the angle α, we decided to use 90° instead of 120°, since a lower ion background was observed for 90°. Ionization of the analytes could be observed even when the miniFAPA ion source was placed relatively far from the spray path (c = 20 mm) (f**ig. 5.2**, bottom panel). While the flowing atmospheric-pressure afterglow (the visible plume) extends over < 10 mm (*cf.* **fig. 5.1C**), this observation suggests that the zone beyond the afterglow region also contains a certain amount of reactive species which can ionize the nebulized molecules of the analytes (see also section 3.5).

Based on the data presented in **fig. 5.2**, we conclude that the CE-miniFAPA-MS interface is relatively insensitive to minor changes to the arrangement of the interface components (*cf.* **fig. 5.1A**). For all the parameters, the ionization efficiency varies within only one order of magnitude (**fig. 5.2**). One possible explanation is that since there is almost no electric field in the area adjacent to the capillary tip, the interface is less affected by deviation of the relative positioning of its key parts (capillary tip, miniFAPA device, MS orifice). Since this interface does not require frequent maintenance and is characterized by stable operation (see also the supporting movie), it is suitable for applications where frequent maintenance and adjustment of key parameters is not possible. Such applications include on-site quality control in production plants and environmental monitoring. Use in conjunction with microfluidic devices, in which the introduction of the ionization potential might affect execution of the sample treatment steps performed in the microfluidic channel (upstream of the MS interface) should also be of interest.

5.4.2 Establishing the electric contact for CE

A technical challenge in CE-MS interfaces in general is to establish a stable electric contact at the end of the capillary while preserving optimum conditions for separation as well as ionization.[99] In the CE-miniFAPA-MS interface, no sheath liquid needs to be used; the electric contact with the silver-coated capillary tip was found to be sufficient for the CE separation. Neither is there a need to apply an electric potential for ionization, which occurs mainly in the gas

phase. In general, narrow capillary emitter tips, used in sheathless ionization, are susceptible to clogging[115] and to deterioration of the conductive coating used as an electric contact.[112] In the interface presented here, the effluent of the CE capillary is nebulized with pure nitrogen gas, and there is no requirement to tune the electric field strength by sharpening the capillary end. The silver paint, used to establish the electric contact for the CE separation in the CE-miniFAPA-MS, adhered very well to the external polyimide layer (**fig. 5.1B**), therefore we did not need to remove the polymer cladding prior to spreading silver paint over the untapered capillary end. Although there is a physical gap (~ 140 µm) between the capillary lumen and the silver coating outside capillary (**fig. 5.1B**), this did not seem to cause problems with the stability of the electric current during CE runs (tested with 20 kV). In fact, the CE current was stable, with fluctuations normally not exceeding ~ 5%.

5.4.3 Coupling CE with miniFAPA-MS

In the next step, we applied CE separation together with the miniFAPA-MS detection. Since dilute acetic acid is frequently used as BGE in CE-MS,[16,20] we decided to use 50 mM acetic acid (pH = 3.1) in this first demonstration of the CE-miniFAPA-MS setup. **fig. 5.3** presents UV electropherograms as well as MS extracted ion currents (EIC) obtained during analysis of a standard analyte mixture (**Tab. 5.1**). The time shift between the UV and MS traces is due to positioning the UV detector ~ 8 cm upstream of the CE-miniFAPA-MS interface (*cf.* **fig. 5.1A**). The migration order of *p*-chloraniline, *N,N*-dimethylbenzamide, and the other four compounds taken together, is as expected, with the migration times being related to the solution-phase charge and hydrodynamic radius. Baseline separation was achieved for almost all pairs of electrophoretic peaks in MS traces (**fig. 5.3**). The CE resolution, as monitored by UV absorption detection, does not seem to deteriorate following ionization of analytes by miniFAPA and detection with Q-TOF-MS (**fig. 5.3**). The baseline in **fig. 5.3** is flat, even though no smoothing was applied before the data display. Limits of detection (LODs) obtained here range from 74 ± 37 to 610 ± 143 fmol for 2,4,6-trimethylpyridine and tripropylamine, respectively (**Tab. 5.1**). In terms of sensitivity, these figures

locate the current CE-miniFAPA-MS version at the level of some of the existing sheath-flow CE-ESI-MS interfaces (see, for example, the review article[111]). However, the CE-miniFAPA-MS is simpler to operate: there is no need for applying sheath liquid or an ionization potential to the CE capillary outlet. Some embodiments of sheathless CE-ESI-MS interfaces have been reported to provide sub-femtomole LODs (see, for example, Refs.[96, 116, 117]).

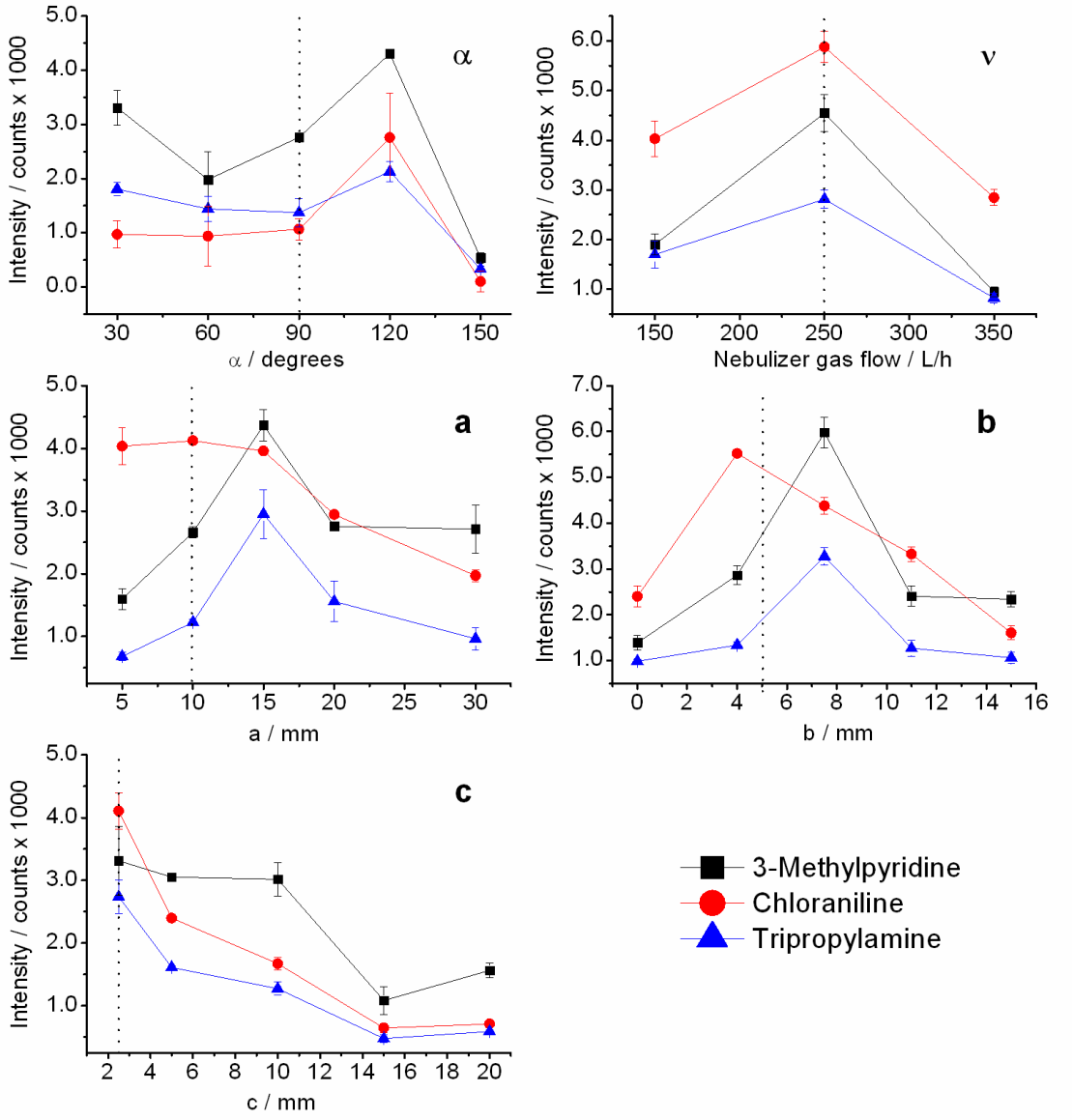

Figure 5.2. Results of the optimization study of five key parameters: *a* (*b* = *a*/2, *c* = 5 mm, α = 90°, ν = 250 L h^{-1}), *b* (*a* = 15 mm, *c* = 5 mm, α = 90°, ν = 250 L h^{-1}), *c* (*a* = 15 mm, *b* = 7.5 mm, α = 90°, ν = 250 L h^{-1}), α (*a* = 15 mm, *b* = 7.5 mm, *c* = 5 mm, ν = 250 L h^{-1}), ν (*a* = 15 mm, *b* = 7.5 mm, *c* = 5 mm, α = 90°). Refer to **fig. 5.1A** for description of *a*, *b*, *c*, α and ν. Each point corresponds to the mean value of three measurements, each one being a sum of intensities recorded over a 30-s period. The dotted lines mark the values selected for further experiments. Test mixture: 3-methylpyridine, 1.02 mM; *p*-chloraniline, 0.951 mM; tripropylamine, 0.526 mM. Sample flow rate: ~ 8 µl min^{-1}.

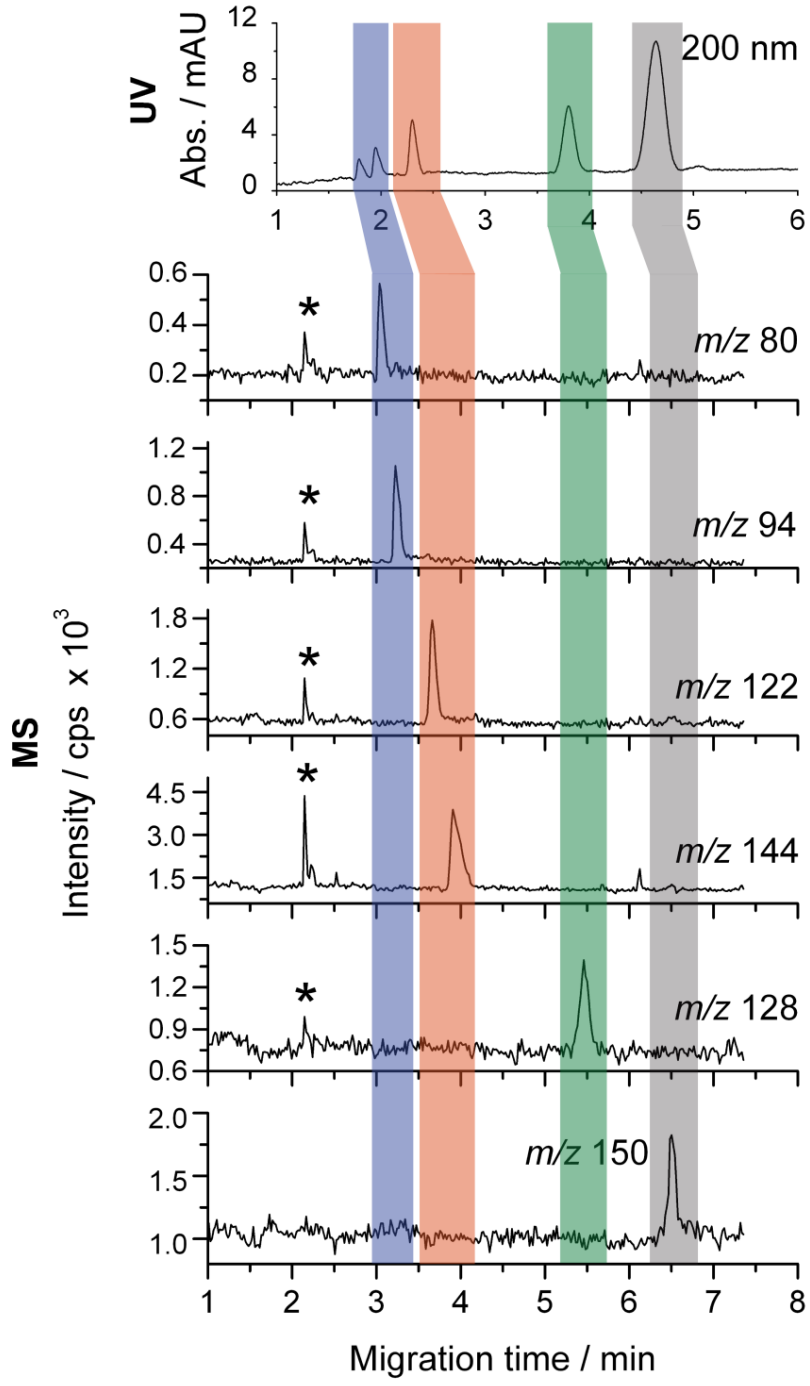

Figure 5.3. Representative UV and MS electropherograms showing electrophoretic separation of the standard mixture: pyridine, 0.124 mM; 3-methylpyridine, 0.102 mM; 2,4,6-trimethylpyridine, 0.0751 mM; tripropylamine, 0.0526 mM; p-chloraniline, 0.0951 mM; N,N-dimethylbenzamide, 0.168 mM. The sample was prepared in a 5 mM solution of acetic acid. CE-MS parameters: fused silica capillary, length × i.d. × o.d.: 58 cm × 75 μm × 363 μm; BGE, 50 mM acetic acid (pH = 3.1); injection, ~ 7 mbar 5 s; separation voltage, +20 kV; hydrodynamic pressure applied to the inlet vial during separation, ~ 7 mbar; UV detection (50 cm downstream from the CE capillary inlet), 200 nm; ionization, miniFAPA (a = 10 mm, b = 5 mm, c = 2.5 mm, α = 90°, ν = 250 L h-1); MS detection, Q-TOF-MS. The injection volume, calculated using a rearranged Poiseuille equation, was ~ 4.5 nL. CE current: ~ 4.1 μA. Color bars mark the corresponding time windows of the UV and MS traces. Asterisk (*) indicates an unidentified feature.

The sensitivity of our design could probably be improved, *e.g.*, when operating it with more sensitive mass analyzers than the one we had available for the present demonstration. On-line preconcentration steps can also be incorporated into CE-MS methods,[109, 118]offering benefits with respect to the concentration sensitivity.

Table 5.1: Molecular weights (M_w), dissociation constants (pK_a), migration times (t_M), observed *m/z* values (protonated form), and limits of detection (LODs, 3× *S/N* criterion) calculated according to the MS traces obtained by CE-miniFAPA-MS.

Compound	M_w g mol^{-1}	pK_a [a]	t_M / min	*m/z* $[M+H]^+$ [b]	LOD [c] / fmol
pyridine	79.10	5.2	3.0	80	277 ± 22
3-methylpyridine	93.13	5.6	3.2	94	149 ± 20
2,4,6-trimethylpyridine	121.18	6.6	3.7	122	74 ± 37
tripropylamine	143.27	10.6	3.9	144	610 ± 143
p-chloraniline	127.57	4.0	5.5	128	251 ± 47
N,N-dimethylbenzamide	149.19	n.f. [d]	6.5	150	425 ± 7

[a] different on-line sources
[b] *m/z* for analyte peaks were rounded to the nearest integer value
[c] ± 0.5× spread
[d] not found

5.4.4 Analysis of samples with complex matrices

Despite the high resolution of TOF analyzers, interferences from the sample matrix and other analytes are often problematic; therefore, separation prior to MS is indispensable.[109] In the next experiment, samples within complex matrices, such as a yeast extract, a soil extract and urine, spiked with the test compounds, were successfully analyzed using the proposed setup. **Fig. 5.4A** illustrates three MS electropherograms of *p*-chloraniline (EIC traces for *m/z* 128) in yeast extract, soil extract and urine. **fig. 5.4B** shows CE-UV and CE-MS electropherograms obtained during analysis of a urine sample spiked with the same standard compounds as in **Tab. 5.1**. Clearly, the miniFAPA-MS system enables detection of all the compounds even when they are injected with a complex matrix (urine). In addition, by performing CE-miniFAPA-MS/MS analysis of selected precursor ions, it was straightforward to obtain fragmentation spectra (data not shown). Some of the species – *e.g. m/z* 142, 144 and 145 – appear at the same time (**fig. 5.4B**); therefore, one can assume a

common origin of these three species. The peak at *m/z* 144 corresponds to protonated tripropylamine, while the peak at *m/z* 145 (*) is the corresponding ^{13}C-isotope peak. The peak at *m/z* 142 (**) represents the species produced by loss of H_2 from the tripropylamine ion. Isotope peaks cannot be seen for most analytes (except for tripropylamine and *p*-chloraniline) due to the signal intensity threshold chosen for displaying the 2D plot (**fig. 5.4B**).

3.5 Comparison with the APCI interface and final considerations

In general, most APCI interfaces are designed for LC-MS and function properly only under high flow-rate conditions; consequently, relatively low *S/N* ratios were observed when high sheath flow rates were used in CE-APCI-MS.[119] In APCI, the initial ionization in corona discharge takes place in a relatively small volume near the needle tip.[120] An interesting APCI interface for CE-MS has been presented by Tanaka *et al.*[95]

(i) Downscaling the ion source body to the size of a pen (8 mm in diameter) enables straightforward positioning and rearrangement of the miniFAPA ion source and a microscale capillary tip.

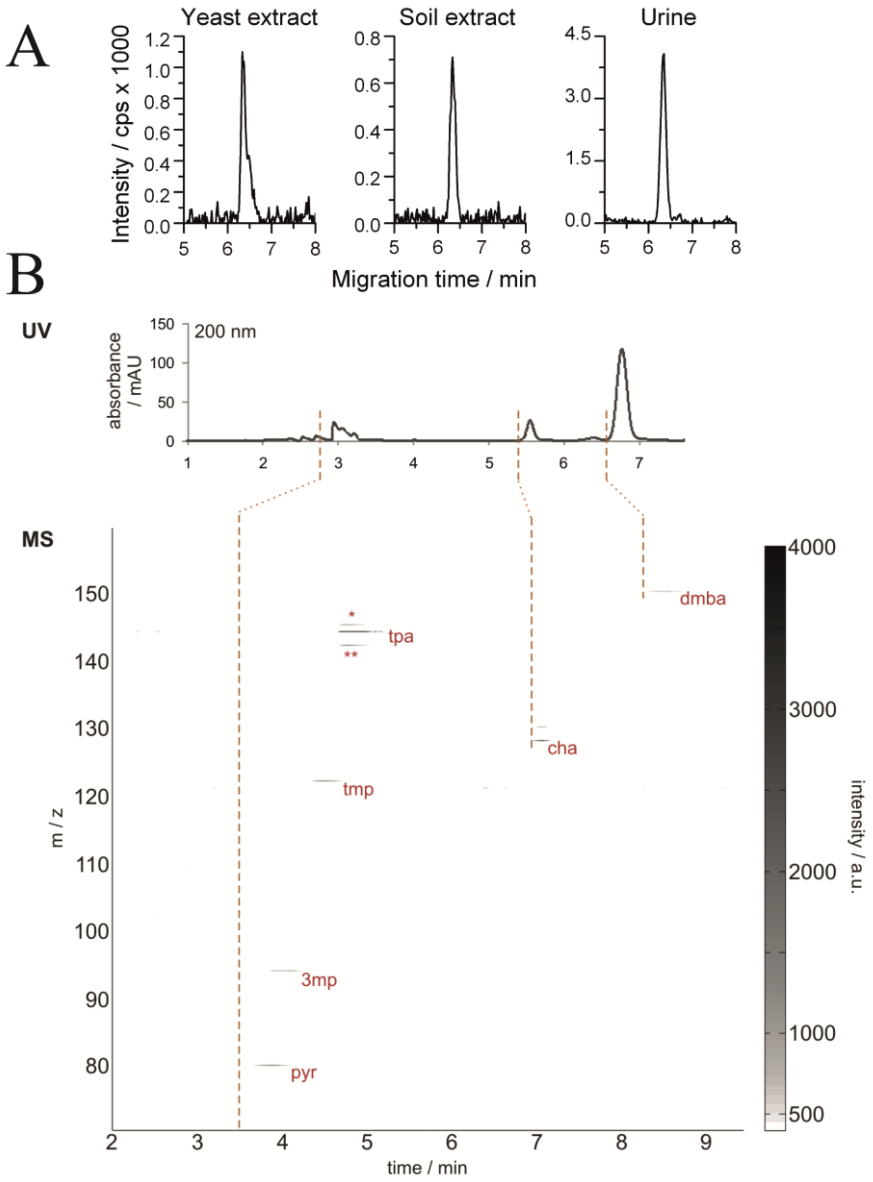

Figure 5.4. (A) Three MS electropherograms (*m/z* 128) of *p*-chloraniline (0.951 mM) in yeast extract, soil extract and urine sample. The samples were prepared by mixing 0.5 mL of filtered yeast extract, soil extract or urine with appropriate amounts of the standards, 100 µL of 50 mM acetic acid, and adjusted to the volume of 1 mL with water. Migration times have been aligned for clarity of graphical presentation. (B) CE-UV and CE-MS electropherograms showing the result of analysis of a urine sample spiked with the test compounds (**Tab. 5.1**) using CE-miniFAPA-MS. Spiked standard compounds: pyridine (pyr), 1.24 mM; 3-methylpyridine (3mp), 1.02 mM; 2,4,6-trimethylpyridine (tmp), 0.751 mM; tripropylamine (tpa), 0.526 mM; *p*-chloraniline (cha), 0.951 mM; *N*,*N*-dimethylbenzamide (dmba), 1.68 mM. One asterisk (*) indicates an isotope variant (*m/z* 145) of tripropylamine (*m/z* 144); two asterisks (**) indicate $[M+H-H_2]^+$ (*m/z* 142), related to hydrogen loss of tripropylamine ion; most isotope variants of the spiked analytes as well as matrix components are not seen due to the preset ion intensity threshold. Dashed lines approximately mark common points on the separation time line, accounting for the shift due to positioning of the UV detector, ~ 8 cm upstream from the CE capillary outlet; fluctuations of migration velocity might cause additional misalignment of the corresponding UV and MS features. Mass increment has been reduced to 0.1 *m/z* values for clarity of graphical presentation. CE-MS parameters in (A) and (B) are the same as in **Fig. 5.3**.

This interface is very dissimilar to our setup: (i) it has a needle to generate a corona discharge, (ii) it uses a sheath liquid, and (iii) it incorporates a vaporizer that heats up to 400°C. Similarly to CE-APCI-MS, the CE-APPI-MS also incorporates a vaporizer.[121] However, in the present study using CE-miniFAPA-MS, the transfer of analytes from the liquid phase into the gas phase was conducted with the optimized nebulizer gas flow rate. Importantly, this did not cause any obvious oscillations of the capillary end.

The miniaturization of FAPA is believed to limit dispersion of the gas-phase species in front of the MS orifice. The reaction time in the present version of the CE-miniFAPA-MS interface is roughly estimated to be in the order of ~ 0.1 ms. One could expect that, in general, downscaling the afterglow region poses a limit on the interaction time between the analyte and reactive species. However, the resulting decrease of sensitivity is outweighed by the compatibility with the low flow rates (down to sub-microliter per minute) of effluents from CE capillaries or microchips. An investigation of the ionization mechanism is not the topic of this study; like for other compounds analyzed with FAPA-MS,[52-54, 114] we also observed formation of protonated molecules $[M+H]^+$. As described by Andrade and co-workers,[52] the FAPA ionization process resembles the one observed in most common APCI sources, operated with corona discharge; therefore, yielding mostly charged water clusters ($[H_2O]_nH^+$) as active species.

5.5 Concluding remarks

Implementation of the miniaturized FAPA ion source in CE-MS brings some practical advantages:

(i) The outer plate electrode of miniFAPA is grounded, which eliminates technical obstacles associated with application of electric potentials for CE and ionization.

(ii) The interface offers good stability of operation; the ion intensity was not strongly affected by slight deviation of the interface alignment from the optimum.

(iii) Downscaling the ion source body to the size of a pen (8 mm in diameter) enables straightforward positioning and rearrangement of the miniFAPA ion source and a microscale capillary tip.

(iv) Construction of the ion source for the interface described here is relatively simple and achieved using inexpensive materials (< $10).

(v) While the miniFAPA ion source is generally maintenance-free, its disassembly is very easy and can be accomplished within one minute allowing for fast but thorough cleaning of the copper electrode.

The limits of detection achieved in this study were in the femtomole range. Further work should thus focus on improving the sensitivity, for instance, by finetuning the ion collection efficiency at the MS orifice, choice of another mass analyzer, and optimization of the acquisition mode (*e.g.* multiple reaction monitoring). Due to the minuscule technical requirements for operating miniFAPA and its anticipated ruggedness, following its further development, the new interface may be useful in conjunction with portable ion trap mass spectrometers designed for performing analysis of target species of interest outside the laboratory,[122] when coupled with microscale capillaries and microchips, or in industrial quality control systems; complementing the list of the established CE-MS interfaces in current use.

Chapter 6

Online Monitoring of Molecular Processes in a Plasma Air Purifying System

This chapter is adapted from:

Schmid, S.; Meier, L.; Berchtold, C.; Zenobi, R., Online Monitoring of Molecular Processes in a Plasma Air Purifying System *Environ. Sci. Technol.* **2012**, *46*, (7), 4067-4073.

6.1 Abstract

Plasma air purifying systems present an interesting alternative to filters for purifying air. In this study, molecular processes in a commercially available ac driven plasma air purifier were studied in detail. This air purifier is supposed to reduce all air contaminants to small nontoxic molecules (e.g., H_2O and CO_2). However, degradation mechanisms are not yet fully understood. In this study, we investigated the exhaust of the plasma air purifier to determine which degradation products are formed. An interface was designed and constructed to allow the direct coupling of the plasma air purifier's exhaust to a mass spectrometer. The compounds studied, primary and secondary amines, were introduced at a concentration of 1 ppmV. Contrary to our expectations, polymerization instead of degradation was observed. The higher the ac voltage applied (max. 9.0 kV) to the plasma air purifier, the higher the mass of the oligomer distribution. Side chain oxidation products as well as oligomers could be observed for all compounds tested. Starting with amines of low mass (m/z < 200), compounds of molecular masses above 1000 Da were observed in the plasma air purifier. Detailed analysis of the observed mass spectra as well as experiments with deuterated dibutylamine helped to unravel the mechanism taking place in the plasma air purifier. Nitrate anions generated in the plasma air purifier (presumably from N_2) are proposed to form ionic clusters with protonated amines.

6.2 Introduction

Purifiers based on non-thermal plasma are a novel alternative to filters for cleaning air. These systems should be able to degrade any air contaminants to nontoxic compounds, while consuming only limited power (50 mW to 17 W; information from suppliers). In recent years, air cleaning systems have become of great interest to both the general public and the economy. Buildings with ever better thermal insulation, humidity and temperature control, result in a smaller exchange rate with the outdoor air, and thus leading to poorer indoor air quality.[1-6] Many infectious diseases are caused by airborne pathogens, the large majority of which is spread in indoor environments.[123] This takes a big toll on people and on the economy,[124] especially since many people spend 80% and more of their time indoors.[7, 8, 125] Indoor air pollution is among the top five environmental risks to public health, and it is suggested to ventilate buildings and rooms several times a day with clean outdoor air. However, this is not always desirable or possible, due to weather conditions or due to energy saving issues. Therefore, air cleaning systems have become increasingly important. From 1998 to 2007, 51 patents for plasma air purifiers (PAPs) were filed, whereas in the last 3 years close to 100 patents for PAPs were applied for. This shows the growing general interest in this technology. Several designs of PAPs have been reported; most of them are using a heterogeneous catalyst and relatively high power for achieving good degradation efficiencies (from 70 to 100%).[14, 22, 28, 70, 74, 126] Until now, there is no standardized method to characterize the degradation efficiency of such plasma based air purification systems, since mechanisms of the reactions and the reaction pathways are still not fully understood. One method to specify the degradation efficiency of a PAP is to study the fate of contaminants such as volatile organic compounds by using adsorption tubes. Although the overall cleaning efficiency can easily be evaluated using adsorption tubes, it is difficult to detect the degradation products generated. Some reactive products formed may not be adsorbed at all, while others (e.g. ozone and radicals)[12] could react with the adsorption material in the tubes, which would therefore render subsequent desorption of such compounds impossible. Unfortunately, it is not at all straightforward to investigate which products are generated in the plasma, since the selection of an

adequate sorption material is very problematic for unknown products.[127] Moreover, in a worst-case scenario, non-toxic compounds could be modified in such way that undesired toxic products are formed upon passing the PAP.

Here, a commercially available PAP was studied using a newly designed interface that allows to directly lead the exhaust of the PAP into a mass spectrometer (MS). This interface helps to circumvent offline sampling, and simplifies the understanding of the molecular processes in the air purification system. The ionization of the compounds in the PAP exhaust was either accomplished using the plasma air purifier itself or with a miniaturized atmospheric-pressure afterglow ion source (miniFAPA).[128] To study the performance of the newly designed MS interface, volatile amines were chosen as reactants since it is well known that amines are easily ionizable. By choosing well defined starting compounds, we also aimed at reducing the complexity of the product distribution for a comprehensive characterization of the molecular processes in the PAP.

6.3 Experimental Section

6.3.1 Materials and sample preparation

Water was purified in-house using a Millipore system (Bedford, MA, USA). Methanol, ethanol, as well as hexyl-, octyl-, decyl-, *tert*-butyl-, dipentyl-, dibutyl- and d18-dibutylamines (HPLC grade) were purchased from Sigma Aldrich (Buchs, Switzerland). Solutions of 1% by weight of all amines in water, water:methanol (1:1, v:v) or ethanol were prepared. Using an air flow of 320 L min^{-1} through the PAP, and an ionfusion rate of 40 µL min^{-1} this a concentration of roughly 1 ppmV results in the ventilation system for all amines. Dilutions were done with the methanol/water mixture unless noted otherwise.

6.3.2 Experimental setup

The schematic of our experimental setup is shown in **fig. 6.1**. It consists of four parts. The sample introduction into the system (**A**) was accomplished using a syringe pump (Fusion 400, KR Analytical Ldt, Cheshire, UK). The syringe pump allows delivering an exact amount of sample per time, which renders comparisons between experiments very reliable. The sample is nebulized using a pneumatically assisted sonic spray-like source.[57] For this, a high voltage is

needed. Air was used as nebulization gas (1.0 L min^{-1}). The flow through the system was generated by a fan which sustained a constant air flow of 320 L min^{-1}. The PAP (**B**) is incorporated into the self-made ventilation system. The diameter of the PAP is 160 mm, its length is 180 mm, and its overall weight

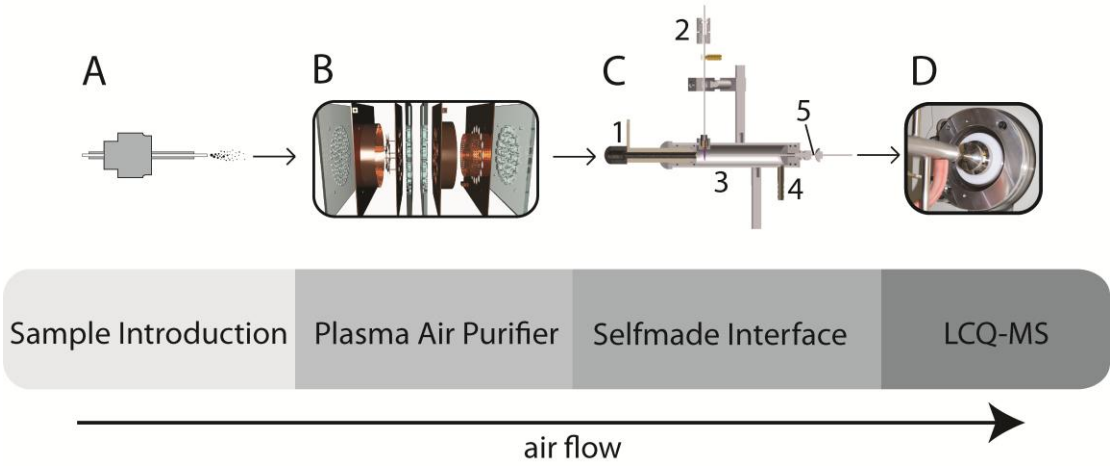

Figure 6.1: Schematic design of the used system for testing the PAP. A, sample introduction accomplished using a sonic sonic ionization like spray source; B, PAP consisting of 4 copperplates and 4 plates made of poly-(methyl-methacrylate) as spacers; C, Self designed Interface, which consist of a heating coil (1), the miniFAPA ion source for secondary ionization (2), an aluminum tube (3), a connection for a vacuum pump (4) and a 150 mm elongated MS cone (5), whose tip is placed 10 mm in front of the miniFAPA ion source; D, the LCQ-MS for mass analysis.

is 10.5 kg. The plasma electrodes inside the PAP are made of nickel, lead, and copper, and are supported by polyvinyl chloride and poly-(methyl-methacrylate) holders. The plasma in the PAP is generated using air, no auxiliary gas is needed. A high AC voltage is applied to the copper plates with a frequency of 50 Hz and an amplitude that can be adjusted from 0 to 9 kV (using an even higher voltage resulted in electrical breakdown inside the PAP, with sparks bridging the gaps between the copper plates). The dwell time in the plasma zone of the compound studied is approximately 0.6 s. Unless noted otherwise, a voltage of 8.5 kV was used. Using these conditions approximately 300 ppb ozone were measured on the exhaust of the PAP. The humidity during our experiments was determined to be in the 10–14 g/m^3 range. Introduction of a sample increased the humidity by no more than 1%. Therefore, a change in the ongoing reactions due to a change in humidity during sample introduction is very unlikely.

Fig. 6.2 shows a characteristic emissions line at 779 which is due to O emission, and the signals between 300 and 450 nm originate most likely from N_2

transitions of the second positive system ($C^3\Pi_u \rightarrow B^3\pi_g$).[129] No indications of reactive species were visible in the emission spectrum, presumably because O and N_2 emissions are much stronger.

The ionization interface (**C**) consists of a heating coil (1), which was used to heat the aluminum body (3) to 473 K. This greatly helped to reduce memory effects between experiments. The ionization of the PAP exhaust was either accomplished using the PAP itself or the miniaturized atmospheric-pressure afterglow ion source (2, miniFAPA). The settings for the miniFAPA ion source were 0.50 kV, 15.0 mA, and a gentle helium flow (~100 ml min^{-1}, 99.999%; PanGas, Dagmersellen, Switzerland).

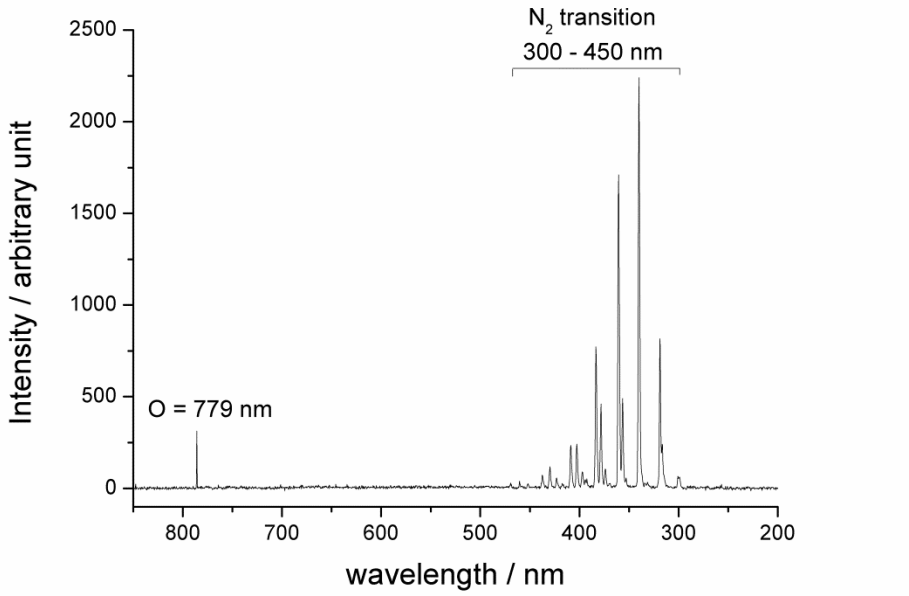

Fig. 6.2: The emission spectrum of the plasma in the PAP was measured with an optical fiber coupled PC-card based UV/VIS spectrometer (ISS-UV/VIS, Ocean Optics, Dunedin FL/USA). For these measurements all ambient light sources were switched off. The background was measured at the same position without activated PAP. The spectrum obtained was background subtracted and shows a number of emission lines.

The ionization processes of the miniFAPA ion source are similar to those taking place in common atmospheric pressure chemical ionization sources, with active species of the composition $[H_2O]_nH^+$.[127] The vacuum port (4) allowed to aspirate 10% (~33 L min^{-1}) of the PAP exhaust through the ionization interface, which was accomplished by connecting it to a vacuum pump (DIVAC 2.2 L, Oerlikon, Cologne, Germany). The tip of the elongated MS cone (5) was placed within the aluminum body at a distance of 1.0 cm from the miniFAPA ion source.

Mass spectrometric analysis was performed using an ion trap instrument (**D**) (LCQ Deca, Thermo Finnigan, San Jose, USA) equipped with a self-made inlet cone. The settings of the LCQ instrument were: capillary voltage, 30 V; capillary temperature, 473 K; tube lens, 55 V. The ion optics and main RF were optimized to obtain the best overall ion yield. The LCQ instrument was controlled by the Xcalibur software, version 2.07 SP1.

6.4 Results and Discussion

In a first set of experiments the performance of the newly designed interface was studied. It was already known that the plasma air purifier itself was capable of ionizing substances that were present in the air ventilation system. To compare this observation to a better known ionization method, we incorporated the miniFAPA ion source into the interface. 40 µL of a 1% dipentylamine solution in water was sprayed for 1 min into the system. The concentration transferred into the interface was calculated to be ~1 ppmV. **fig. 6.3** shows the mass spectra using either the miniFAPA ion source (upper panel, PAP turned off) or the PAP (lower panel) for ionization. Helium was used in the miniFAPA to generate an active species which reacts with the analyte. The ionization process resembles the one observed in most plasma ion sources, presumably involving mostly charged water clusters ($[H_2O]_n\ H^+$). No details are known about the ionization mechanisms in the PAP, but we assume that it is similar to that in a corona discharge plasma. Upon injecting dipentylamine, the intensity observed of the parent ion (*m/z* = 158) was more than one order of magnitude higher using the miniFAPA ion source compared to the PAP. In the mass spectra obtained using the PAP, a huge signal could be observed at *m/z* = 378. This signal must be generated in the PAP when dipentylamine is injected, since it was not observed with the miniFAPA ion source. This also shows that the compound causing this peak is not present in solution. The two signals at *m/z* = 174 and *m/z* = 190 represent oxidation products of the alkyl chain. Such products have been described in previous work conducted with common volatile organic compounds.[127] The same oxidation products could also be detected using the miniFAPA ion source. The signal-to-noise ratio when applying the miniFAPA was not as good as for the PAP, though. Finding signals

with *m/z* higher than 158 (except for the oxidation products) was surprising, as degradation products were expected to be formed exclusively.

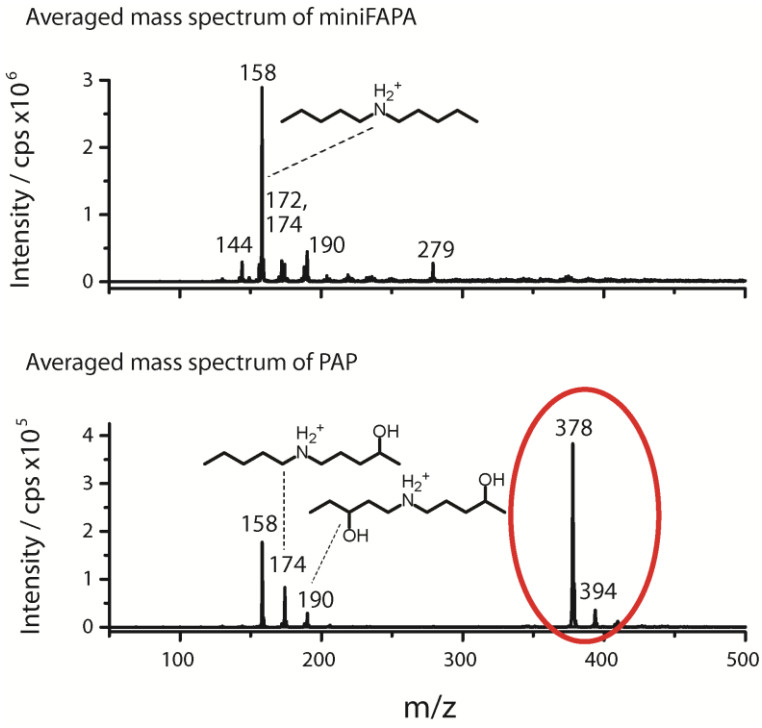

Figure 6.3: Performance test of the newly designed interface injection dipentylamine for 1 min. The upper graph show mass spectrum using the miniFAPA ion source for ionization (PAP turned off). The lower graph show the same, but using only the PAP as ionization source.

In a next set of experiments the mass-to-charge range was increased to 2000 and the dependence of the voltage applied to the PAP was studied using different amines. **Fig. 6.4** shows spectra for octylamine and dibutylamine (parent ions = 130 *m/z*) without using the miniFAPA ion source. The voltage of the PAP was gradually increased from 6.0 to 9.0 kV in steps of 0.5 kV. For all amines measured, oligomer-like signal series were observed in the mass spectra from 7.0 kV on upwards, especially in case of primary amines. The results obtained show that the higher the applied voltage, the higher the degree of oligomerization. No decomposition products were found. Using the highest possible voltage of 9.0 kV, the parent ion of octylamine (*m/z* = 130) was much less intense compared to the most intense product ions. It seemed that a large fraction of octylamine introduced reacted to higher molecular weight oligomers. When studying dipentylamine (parent ion = 158 *m/z*) at an applied voltage of

7.0 kV or higher, the most intense signal changed from the parent ion (m/z = 158) to the first oligomerization product (m/z = 378). This shift towards higher molecular weight products when applying a high voltage to the PAP was found for all compounds tested. The mass steps of 14 and 16 Da observed are very likely due to OH radical side chain oxidations forming alcohols or ketones/aldehydes.[1, 130-132] Kalberer *et al.*[133] have previously shown that reactions of carbonyls and their hydrates can generate polymers, which were found to be a substantial fraction of the organics on aerosols. Similar results, with regular mass differences of m/z = 14, 16, and 18 were observed in our study. By increasing the voltage, the maximum of the polymer mass shifted gradually to higher masses. Kalberer et al. observed analogous effects when they increased the reaction time.

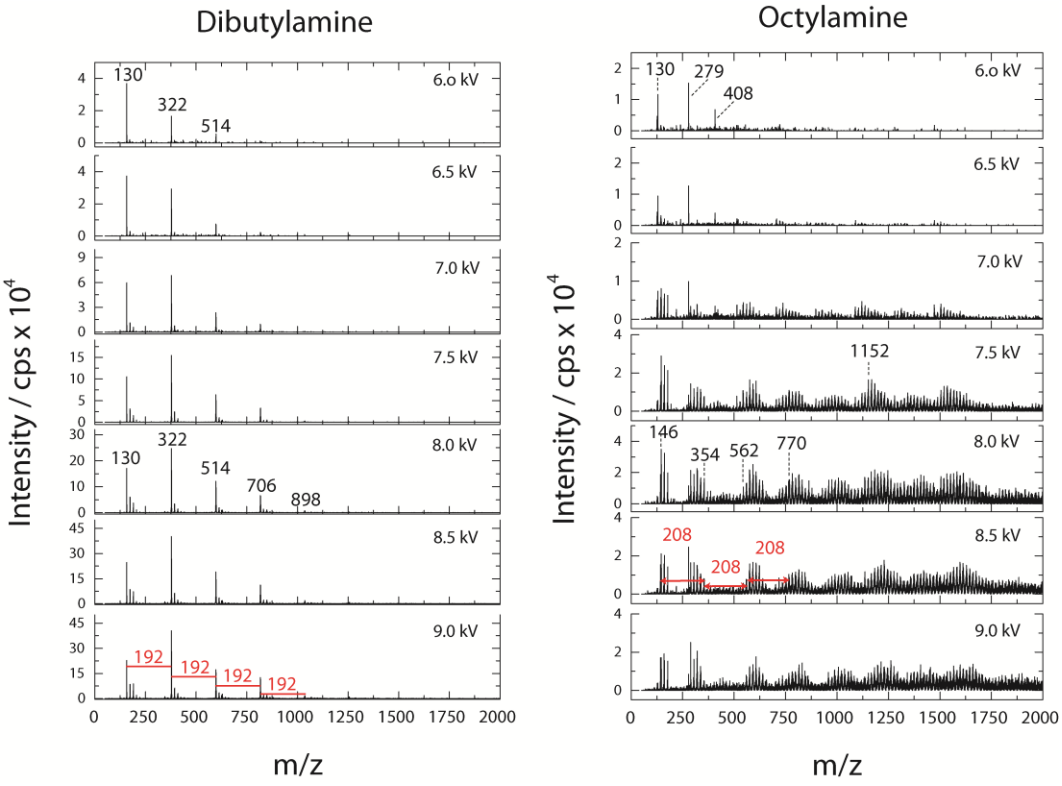

Figure 6.4: Illustration of the influence of the voltage applied to the PAP von the mass spectra when injecting octyl- and dipentylamine. The voltage was gradually increased in 0.5 kV steps from 6 to 9 kV. Regular mass steps of m/z =192 for dibutylamine and m/z = 208 for octylamine could be observed for all voltages tested. Every spectrum was obtained by summing up 1 min of data. The m/z range was set to 50 … 2000.

Fig. 6.5 shows details of four different amines studied. For dipentylamine (parent ion = 158 *m/z*), a common oligomerization pattern with steps of *m/*z = 220 was observed. We first assumed that dipentylamine was strongly oxidized to a reactive oxygen radical intermediate on the copper plates with an overall molecular weight of 221 Da that further reacted with ammonium ions passing the PAP. A reactive intermediate with a mass of 221 Da was assumed since a covalent bond formation between the dipentylammonium ion and the reactive intermediate should lead to a loss of 1 Da. The mass difference between the putative reactive intermediate and the dipentylamine is 64 Da. For tert-octylamine, octylamine and hexylamine the very same mass difference between the reactant and the intermediate were observed.

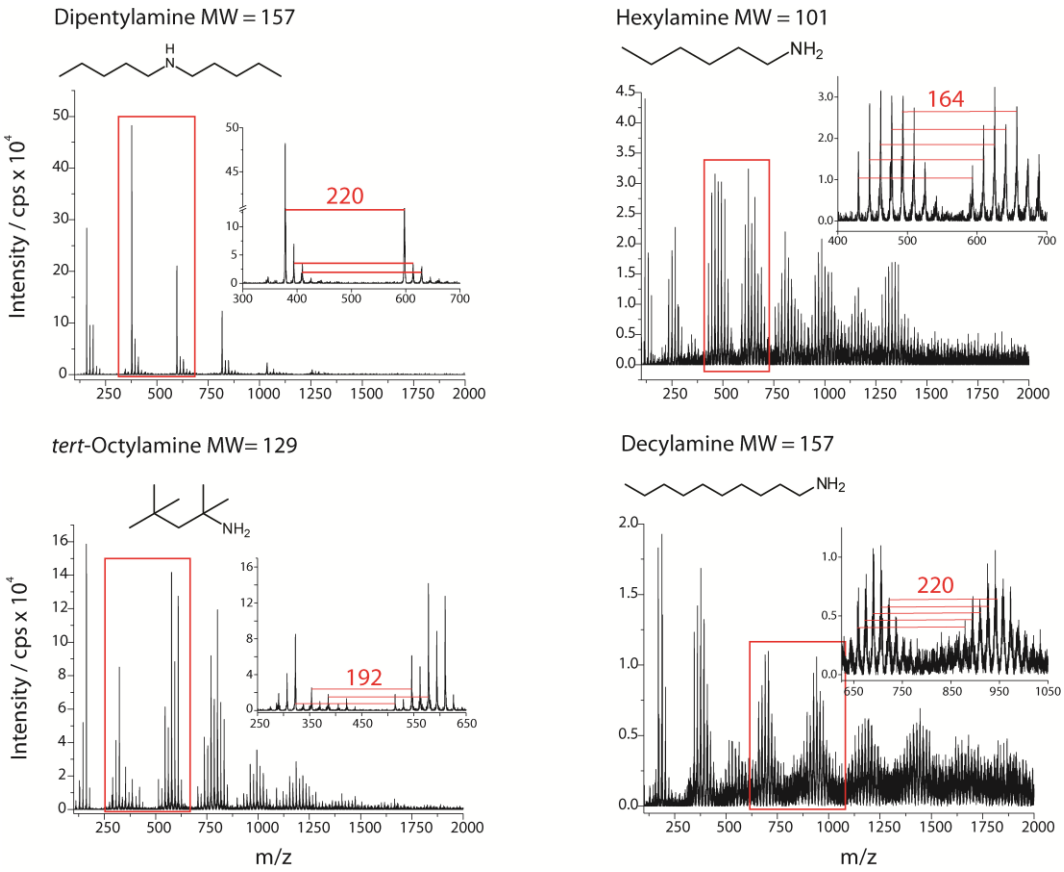

Figure 6.5: Four mass spectra of different amines studied are presented. In each of those spectra, regular mass steps could be observed: regular mass steps of *m/z* = 220 were found for dipentylamine, 164 for hexylamine, 192 for tert.-octylamine and 220 for decylamine.

In a next set of experiments, we tried to verify the hypothesis of covalent bond formation and therefore prove the existence of a reactive intermediate

which would explain the results observed above. Dibutylamine (parent ion = 130 *m/z*) was chosen as model compound because the mass spectra were not as complex as those for the primary amines. For this reason, per deuterated dibutlyamine (parent ion = 148 *m/z*) was studied in the PAP. Part **A** of **Figure 6.6** shows mass steps of *m/z* = 15 observed for the side chain oxidation products, which is 1 Da less than in the experiments with undeuterated dibutylamine. This can only be explained by the loss of deuterium instead of hydrogen. For two covalent bonds being formed and the consequential loss of two deuterium atoms, oligomerization steps of Δm = 208 instead of 210 would be expected. However, a Δm = 210 was still observed. Therefore, the formation of a reactive intermediate

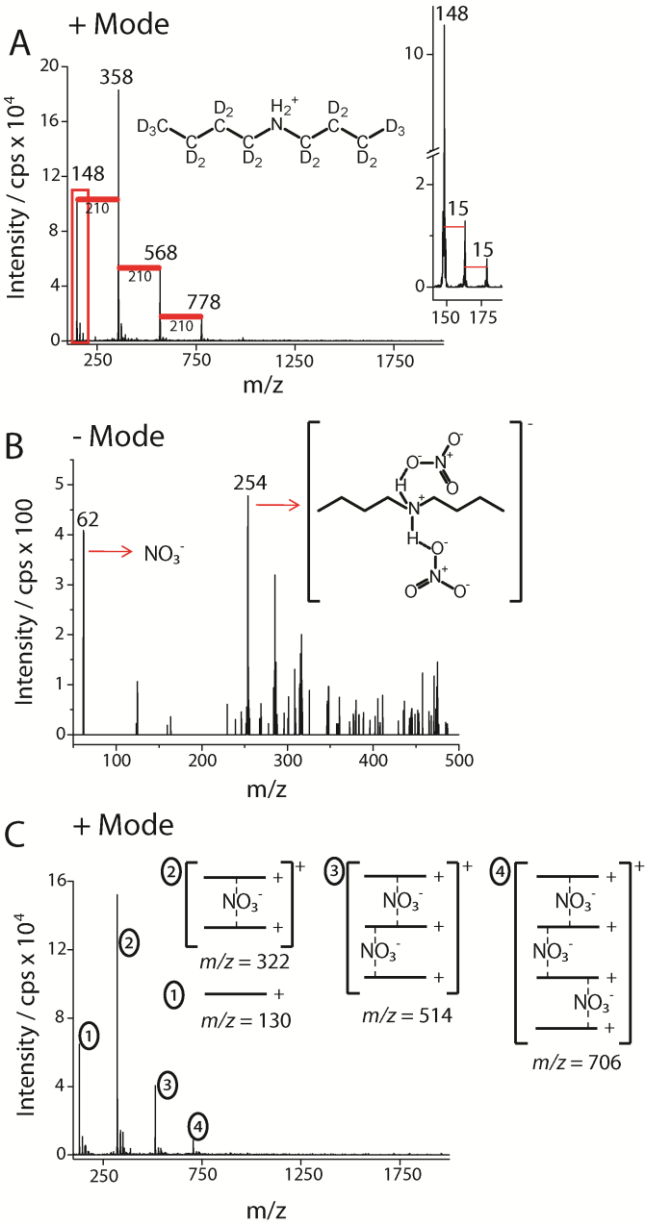

Figure 6.6: (A) Mass spectrum of the deuterium labeled dibutlyamine studied in the PAP. Regular mass steps of 15 and 210 are found. The mass steps of 15 confirm clearly the side chain oxidations. (B) Mass spectrum of dibutlyamine measured in the negative ion mode. Nitrate and a nitrate-dibutlyammonium-nitrate ionic cluster could be seen. (C) Mass spectrum and schematic representation of the polymeric products generated from dibutylamine in the PAP.

that forms covalent bonds had to be excluded to explain the observed oligomerization series in the mass spectra. Repeating the experiments using water, methanol and ethanol as solvents had no discernible influence to the mass spectra observed.

When running the LCQ-MS in negative ion mode, a signal at *m/z* = 62 was found. Part **B** of **fig. 6.6** shows the mass spectrum of dibutylaime in negative ion mode. In addition to the negatively charged ion at *m/z* = 62, an intense signal at *m/z* = 254 was detected. The signal observed at *m/z* = 62 could correspond to nitrate, which is known to form from N_2 in an air-operated corona plasma.[84, 134, 135] To prove the existence of nitrate, the exhaust of the PAP was bubbled through water for 4 h. Ion chromatography measurements of the water supported the production of nitrate and nitrite (NO_X) by the activated PAP. In a control experiment without the PAP activated, only traces of nitrate but no nitrite could be detected. The signal at *m/z* = 254 could thus be assigned to a cluster of protonated dibutylamine and two nitrate anions.

Ionic cluster formation with nitrate explains the observed mass steps shown in **fig. 6.5**, and it is in an excellent agreement with the observed masses.

Part **C** of **fig. 6.6** shows the positive mode mass spectrum, along with the suggested sandwich clusters between the positively charged dibutlyamine ions and the nitrate anions, which were obtained when injecting dibutylamine into the PAP. The higher the voltage of the PAP, the more nitrate was generated and the larger and therefore heavier the ionic clusters became. Primary ammonium molecules can form more clusters because steric hindrance could at least partially explain the much more crowded mass spectra observed for primary compared to secondary amines. MS/MS experiments showed that the high mass ionic clusters are related to the lower mass ionic clusters. Isolating the signal at *m/z* = 706 generated from dipentylamine and using an arbitrary collision energy of 30% in the MS/MS mode, a product ion of *m/z* = 514 was observed. Using MS^3 (1, 706; 2, 514) it was possible to detect a signal at *m/z* = 322 and even dibutlyammonium could be seen conducting MS^4. Therefore, it is clear that the ionic clusters observed were from the dibutlyammonium interacting with nitrate, which is generated in the PAP. **Fig. 6.7** shows the MS/MS of the first

oxidized ionic cluster. Both signals at *m/z* = 130 and at *m/z* = 146 can be seen, showing that the oxidized cluster of the oxidized dibutlyammonium, the dibutlyammonium and the nitrate is formed.

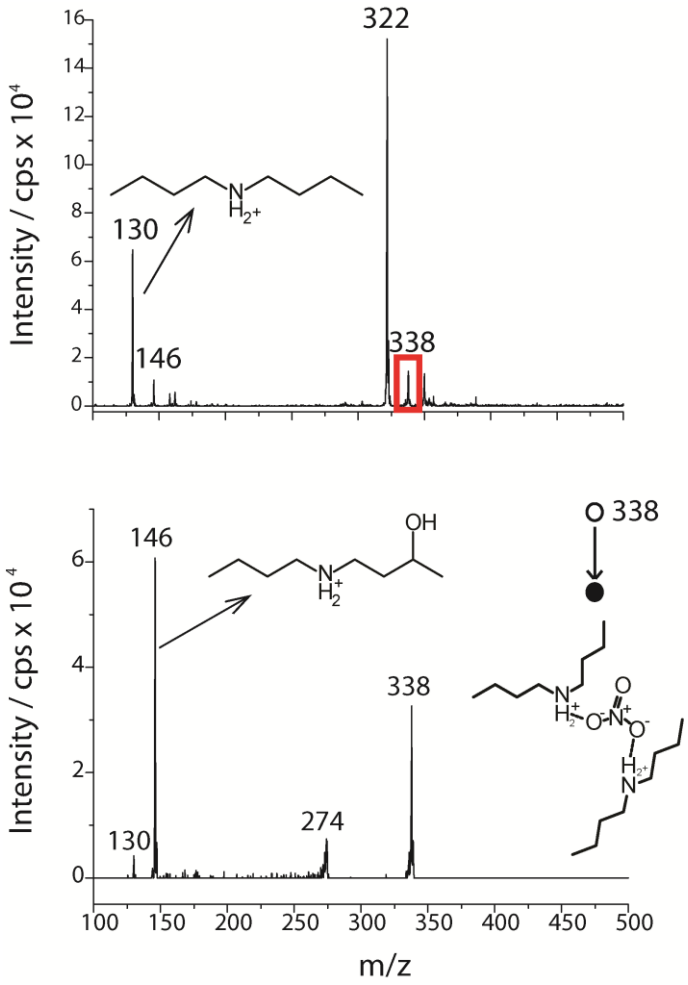

Figure 6.7: (top) Mass spectrum of the product distribution generated from dibutylamine after passing through the PAP. (bottom) MS/MS spectrum of the first oxidized ionic cluster at *m/z* = 338. Collision energy was kept at 30% (arbitrary unit).

This study shows that most products in the PAP are generated from reactions with OH radicals and subsequent formation of ionic clusters involving nitrate. The distance from the exhaust of the PAP to the LCQ-MS is more than 1 m, i.e., the ionic generated clusters are rather stable. The method of coupling the PAP directly to the MS offers significant advantages compared to offline sampling methods (e.g. using adsorption tubes): (i) a short measurement time, which allows covering a wide range of experimental parameters; (ii) first results for compounds of interest are obtained within minutes; (iii) adjusting the setup

to find the most efficient experimental conditions is easily possible; (iv) neither time-consuming desolvation nor sample preparation steps are necessary; (v) the compounds to analyze do not need to be known in advance to get valid results (no need to select different adsorbing media).

Complete breakdown of the amines studied, as stipulated by manufacturers of such devices, was not observed. On the contrary, higher molecular weight products are generated. It is quite possible that even higher mass polymers are generated that are not detected in the MS, since the instrument used here was optimized for the mass range m/z = 100-1000. Signal intensity in the higher mass range is lost i.e., the intensity of even higher molecular weight products, if present, are discriminated against. We assume the reactions in the PAP in a fashion similar to those proposed by Atkinson for the tropospheric gas phase chemistry[136] (abstraction of an H atom by OH radicals; O_2 addition to the alkyl radical, forming an alkyl peroxy radical; further reaction with NO to the alkyl radical and with NO_2 in an isomerization reaction to a hydroxyl alkyl radical). However, pinning down details of the reaction mechanisms that occur in the PAP has to await further, detailed study.

It is not known if the compounds formed in the PAP are toxic or not. Therefore, it is generally recommended to study other air purifiers based on plasma using an approach similar to the one shown in this work. Our results suggest that the design of the PAP studied in this work needs to be improved. In its current state it cannot be recommended as an all-round air purification system, since it is not known what influence the molecules generated have on public health. The production of high-mass polymers from small compounds could also present an alternative strategy for removing volatile compounds from polluted air, because polymeric compounds are non-volatile. Non-volatile species could easily be trapped on an electrostatic filter.

6.5 Safety Considerations

We made sure that the entire gas exhaust of the used experimental setup was guided into the laboratory gas exhaust. A special vent was mounted over the (ambient pressure) inlet to the mass spectrometer to guarantee safe working conditions.

Chapter 7

Studying the Degradation Processes of non-Volatile Organic Compounds in a Commercial Plasma Air Purifier

This chapter is adapted from:

Schmid, S.; Seiler, C., Gerecke, A. C.; Hächler, H.; Hilbi, H.; Frey, J.; Weidmann, S.; Meier, L.; Berchtold C.; Zenobi, R., Studying the Degradation Processes of non-Volatile Organic Compounds in a Commercial Plasma Air Purifier, submitted to *J Hazard Mater*.

7.1 Abstract

The performance of a commercially available air purifier based on a cold plasma was studied in detail. This system is capable of handling air flow rates up to 3200 L min^{-1}, much higher than other plasma-based reactors described in the literature, which generally can only handle air flow rates below 10 L min^{-1}. Environmental toxins such as methyltriclosane and phenanthrene were studied as representative of low molecular weight molecules, bovine serum albumin (BSA) as a representative of a high-mass protein, and *Legionella pneumophila* as well as *Bacillus* spp. were chosen to study bioparticles. When passing through the plasma air purifier, we always found a reduction in concentration of the compounds/particles studied. The measured elimination from the gas steream was 31.0% for phenanthrene and 16.9% for methyltriclosane. Since no degradation products were detected by GC-MS analysis, a mass balance study of the entire system was done. It was found that 17.4% of the injected methyltriclosane was deposited on the plasma air purifiers copper electrodes, almost identical to the quantity determined as "degraded" methyltriclosane when switching on the plasma air purifier. For BSA, a reduction of the injected amount of up to 80% was observed. 33% of the bovine serum albumin was deposited on the copper electrodes, when the plasma air purifier was switched on. Due to the rather high standard deviation of our sampling method for BSA, deposition is probably still the major source of reduction. The analysis of a water insoluble portion using matrix-assisted laser desorption mass spectrometry coupled with a high mass detector showed that around 1% of the bovine serum albumin oligomerized in the plasma air purifier. This observation suggests that many different and poorly understood chemical reactions take place in the plasma air purifier. No *L. pneumophila* bacteria survived in the exhaust of the plasma air purifier. The same experiment showed that the plasma air purifier reduced the cell count of aerosolized spores of *B. subtilis* and *B. anthracis* by 26 and 15 fold, depending on whether it was run at 10 Hz or 50 Hz, respectively. At first glance, this suggested that the plasma air purifier worked well for larger bioparticles. However, surviving *Legionella* bacteria as well as *Bacillus* spores were also found on the copper electrodes, which again suggest that a large fraction of the amount introduced is deposited on the electrodes rather than

being destroyed. All the data showed the same result: putative "degradation efficiencies" were largely due to electrostatic precipitation combined with impaction of particles on the copper plates, rather than due to decomposition into smaller molecules.

7.2 Introduction

Air purifiers based on a plasma – most of which incorporate a catalytic stage – are designed to reduce all air contaminants to small nontoxic molecules.[22, 28, 74, 126, 137-139] However, neither the degradation mechanism nor the degradation efficiencies are well understood. In this work we performed a detailed study of the performance and efficiency of a commercial prototype plasma air purifier (PAP), which is driven by alternating current, and forgoes a catalytic stage, and investigated how and whether degradations in such a system is accomplished. Conventional (catalytic) systems can only deal with rather small air flow rates < 10 L min^{-1} [127], whereas the PAP studied here is designed to handle air velocities up to 3 m s^{-1} (corresponding to a flow rate of 3200 L min^{-1}). This particular PAP is supposed to achieve the same degradation efficiency even in the absence of a catalyst. Since the catalytic material needs to be replaced from time to time, the PAP studied here offers the advantage of being completely maintenance free.

To investigate the capabilities of the PAP, we decided to study examples of low-mass environmental toxins, proteins, and various bacteria representative for very high mass bioparticles. For the small mass molecules, we chose waste incineration plant toxins, namely phenanthren and methyltriclosan. These two compounds were studied since the manufacturer of the PAP wanted to incorporate their systems into waste incineration plants. As a high-mass model protein we chose bovine serum albumin (BSA), since it can be obtained in large quantities with sufficient purity. Airborne pathogens are responsible for the majority of infectious diseases and can easily spread indoors. Therefore, we selected Gram-negative bacteria and spore forming Gram-positive bacteria that are known volatile environmental- or airborne infectious agents to be studied in the PAP. Specifically, *Legionella pneumophila, Bacillus subtilis* and *Bacillus anthracis* were chosen, for the following reasons: *L. pneumophila*, the causative

agent of Legionnaires disease, is a Gram-negative human pathogen that is transmitted by aerosols. Many household appliances including showers, hot tubs or warm water supply systems are possible sources of *L. pneumophila*-containing aerosols. Legionnaires disease is of considerable concern especially among elderly and immuno-compromised people.[140, 141] *Bacillus* spp. are Gram-positive bacteria that form spores. Bacterial spores are extremely resistant to physical and chemical stress.[142] Moreover, spores of *B. anthracis* have been successfully weaponized and abused, e.g. during the anthrax letter crisis in the USA in October 2001.

The main goal of this work was to carefully study the performance of a commercially available PAP, focusing on its air-cleaning efficiency as well as the resulting degradation products.

7.3 Materials and Methods

7.3.1 Experimental setup

The PAP used in this study is a catalyst-free, pure AC corona plasma device. It is a commercial prototype incorporating proprietary technology, i.e., some details of its construction cannot be disclosed. However, we provide here all necessary figures of merit and technical data for its characterization. A set-up simulating common heating, ventilation and air conditioning (HVAC) systems was designed in such a way that the PAP could be studied under realistic conditions. **Fig. 7.1** shows the schematic design of the system, which is used in the part of our study with waste incineration plant toxins. From left to right, the experimental setup consists of a high-efficiency particulate air (HEPA) filter that prevents the system from being contaminated by laboratory air. This is followed by a fan that delivers the air flow through the whole system, with a flow rate of 320 to 3200 L min^{-1} (0.3 to 3.0 m s^{-1}). The nebulization interface is located in the middle of the nebulization chamber and is fed with a syringe pump (Fusion 400, KR Analytical Ltd, Cheshire), using flow rates from 25 to 375 µL min^{-1}. Air with a pressure of $3x10^5$ Pa was used as nebulizing gas. For the experiments with *Legionella*, and *Bacillus* spp. an ultrasonic generator (NU52S, Europe Médical) was used for nebulization, and different PAP voltage (20V, 10Hz), and air flow rates of 3200 L min^{-1} through the completely closed system were used.

The core of our system is the PAP itself, which is directly placed after the nebulization chamber. The diameter of the PAP is 160 mm, its length is 180 mm, and its overall weight is 10.5 kg. The plasma electrodes inside the PAP are made of nickel, lead, and copper, and are supported by polyvinyl chloride and poly-(methyl-methacrylate) holders. The dwell time of the compounds in the plasma zone is strongly dependent on the flow velocity through the system, and varies from 0.06 to 0.6 s (0.3 m s^{-1} to 3.0 m s^{-1}). Air flow velocities through our test bench system were measured with an anemometer (PCE group, Germany) at the exhaust and were afterwards converted to air flow rates. In our earlier work on the fate of volatile organic compounds passing through the same PAP it was shown that the higher the air flow rate the weaker the degradation efficiency.[127]

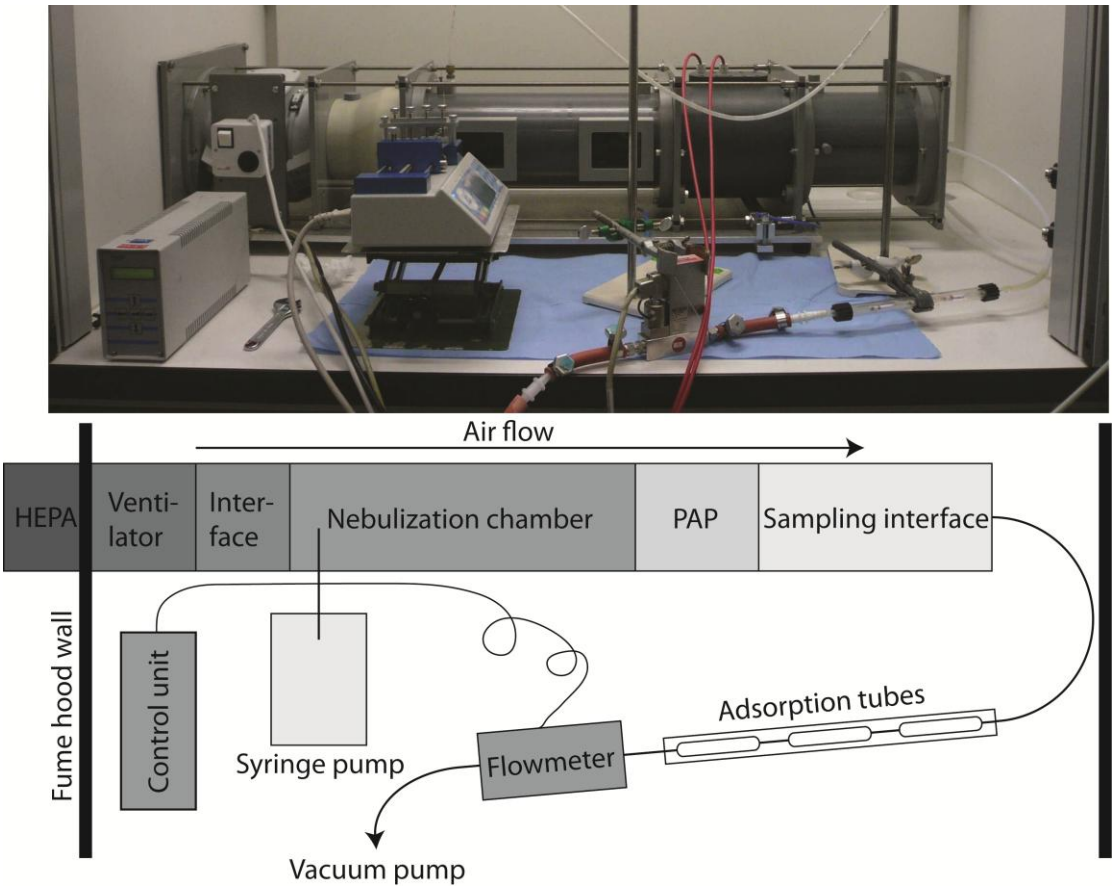

Figure 7.1: Experimental setup used for studying the fate of phenanthrene, methyltriclosane and BSA. Components from left to right: HEPA filter, a high-efficiency particulate air filter that cleans the air before entering the system; fan, continuously adjustable from 0.1-3.0 m s^{-1}; nebulization chamber, is fed with a flow of 25 to 375 µL min^{-1} by a precise syringe pump and capable of putting all components into the gas phase; PAP, plasma air purifier connected to a high voltage power supply; sampling interface, connected to the adsorption tubes; flow meter, used to ascertain a flow rate of 1.0 L min^{-1}; vacuum pump, connected to the flow meter and run at full power.

The plasma in the PAP is generated using normal air, no auxiliary gas is needed. Therefore, it can be installed into all existing heating ventilation and air conditioning systems without high-price modifications. Using an operation voltage of 8.5 kV, an ozone concentration of approximately 300 ppb was measured in the exhaust of the PAP. The humidity during our experiments was determined to be in the 10–14 g/m^3 range. Introduction of a sample increased the humidity by less than 1%. Hence, a change in the ongoing reactions due to a change in humidity during sample introduction is very unlikely. The optical emission spectrum of the plasma generated in the PAP showed a characteristic line at 779 nm due to excited O radical emission, and signals between 300 nm and 450 nm clearly showed the N_2 transitions of the second positive system ($C^3\Pi_u \rightarrow B^3\pi_g$).[69] The next stage consists of the PAP sampling interface, which was adapted with an optimized sampling method for the different compound classes tested. A mass flow controller was used (F 201-CV, Bronkhorst High-Tech B.V., B.V., Ruurlo, Netherlands) to precisely control the volume flow, assuring that in each experiment the same total volume was analyzed. For more information about the experimental setup we refer to our earlier publication.[127] The design of the experimental setup was adapted for suitable analysis for all three substance classes. To test the microbicidal capacity of the PAP in the third part of our study, the system was used in a closed circular way, as opposed to the other two parts of our study, where an open tube was used.

7.3.2 Sample preparation, collection and detection

For the first part of our study, analytical grade methyltriclosane and phenanthrene were purchased from Sigma-Aldrich (Buchs, Switzerland). 54.3 mg methyltriclosane were dissolved in 1200 µL benzene (>99.7%, Sigma-Aldrich) resulting in a concentration of 45.3 g L^{-1}. Phenanthrene was treated in the same way, giving a final concentration of 30.2 g L^{-1}. A sample flow rate of 25 µL mL^{-1} (500 µL total) fed the nebulization interface, which was assisted with pressurized air (3x10^5 Pa) used for complete nebulization. An air flow of 320 L min^{-1} through the experimental system was used throughout all experiments. Sampling was achieved by aspirating exactly 1 L min^{-1} of the exhaust over three adsorption tubes (Supelco ORBO 60, Sigma-Aldrich). Three

absorption tubes were used to assure that everything could be retained during the measurements. Desorption from the adsorption tubes was realized using carbon disulfide (analytical grade, Merck, Darmstadt, Germany). Two external calibrations were established for methyltriclosane and phenanthrene, which were determined using gas chromatography (GC, Thermo Fisher, TRACE GC Ultra, Waltham, USA) either equipped with a flame ionization detector (FID) or a mass spectrometric detector (MSD). Every sample was injected at least twice and the signal areas were averaged. The FID detector was used for quantification while the MSD was used for identification of the observed signals.

Bovine serum albumin (BSA, lyophilized, > 95%, Fluka, Buchs, Switzerland) was used as an example for a high mass protein in the PAP for the second part in our work. In every experiment, 10 mL of a 10 mg mL^{-1} aqueous BSA solution were fed into the nebulization interface with a constant sample flow rate of 375 µL min^{-1}. The sampling in the PAP exhaust was accomplished by bubbling 10% of the whole air flow through water. For this purpose, an impinger was used, which was filled with 80 mL water. After the sample collection step, exactly 50 mL of the resulting solution were transferred into a falcon tube. BSA was quantified on a high performance liquid chromatography (HPLC) system (Agilent, 1100 Series, Santa Clara, California, USA) using a seven-point external calibration. The following dilutions of BSA were made: 7.53 µmol L^{-1}, 3.76 µmol L^{-1}, 1.88 µmol L^{-1}, 0.94 µmol L^{-1}, 0.47 µmol L^{-1}, 0.24 µmol L^{-1} and 0.12 µmol L^{-1}. The coefficient of determination for this calibration was found to be 0.9983. The HPCL method used the following conditions: solvent A, water containing 0.1% trifluoroacetic acid (TFA); solvent B, acetonitrile containing 0.1% TFA; column, symmetry C4 3.5 µm (Waters, Milford USA); detection, 210 nm; loop, 10 µl; gradient, 70:30 A:B for 3 min, followed by a gradient towards 30:70 within 8 min. This ratio was then held for 1.5 min, which resulted in a retention time of 7.1 min for BSA. One measurement included disassembly of the entire PAP and extraction of BSA trapped on the copper electrodes. A beaker was filled with 1 L water, and each of the 4 copper plates were carefully submerged for 5 min in the water to dissolve any deposited BSA. The water was afterwards reduced in a round-bottom flask to a volume of 50 mL. Quantitative analysis was accomplished using a photo array detector coupled to the HPLC system. Every

sample was injected at least twice and the signal areas were averaged. Identification was performed using matrix-assisted laser desorption ionization (MALDI) using a commercial mass spectrometer (ToF/ToF 4800, ABSciex, Darmstadt Germany) equipped with a high-mass detector (HM2tuvo, CovalX, Schlieren, Switzerland).

The following bacterial strains were used for the third part of our study: *L. pneumophila* JR32 (wild-type) [143], *L. pneumophila* GS3011 (avirulent derivative of JR32, deleted in *icmT*, encoding a component of the Icm/Dot transporter),[144] *B. subtilis* (commercially available dry spore preparations used for biological counter-action of plant infections caused by *Erwinia amylovora*) (Andermatt Biocontrol, Grossdietwil, Switzerland), and *B. anthracis* A58 (avirulent derivative of CDC 1014 lacking both virulence plasmids pXO-1 and pXO-2; courtesy of R. Böhm). *L. pneumophila* was grown on CYE agar plates for 3-4 d [145], and *B. anthracis* was grown overnight on LB agar plates,[146] respectively. The F-specific RNA bacteriophage MS2 (ATCC strain: 15597-B1) was propagated in a culture of *Escherichia coli* (*E. coli* K12-Hfr –ATCC 23631) in TYG broth.[147] Spore suspensions were prepared in the following way: The *B. subtilis* dry spore preparation was suspended in sterile water and diluted to yield 10^9 colony forming units per ml (cfu mL^{-1}). Spores from *B. anthracis* A58 were prepared according to a modified protocol from Böhm:[148] Five plates containing sheep blood agar were inoculated with the strain, incubated for 48 h at 37°C, and left to stand in the dark in a biosafety cabinet at ambient temperature for 5 weeks. Spores and surviving vegetative cells were harvested with 10 ml sterile water, pooled and centrifuged for 30 min at 5000 g at 4°C. After elimination of the supernatant, the pellet was resuspended in 5 ml 65% isopropanol and left to stand at ambient temperature for 1 h to eliminate vegetative cells. After addition of 5 ml of sterile water and shaking, the suspension was re-centrifuged as above. The pellet was washed several times each with 5 ml of sterile water, followed by centrifugation, until the supernatant was clear. The pellet was then resuspended in water, diluted to yield 10^9 cfu mL^{-1} and stored at 4°C. This was the final spore count of the suspensions which were afterwards placed in the nebulizer. Samples were taken at intervals of about 1 min according to procedure. After a stable aerosol developed, samples of 20 L air were taken from the exhaust of the PAP.

At each time point, the agar strips were removed from the aspiration sampling device, wrapped in sterile containers and incubated for 3 d (*L pneumophila*) or overnight (*B. subtilis*) before colonies were counted. To quantify the cfu, the PAP was switched off, and the sampling was repeated in an identical manner.

7.3.3 Safety precautions

For the work with the bioparticles, the PAP system was run in a closed loop, and was placed in a fume hood during all experiments performed, to minimize exposure to possible toxic degradation products which could be formed due to the plasma treatment. In order to fulfill biosafety requirements for *L. pneumophila* and *B anthracis*, the following precautions were taken: 1, experiments were carried out in a biosafety level 2 (BL2) (*L. pneumophila*) or in a BL3 facility (*B. anthracis*); 2, the air-tightness of the experimental setup was checked prior to each experiment. Leaks were sealed with silicone; 3, after each experiment, the system was flushed with formaldehyde gas by passing pressurized air through a container containing 37% formaldehyde in water until a final concentration of 300 ppm was reached. Under these conditions, the system was left overnight with the fan running. After this decontamination step, the formaldehyde was neutralized by flushing with ammonia gas generated from a 25% aqueous solution of ammonium hydroxide. The closed loop was opened and dismanteled after the formaldehyde concentration had decreased to less than 20 ppm; 4, after experiments involving *B. anthracis*, the PAP was removed from the system following decontamination step 3, dismantled and disinfected, partly chemically, partly by autoclaving. This step proved to be necessary, because some viable spores surprisingly even survived the overnight formaldehyde decontamination.

7.4 Results

7.4.1 Effect of the PAP on phenanthrene and methyltriclosane

In a first set of experiments, the degradation efficiencies of phenanthrene and methyltriclosane in the PAP were measured. Benzene was chosen as solvent, since it had shown the smallest degradation efficiency in our previous work.[127] The negative controls carried out with benzene did not show any oversaturation

of the adsorption tubes. Furthermore, no signal other than that of benzene was observed in the GC-MS experiments, which confirmed it as a suitable solvent. All experiments were done with and without the PAP switched on, to obtain the quantitative information needed. The experiment with phenanthrene was repeated three times to determine how reproducible the measurements were. 500 µl of a 30.2 g L^{-1} phenanthrene solution were introduced into the system, with a constant sample flow rate of 25 µL min^{-1}. This resulted in a total of 15 mg of phenanthrene introduced. In all three experiments, a reduction of the amount of phenanthrene could be observed when working with the PAP switched on. The mean reduction determined in the three measurements was 31±4%. Besides phenanthrene, it was not possible to identify any other compound by GC-MS and using the National Institute of Standards and Technology (NIST) library. Performing the same experiment with methyltriclosane, a reduction of 16.9% was observed. A second experiment with methyltriclosane was only carried out to see whether deposition in the PAP occurs. **Fig. 7.2** shows the spots where samples were taken. Sampling was done with a benzene wetted Q-tip in an area of approximately 2 cm^2. The table in **Fig. 7.2** shows the qualitative signal intensity in different spots. Surprisingly, most material was deposited on the surface of the copper electrodes. According to these results, it was decided to conduct a mass balance for methyltriclosane to determine how much of it adhered to the copper plates. The experiment was repeated twice, once with and once without the PAP switched on. Each of the four copper plates were then submerged in CH_2Cl_2 for 5 min to dissolve all deposited compounds. The solution was filtered, reduced to 10 mL, and analyzed with GC-MS. With the PAP switched on, 3.9 mg of methyltriclosane were found to be deposited on the copper electrodes, which corresponds to 17.4% of the injected methyltriclosane. The negative control experiment with the PAP switched off showed that only 0.3% methyltriclosane were trapped on the copper electrodes. These results suggest that the observed reduction in the amount of methyltriclosane and phenanthrene is entirely due to deposition on the copper plates, not from any decomposition of these molecules into small fragments such as H_2O and CO_2. Neither oxidation products of methyltriclosane and phenanthrene nor compounds other than methyltriclosane were found in the extract of the copper

plate. These results let us conclude that electrostatic precipitation is responsible for the apparent decrease in the compound amounts, rather than chemical/physical degradation as previously assumed.

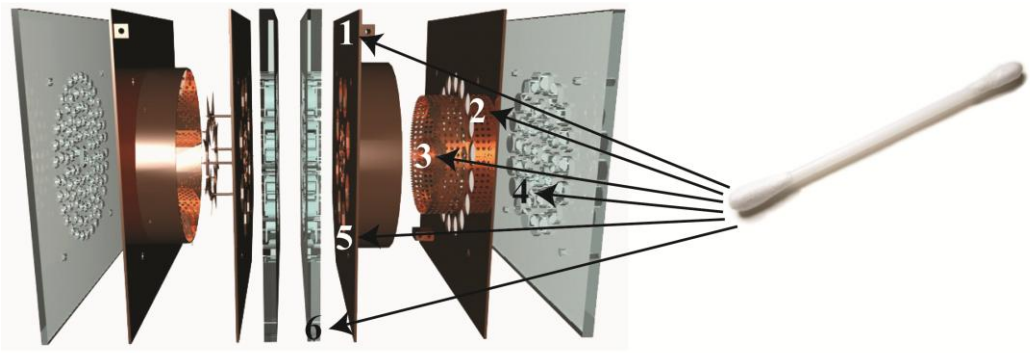

Location	Position Name	Observed Phenanthrene			Observed Methyl Triclosane		
		Not observed	Small signal	Strong signal	Not observed	Small signal	Strong signal
1	PVC tube	X			X		
2	Cu plate inside		X				X
3	Cu grid		X				X
4	Plexiglass back	X			X		
5	Cu plate with ring		X				X
6	Plexiglass middle	X				X	

Fig. 7.2: PAP wipe test: samples were taken at 6 different 2 cm^2 spots. They were then analyzed and quantified using GC-FID.

7.4.2 Effect of the PAP on bovine serum albumin

Next, the effects of the PAP on a protein such as BSA were investigated. A 7-point external calibration curve for BSA was established on an HPLC equipped with a photo diode array detector for quantification. Identification of the BSA was done using MALDI-MS for all samples taken. Based on the results for the small toxic compounds, it was decided to estimate the mass balance experiments. Therefore, each experiment included spraying the BSA solution and collecting 10% of the exhaust by bubbling it through water, as explained in detail in the materials and methods section. Experiments with the PAP switched on or switched off were repeated 4 times. A BSA reduction of 81% was observed when the PAP was on. However, the experiments with the PAP switched on showed a rather high relative standard deviation of > 20%. After performing the experiments with the PAP switched on, a clearly visible white coating covered the copper plates (see **Fig. 7.3**), whereas this was not observed in the experiments with the PAP switched off. Analysis of the copper plate extracts showed that 29±4% of the introduced BSA was deposited on the plates during a

measurement with the PAP switched on. We assume that a portion of the introduced BSA is also deposited on the plexiglas and PVC pieces in the PAP. However, we do not assume this to be major fraction of the total amount of BSA introduced, since during the measurements with the PAP deactivated only 0.8±1.0% BSA was deposited on the copper plates. Surprisingly, solid white particles were found in the copper plate extract. The particles could not be

BSA	PAP	Introduced [mg]	Measured [mg]
Water phase	off	100	1.95±0.01
Water phase	on	100	0.37±0.11
Copper electrodes	off	100	0.85±1.01
Copper electrodes	on	100	32.69±2.29

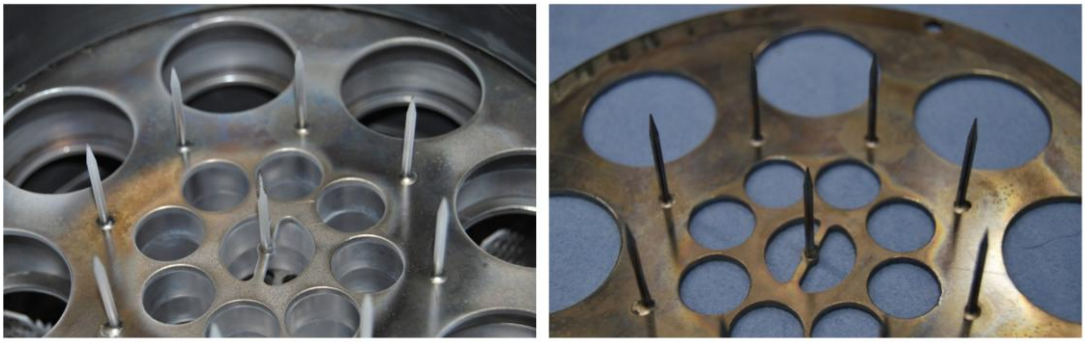

Copper electrode, PAP on | Copper electrode, PAP off

Figure 7.3: BSA experiments: measured amount of BSA in the exhaust of the PAP as captured by drawing the exhaust through water (table). BSA deposited on the PAP electrodes is described as "copper electrodes" in the table. The image on the left shows the second copper plate after one BSA experiment with the PAP switched on. The image on the right shows the second copper plate with the PAP switched on.

dissolved in organic solvents. After 10 washing steps with water (to get rid of the BSA), the white particles were lyophilized, weighted, again dissolved with acetonitrile and afterwards analyzed with a MALDI-MS equipped with a high mass detector. **Fig. 7.4** clearly shows that the particles contained oligomeric BSA. The only explanation for this finding is a polymerization reaction that must have occurred either on the copper plates, in aqueous phase, or in the gas phase. As no BSA polymers could be found elsewhere in the system, it is very likely that the bigger the particles are, the higher the collection efficiency of the PAP is. The polymerized BSA corresponds to approximately 1% of the introduced BSA, which means that the majority of the BSA was not in the polymerized form. We assume that the rather high variance between the different experiments is due to sampling error, which could explain the missing BSA in our mass balance. Again,

we surmise that in this particular PAP, a mineralization (degradation to H_2O, CO_2 etc.) of the BSA is not taking place or only to a negligible extent. For BSA, too, the PAP most likely works like an electrostatic precipitator[149] combined with impaction,[150] whereas the anticipated degradation to smaller, nontoxic compounds is unlikely to occur.

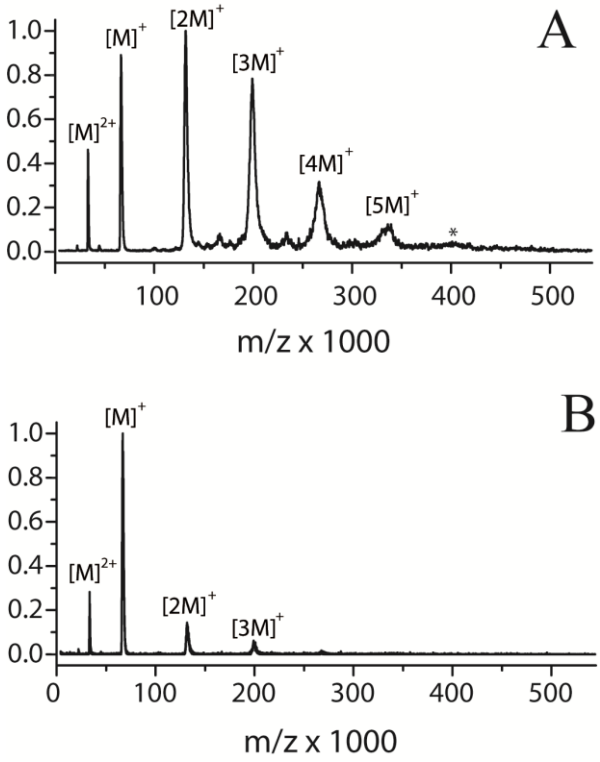

Figure 7.4: A: Mass spectra of the polymerized BSA suspended in H_20:ACN (1:1). B: Mass spectra of BSA standard using the same conditions. The mass spectra were recorded using a MALDI-TOF system equipped with a high-mass detector. The signal marked with an asterisk could be the $[6M]^+$ oligomer.

7.4.3 Effect of the PAP on various bacteria

To test the capacity of the PAP to destroy Gram-negative bacteria, *L. pneumophila*, an airborne human pathogen was chosen. The effect of the PAP on *Legionella*-containing aerosols is shown **in fig. 7.5**. When the PAP was switched on, non-pathogenic (**fig. 7.5A**) or pathogenic (**fig. 7.5B**) *L. pneumophila* could not be detected in the exhaust of the PAP. In contrast, when the PAP was switched off, the number of cfu detected in 20 L of air increased over a period of about 5 to 7 min to 2200 (non-pathogenic *L. pneumophila* strain GS3011) or

1500 (pathogenic *L. pneumophila* strain JR32). After a maximum, the cfu count dropped again.

In these experiments, a highly concentrated aerosol of virulent *L. pneumophila* (75'000 cfu m^{-3}) was introduced, and the PAP seemed to be very effective in removing the *L. pneumophila*-containing aerosol at this concentration, since no viable *L. pneumophila* could be detected in the airspace of a chamber located immediately after the PAP. It is possible that some bacteria did not survive the ultrasound treatment used for the aerosolization or adsorbed to the surface of the experimental setup. Deposition on the copper plates might also account for the decrease in bacteria numbers after a peak of 1500 and 2200 cfu in 20 L of air, respectively.

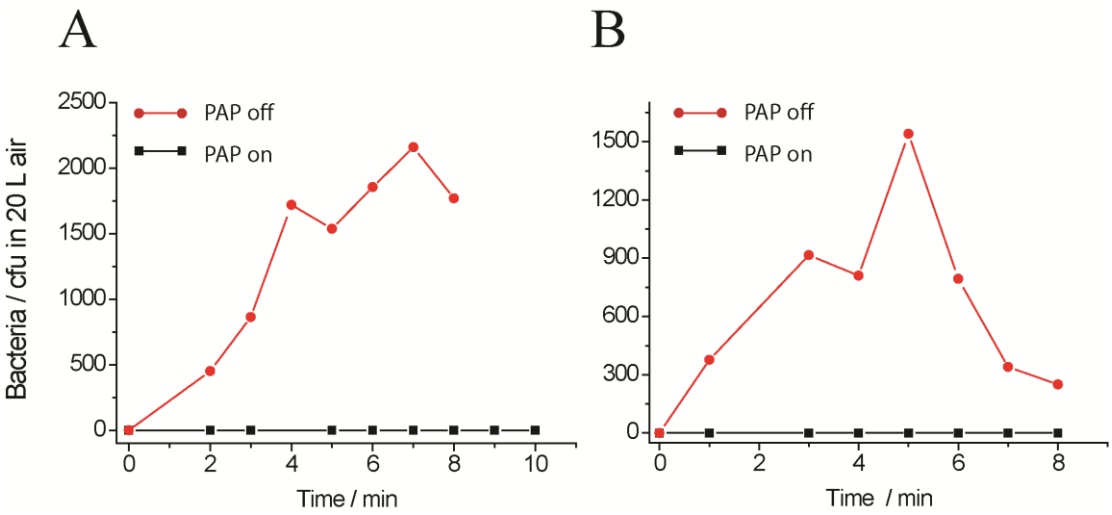

Figure 7.5: A: Survival of aerolized, non-pathogenic *L. pneumophila* under conditions where the PAP was either switched on or off. Non-pathogenic *L.pneumophila* strain GS3011 in 20 L of air was quantified on CYE agar strips. B: Survival of aerosolized, pathogenic *L. pneumophila* under conditions where the PAP device was either switched on or off. Pathogenic *L. pneumophila* strain JR32 in 20 L of air was quantified on CYE agar stripes.

7.4.4 Effect of the PAP on spores

The effect of the PAP on bacterial spores was assayed by using spores of Gram-positive *B. subtilis* and *B. anthracis*. The following protocol was applied to test the activity of the PAP on spores of *B. subtilis* (**fig 7.6A**): First, a negative control sample with the fan and the PAP running at 20 V and 10 Hz but without spore supply was taken. Subsequently, aerosolization of the spores was initiated and samples were taken for about 11 min. Then, the AC frequency was changed to 50 Hz and after about 22 min, the PAP was switched off while ventilation and

aerosolization continued for another 10 min. Viability of the spores was recorded at intervals of around 1 min.

The mean decrease in viable spores was calculated according to the formula given below.

$$d = \frac{\sum \text{cfuPAP}^{+} / \text{nPAP}^{+}}{\sum \text{cfu PAP}^{-} / \text{nPAP}^{-}}$$

d = mean decrease; PAP+ = PAP switched on; PAP- = PAP switched off; n = number of data points per measuring sequence. The mean decrease of viable spores when running the PAP at 10 Hz or 50 Hz was found to be a factor of 26.4 or 15.1, respectively.

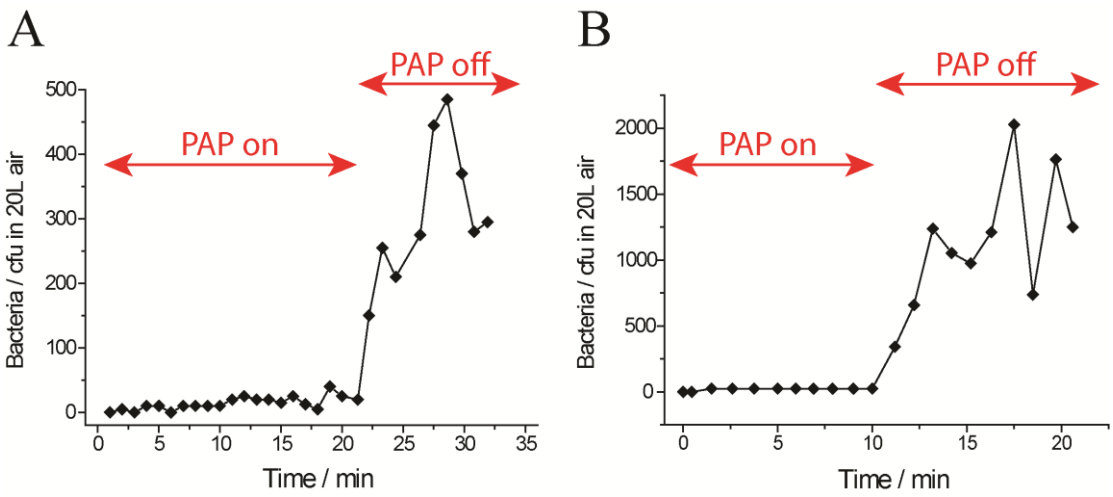

Figure 7.6: A: Survival of *B. subtilis* spores in 20 L of air was quantified on LB agar strips. During the experiments, the PAP was running at 10 HZ and 50 Hz respectively, or switched off. **B**: Survival of *B. anthracis* spores in 20 L of air were quantified on LB agar strips. During the experiments, the PAP was running at 10 Hz and 50 Hz respectively, or switched off.

Another experiment was carried out on *B. anthracis* A58 spores using two serially connected PAPs rather than just one, in order to assess the expected synergy effect (**fig. 7.6B**). The first device was operated at 10 Hz, the second one at 50 Hz. Otherwise, the experimental settings were as above. The data (not shown) allowed calculation of a mean decrease of viable cfu by *B. subtilis* of d = 73.9-fold. This is higher than either rate reached with a single device, but not as high (398-fold) as might have been expected by simple multiplication of the rates determined in the experiments with a single PAP. Obviously, air current and

dynamics of inactivation of spores are more complex. To determine whether PAP caused spores to absorb to surfaces, and what the effect of the plasma inside the PAP was on surface-absorbed spores, the aerosolization of *B. subtilis* was stopped in the experiments, while the PAP was still running at 20 V and 10 Hz for 15 min. Then, several sites inside the aerosol generator, the PAP and the wind tunnel were wiped with sterile swabs for detection of viable spores on surfaces before disinfection with formaldehyde. At each site, an area of about 2 cm^2 was wiped, and the swab was rolled onto blood agar. All tested surfaces were found to be still contaminated. Interestingly, rather high concentrations (101-300 cfu) of living spores could be found on the copper electrodes of the PAP.

These results showed that the PAP did not or only insufficiently decontaminate surfaces, regardless of whether the surfaces were located outside or inside the device. Even on the electrodes of the device, spores survived. These results are in a good agreement with the data measured in the previous experiments, where a major part of the organic compounds studied were deposited on the copper electrodes. Unfortunately, it cannot be deduced if and how much of the spores are deactivated. Nevertheless, it seems again that the reduction in the number of bioparticles by the PAP is due to a combination of electrostatic precipitation and impaction; degradation to smaller molecules is probably largely absent rather than being the main reason for the decreased number of bacteria or spores after passing the PAP. Since a flow rate of 3200 L min^{-1} was used to study the fate of bioparticles passing through the PAP, it seems to work efficiently with flow rates in the range of those used in heating, ventilation, and air conditioning systems. Notably, compared to other plasma based air purifying systems the PAP studied here works with rather low specific input energies. The specific input energy (SIE, in J L^{-1}) is defined as the discharge power (J s^{-1}) divided by the air flow rate in L s^{-1}. Higher air flow rates thus result in lower specific input energies. With a flow rate of 3200 L min^{-1} the PAP has a rather low SIE of around 0.5 J L^{-1}, much smaller compared to model reactors described in the literature that sometimes reach SIE values up to 760 J L^{-1}.[20, 21, 27-29, 33] Hence, such model reactors are not suitable to be incorporated into

heating ventilation and air conditioning systems, whereas the PAP can be operated with suitable air flow rates.

For all substances, passage through the PAP caused deposition on the copper plates. Oligomerization of BSA was indicated by a white (and water insoluble) material adhering to the copper plates. Reduction in the numbers of aerosolized bacteria showed that the PAP is capable of reducing the numbers of bacteria in heating and ventilation systems. However, the reduction is thought to be mainly due to adherence to the copper plates rather than to degradation to smaller particles, which is the main degradation mechanism in other plasma based air purification systems incorporating catalytic stage.[22, 27, 28, 74, 126, 137-139]

Table 7.1: Percentage of compound deposited on the copper electrodes as well as the reduction in the PAP exhaust (in %) with the PAP switched on.

	Compound Studied	Measured reduction [%]	Amount deposited on the copper electrodes, PAP switched on [%]
Low molecular weight molecules	Methyltriclosane	16.9	17
High molecular weight protein	Bovine Serum Albumin	81	33
Bioparticles	*L. pneumophila*	100	Survivals
	B. anthracis	>90	Survivals

Table 7.1 compares the reduction efficiency to the measured deposition efficiencies of the PAP. The results indicate that the larger the molecule, the higher the deposition efficiency inside the PAP. One reason for different deposition efficiencies is likely an effect of electrostatic precipitation where particles get charged by the attachment of ions, which are presumably produced in the PAP. Charged particles are attracted by the electrical field to their counter electrode. This effect is called “field charging” and is known to be dominant for larger particles.[149] Small particles diffuse much more easily and stay in the air whereas larger particles cannot follow the airflow and collide with the copper electrodes.

In summary, the results of this study show that the PAP studied here, which is purely plasma based, does not seem to efficiently degrade air pollutants to small nontoxic compounds. Although a reduction in the number of particles was always observed when working with the PAP switched on, this reduction is suggested to be due to electrostatic precipitation combined with the principle of an impactor.

Chapter 8

Electrosonic Spray Ionization - an Ideal Interface for High-Flow Liquid Chromatography Applications

This chapter is adapted from:

Schmid, S.; Jecklin, M. C.; Zenobi, R., Electrosonic spray ionization—An ideal interface for high-flow liquid chromatography applications. J. Chromatogr. A **2011**, *23*, (1), 3704-3710.

8.1 Abstract

Electrosonic spray ionization (ESSI) has been studied as an interface between high-performance liquid chromatography (HPLC) and mass spectrometry (MS), using sample flow rates up to 3.0 ml min^{-1}. This ionization interface was compared with pneumatically assisted electrospray ionization (ESI) using mass spectrometry for detection. For experiments that did not involve direct comparison of different flow rates, the ESI experiments were performed using post column splitting to work at optimal conditions. ESSI allows the interfacing of conventional or high-resolution liquid chromatography (LC) methods to mass spectrometry without post column splitting. High sample flow rates could be handled without a significant loss of signal intensity using a nebulization gas flow rate of 5.5 L min^{-1}. Since ESI needs to be operated with lower sample flow rates, it is limited to micro/nano LC systems, or post column splitting must be used. In particular, nano LC systems have to be treated with great care and require constant maintenance. When using post-column splitting, the increased diffusion can become a problem especially when using systems with very small void volumes. In all experiments ESSI showed better signal intensities than a commercially available, pneumatically assisted ESI source. ESSI does not require heating of the nebulizer gas, which should help to preserve the original structure of thermally unstable molecules. The observed LC-ESSI-MS ion chromatograms are shown to be very stable even when using flow rates higher than 1.0 ml min^{-1}, which could be very suitable for ultra-high performance LC, where sample flow rates up to 2.0 mL min^{-1} with backpressures up to 1200 bar are used. Also, a difference in the relative intensities of singly and doubly protonated peptide monomers and dimers was observed between the two ionization methods. The coefficients of determination for the calibration of instrument response for Val-Tyr-Val and Met-Enkephalin showed excellent linearity over a wide concentration range (0.1 to 100 µM), while ESI results were only linear over a much smaller range (0.1 to 20 µM). The observed behavior is thought to be caused by insufficient ionization efficiency of solutions above ~20 µM by ESI, exemplifying the robustness of ESSI as an interface between LC and MS.

8.2 Introduction

Liquid chromatography-mass spectrometry (LC-MS) has become one of the most popular analytical techniques during the last 10-20 years for the analysis of a wide range of compounds.[151, 152] The three most widely used atmospheric pressure ionization (API) technique that have been developed for a facile coupling of LC with MS are electrospray ionization (ESI), atmospheric pressure chemical ionization (APCI), and atmospheric pressure photoionization (APPI), as recently reviewed by Kostiainen and Kauppila.[152] Among the most widely used API technique today is ESI. LC-ESI-MS is a highly sensitive and specific analysis method for small polar organic compounds and large biomolecules.

In LC-ESI-MS, water is a poor solvent compared to organic solvents due to its higher surface tension, lower volatility and high dissolving energy, which makes it hard to electrospray aqueous solutions. This is a real drawback if highly aqueous conditions are required for good separation in the LC procedure. A further drawback for LC-ESI-MS is the relatively low maximum tolerable flow rate, which is around 20 µL min^{-1}.[153] This means that conventional LC columns (4.6 mm ID) require post column splitting. Higher flow rates, up to 200 µL min^{-1}, can be handled using a pneumatically-assisted electrospray, formerly referred to as ionspray, an interface developed by Bruins et al.[154] Most of the modern ESI interfaces in use today are pneumatically assisted, usually using nitrogen as a "sheath" gas. In 1992, Lee and Henion[155] described a thermally assisted interface capable of operating with flow rates up to 500 µL min^{-1} using temperatures from 150 to 240 °C. Hopfgartner *et al.*[156] presented a high-flow LC-ESI-MS interface, which allows for the use of flow rates up to 2 mL min^{-1} by adding a simple liquid shield between the ion sampling capillary and the pneumatically-assisted (nitrogen gas pressure $5.4x10^5$ Pa) ESI. At the same time Hiraoka *et al.*[157] presented pneumatically assisted ESI parallel to the ion sampling orifice using $2\text{-}2.8x10^5$ Pa nebulizer gas (N_2), which gave them the opportunity to accommodate sample flow rates up to 4.4 mL min^{-1}. However, at 4.4 mL min^{-1} the measured ion intensity decreased by nearly a factor of 10. Furthermore, the entire optimization of their setup was done with a much smaller sample flow rate, 100 µl min^{-1}. Sonic spray ionization (SSI) was

introduced as an interface for CE-MS and LC-MS in 1994. In this technique, charged droplets are produced without a heating capillary or applying an electric voltage to the capillary tip. A sample solution is introduced through a capillary with a coaxial gas flow. It was shown that charged droplets are produced in the spray at atmospheric pressure at high gas velocities. Gas flow rates up to 6 L min^{-1} could be used, with an optimum at 3 L min^{-1}. It was also found that the ion intensity strongly depended on the gas velocity; an intensity maximum was reached at sonic speed (around Mach 1).[57, 158] A study reported a linear nitrogen velocity between Mach 1 (333 m s^{-1}) and Mach 3 (1000 m s^{-1}) using SSI to couple LC with MS.[62] Ion formation can be explained by the proposed statistical charging model.[159] In 2002, the performance of SSI was compared to the better known ESI interface for LC-MS. Similar results were found and in some cases even better sensitivities for opiate analysis were obtained using the SSI interface.[61] Recently SSI has become commercially available as an interface for LC-MS systems.[62, 63]

In 1994, SCIEX introduced turbo-ionspray, which is capable of handling a flow rate of 1 mL min^{-1}, by the use of a heated gas beam to improve the desolvation of the sprayed droplets. After 2003, several manufacturers have introduced ion sources for high flow applications using heated desolvation gas, which underscores that there was and still is a need for interfacing to high chromatographic solvent flow rates. A solvent flow rate of 1 ml min^{-1} could be handled with the ESI source offered by Waters, which uses additionally to the nebulizer gas heated desolvation gas to handle this flow rate. SCIEX introduced in 2003 the TurboV source, a further improvement of the turbo-ionspray.[160, 161] The HESI II (2008) source is the improved version of the HESI source from Thermo Fisher which uses a nebulization gas temperature of 773 K and an ion transfer tube temperature of 673 K. Using this source, solvent flow rates up to 1 mL min^{-1} can be handled. A flow rate up to 2.5 mL min^{-1} can be efficiently nebulized using the Agilent Jet Stream system (2009) with the aid of a coaxial super-heated sheath gas to create a higher ion density in front of the MS cone. AB SCIEX markets the API 4000 system, which uses a dual heater technology with improved gas dynamics. This ion source is promoted for handling flow rates up to 3 mL min^{-1}.

Electrosonic spray ionization (ESSI) is a new variant of pneumatically assisted ESI, which achieves very efficient nebulization without heating to high temperatures. It was introduced by Takats *et al.*[64] in 2004 combining a supersonic gas jet (similar to SSI) with ESI. When analyzing protein samples, extremely narrow charge state distributions and sensitivities similar to nanoESI were described. Varying the spray potential from 0 V (pure SSI) to 3.0 kV, the intensity was found to increase by a factor of 2. It was argued that increasing the gas flow rate leads to very efficient solvent evaporation and causes a lower temperature of the spray by adiabatic expansion of the nebulization gas. Moreover, low peak broadening and the observation of one predominant charge state were notable. From their observations it was concluded that proteins are close to a "native-like" conformation in the gas phase when sprayed by ESSI.[64] ESSI-MS has therefore generated interest to study non-covalent protein interactions.[64, 66]

The aim of this work was to study the figure of merit of ESSI as an alternative HPLC-MS interface to the commercially available heated ESI sources by AB SCIEX, Thermo Fischer, Agilent and Waters. Using higher sample flow rates combined with small diameter columns help to reduce the overall solvent consumption as well as the separation time of an analyses.[162] Therefore, interfaces which can handle high sample flow rates are becoming more interesting. In ESSI, one order of magnitude higher nitrogen pressure (up to $2.3*10^6$ Pa) and nebulization gas flow rates are used than typically employed in pneumatically assisted ESI.[156] The higher nebulization gas flow rate produces smaller droplets, which help to get more molecules into the gas phase even when the water content of the solvent is quite high. Moreover, no heating of the nebulization gas is needed, and ESSI is thought to be a much softer ionization source compared to other commercially available ion sources.[66]

8.3 Experimental Section

8.3.1 Materials and sample preparation

Water was purified in-house using a Millipore system (Bedford, MA, USA). Acetonitrile (HPLC grade, Sigma Aldrich, Buchs, Switzerland) and trifluoroacetic acid extra pure >99% (TFA, Acros Organics, Chemie Brunschwig, Basel,

Switzerland) were used to prepare the mobile phases for sample separation. A HPLC standard mixture of the peptides used in this work (0.5 mg Gly-Tyr (G3502) MW 238.2, 0.5 mg Val-Tyr-Val (V8376) MW = 379.5, 0.5 mg Met-Enkephalin (M6638) MW = 573.7, 0.5 mg Leu-Enkephalin (L9133) MW 555.6, 0.5 mg Angiotensin II (A9525) MW 1046.2, was purchased from Sigma Aldrich (Buchs, Switzerland). This peptide mix was dissolved in 1.00 ml (±0.01) water and afterwards used as stock solution. Calibration was performed using seven dilutions of the stock solution (50 μg mL^{-1}, 10 μg mL^{-1}, 5 μg mL^{-1}, 1 μg mL^{-1}, 0.5 μg mL^{-1}, 0.1 μg mL^{-1} and 0.05 μg mL^{-1}) in water/acetonitrile (1:1) containing 0.1% TFA. A 10 μg mL^{-1} Tyr-Tyr-Tyr (Sigma Aldrich, Buchs, Switzerland) solution used for the performance optimization was prepared by diluting 100 μL of a 10^4 μg mL^{-1} Tyr-Tyr-Tyr stock solution in 75:25 acetonitrile/water containing 0.1% TFA.

8.3.2 Liquid chromatography

All experiments described in this work were performed on an HPLC (Model Shimadzu SCL-10A VP, Duisburg, Germany) equipped with a photo diode array detector (SPD-M10A VP). The LC effluents were delivered by an LC-10AT VP pump which itself was connected to a low pressure mixing valve (FCV-10AL VP). The samples were loaded with an external manual sample injector (Rheodyne, Whitstable, UK) using a 20 μl loop. Method development was done off-line with the photo diode array (PDA) detector set to 220 nm. A flow rate of 1.0 mL min^{-1} was used throughout, unless otherwise noted. The chromatographic separation of the peptide mix was accomplished with a Waters Symmetry300™ C4 column (4.6x150mm, 3.5 μm, Waters, Milford, MA, USA) using the following method: starting with 100% A, holding this ratio for 4 min, decreasing in 7 min to 70% A and finally holding this ratio again for 2 min (A = 5:95 acetonitrile/water containing 0.1% TFA; B= 75:25 acetonitrile/water containing 0.1% TFA). The HPLC was controlled by the CLASS-VP version 614_SP1 software.

8.3.3 ESI source

ESI measurements were carried out using a commercial source (Waters/Micromass Ltd.). The inner diameter of the stainless steel (SS) spray

capillary was 75 µm and the spray distance (capillary tip to the orifice of the Q-TOF) was adjusted to 1 cm. The ESI probe was mounted in the commercially available housing, which fixes the ESI source perpendicular to the MS cone. The tip of the SS capillary was adjusted to protrude 0.5 mm from the nebulizer capillary. The ESI source is capable of handling a flow rate of 1 mL min^{-1}, since it is designed for coupling with standard HPLC systems; for best performance the manufacturer suggests a flow rate of around 200 µL min^{-1}. The nebulization gas flow was set to 2.5 L min^{-1} and the desolvation gas valve was fully opened (~ 500 L h^{-1}, 523 K, for further information see supporting information). A capillary voltage of 3.5 kV was applied to the SS capillary. For all comparisons between ESI and ESSI except the experiments where the solvent flow was directly compared, post column splitting was used for the ESI to operate it in optimal conditions. **Fig. 7.1** shows the schematic of the commercial available ESI source from Waters (Manchester, UK). The ESI source used for the presented work was acquired in

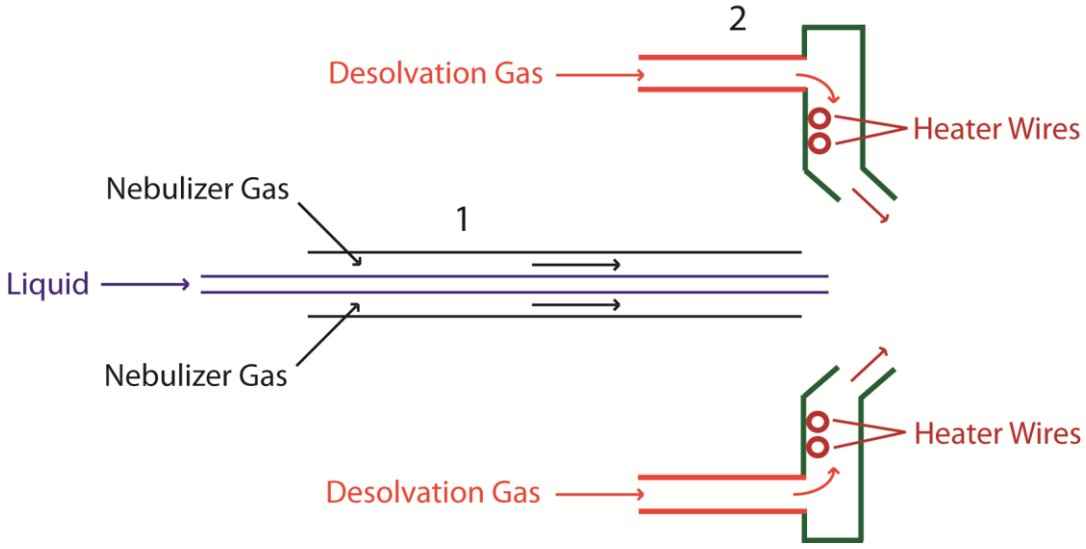

Figure 7.1: Schematics of the standard ESI source from waters. 1. ESI source, 2. Desolvation gas delivered by the QToF Ultima system

2009 and used throughout for all ESI experiments. The desolvation gas can be heated, whereas the nebulizer gas cannot. The used ESI (cf. **fig. 7.1**) ion source is on the market since around 1990. Improvements have been done with the heated desolvation gas (cf. **fig. 7.1**) when the QToF Ultima system was available on the market. The highest applicable solvent flow rate using the Waters ESI ion source is 1 mL min^{-1} (according to Waters). However, it is suggested to split the

flow rate if it is higher than 200 µL min^{-1}. Hence, post column splitting was used for the most experiments using the commercial ESI source.

8.3.4 ESSI source

ESSI measurements were performed using a modified design of the ESSI source described by Takats *et al.*[64] For a detailed description of the ESSI source used for this work see Jecklin *et al.*[66] A spray angle of 90° was used throughout, similar to the Z-shaped ESI interface, in order to minimize contamination of the source region.[66, 163] Note that the 90° angle differs from that used in our previous work. The spray distance was kept at 1 cm, unless otherwise noted. Nitrogen was used as nebulizing gas at a pressure of 20 bar (5.5 L min^{-1}), unless noted otherwise.

8.3.5 Mass spectrometer

Mass spectrometric analysis was performed with a hybrid quadrupole time-of-flight mass spectrometer (Q-TOF Ultima; Waters/Micromass Ltd., Manchester, UK, Our QToF Ultima MS system was installed on the 17 November in 2004. The last revision of our system was executed in 2009. This included also the change of the detector (microchannel plate).) equipped with a Z-spray interface. The instrument was controlled by the MassLynx version 4.0 software. All measurements were performed in positive ion mode. The source temperature was kept at 353 K for ESI and ESSI measurements. The sampling cone voltage was kept at 35 V for all the measurements. The RF1 voltage, the potential applied to the first ion tunnel in the linear flight path before the quadrupole, was varied from 40 to 100 V. The cone gas flow on the other hand was set to ~1 L h^{-1} for ESI as well as ESSI.

8.3.6 Safety considerations

Since a huge amount of solvent is being evaporated during the experiments, an additional gas exhaust close to the ESSI source is recommended. Since ESSI generates more noise than conventional ESI, it is recommended to use the interface in a noise reducing housing.

8.4 Results and Discussion

In the first set of experiments, the gas flow rate and spray distances of the ESSI setup were optimized in order to get the highest signal intensity in the absence of the HPLC system. To minimize contamination of the mass spectrometer from the high rate of sample delivery, all experiments were performed using a Z-spray configuration. The summed ion current of Tyr-Tyr-Tyr (*m/z* 508) from a 30 s acquisition at three different sample flow rates and two ESSI positions as a function of nebulizer gas flow is presented in **fig. 7.2a**. The results were obtained by direct infusion experiments. Three sample flow rates (0.1 mL min^{-1}, 1.0 mL min^{-1} and 2.0 mL min^{-1}) were tested at eight different nebulizer gas flow rates (1.5 L min^{-1}, 2.2 L min^{-1}, 2.8 L min^{-1}, 3.5 L min^{-1}, 4.2 L min^{-1}, 4.8 L min^{-1}, 5.5 L min^{-1}, and 6.2 L min^{-1}). Every point was measured three times by acquiring data for 30 s. The spray position (1 to 6 cm) was optimized by monitoring *m/z* 508 $[M+H]^+$ for a sample flow rate of 0.1 mL min^{-1}. The spray distance resulting in the best signal intensity was found to be ~ 1 cm. This is in excellent agreement with the data found in the literature where 1 cm has been determined to be the optimal spray distance with various protein samples.[64] When compared to a spray distance of 6 cm, the signal intensity could be improved by a factor of ~ 6 (*cf.* **fig. 7.2a**). When using a higher sample flow rate the spray plume becomes wider and thus a smaller percentage of the total plume was sampled by the MS cone. This resulted in a decrease of signal intensity. A higher nebulizer gas flow helps to reduce this effect by allowing for better focusing of the spray in the direction of the MS cone. At a spray distance of 1 cm and a nebulizer gas flow rate of 3.5 – 4 L min^{-1} the intensity seems to reach a plateau. For a sample flow rate of 0.1 mL min^{-1}, this plateau was reached at a nebulizer gas flow rate of 3.5 L min^{-1}. For a sample flow rate of 1.0 mL min^{-1} the maximum intensity occurs at the highest nebulizer gas flow tested. Using a sample flow rate of 2.0 mL min^{-1} a plateau appears at 5.5 L min^{-1}. A nebulizer gas flow rate of 5.5 L min^{-1} seemed optimal for all studied sample flow rates, which was the value chosen for all further experiments. However, at a certain point complete desolvation will be reached, as indicated by the plateau. These measurements were repeated for a spray distance of 6 cm. The observed intensity maximum, however, seemed to be reached at higher nebulizer gas flow

rates, and the absolute ion current intensity obviously has decreased. The reason for this ion loss is that the spray has a much wider spatial distribution using a distance of 6 cm. Therefore a spray distance of 1 cm has been chosen for the ESSI distance of 1 cm. The partial pressure of the solvent in the spray region using ESSI will be rather low and the resolvation of the analyte is slow even though very high flow

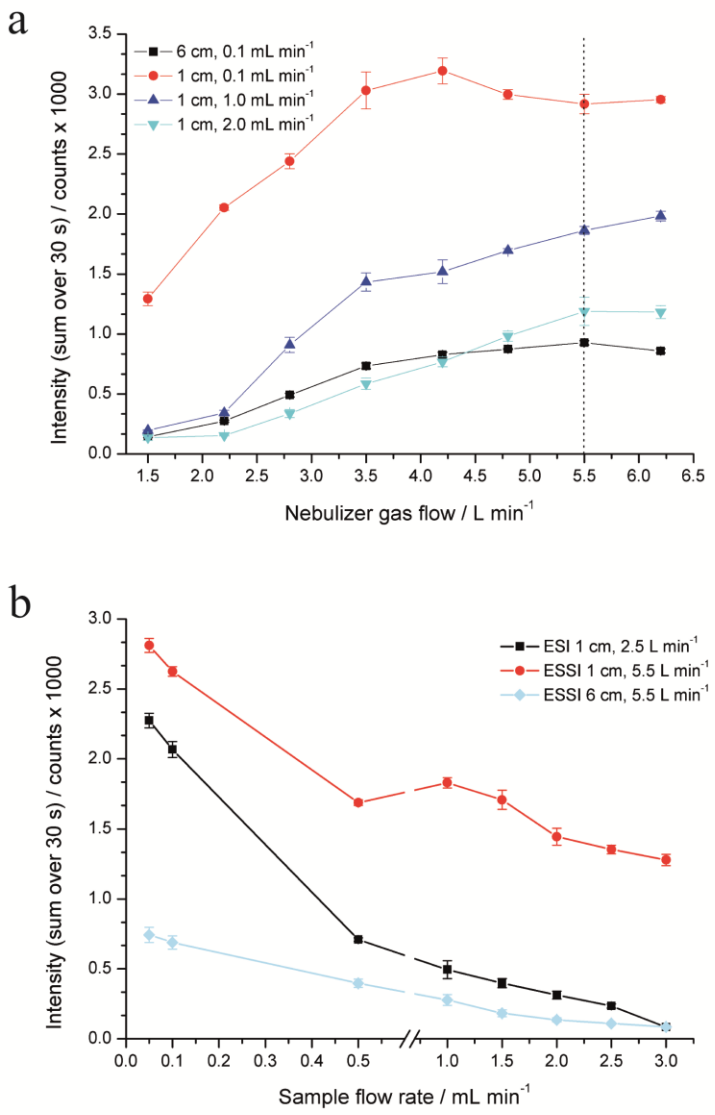

Figure 7.2: a) Dependence of the signal intensity on nebulizer gas flow, for three different sample flow rates and two different distances to the orifice, using the ESSI interface. The sample was delivered to the interface by the LC pump system. Nitrogen was used as nebulizer gas. 30 s of the measured data were averaged (n=3). The dashed line indicates the nebulizer gas flow rate near the optimum that was used in all subsequent measurements. b) Signal intensity versus versus nebulizer gas flow for ESI and ESSI, for two distances to the orifice. Sample delivery was achieved using the LC system. The nebulizer gas flow was adjusted by changing the nitrogen gas pressure. 30 s of the measured data were combined (n=3). The measurements at 6 cm were also performed with ESI but no significant signals were detected.

rates are used. This is thought to be one of the key reasons why ESSI was observed to outperform ESI.

At a spray distance of 1 cm and a nebulizer gas flow rate of 3.5 – 4 L min^{-1} the intensity seems to reach a plateau. For a sample flow rate of 0.1 mL min^{-1}, this plateau was reached at a nebulizer gas flow rate of 3.5 L min^{-1}. For a sample flow rate of 1.0 mL min^{-1} the maximum intensity occurs at the highest nebulizer gas flow tested. Using a sample flow rate of 2.0 mL min^{-1} a plateau appears at 5.5 L min^{-1}. A nebulizer gas flow rate of 5.5 L min^{-1} seemed optimal for all studied sample flow rates, which was the value chosen for all further experiments. However, at a certain point complete desolvation will be reached, as indicated by the plateau. These measurements were repeated for a spray distance of 6 cm. The observed intensity maximum, however, seemed to be reached at higher nebulizer gas flow rates, and the absolute ion current intensity obviously has decreased. The reason for this ion loss is that the spray has a much wider spatial distribution using a spray distance of 6 cm, whereas less ions can enter the MS compared to a spray distance of 1 cm. Therefore a spray distance of 1 cm has been chosen for the ESSI interface. The partial pressure of the solvent in the spray region using ESSI will be rather low and the resolvation of the analyte is slow even though very high flow rates are used. This is thought to be one of the key reasons why ESSI was observed to outperform ESI.

In the next set of experiments, the dependence on the sample flow rate delivered by the HPLC system was studied using the optimal gas flow conditions determined above. This is a key parameter to consider when coupling with LC, in order to figure out which flow rates are tolerated by an ESSI setup. **Fig. 7.2b** reports the signal intensity of Tyr-Tyr-Tyr (*m/z* = 508) monitored as a function of sample flow rate. Experiments were carried out with ESI and ESSI, where the latter was operated at two different spray distances (1 cm and 6 cm). Sample delivery by the HPLC pump ensured stable sample flow rates ranging from 0.1 to 3.0 mL min^{-1}.

ESI and ESSI both show a decrease of the signal intensity with increasing sample flow rate, however this effect is substantially greater in the case of ESI. For instance, keeping the spray distance fixed at 1 cm, when the sample flow rate was increased from 0.1 to 2.0 mL min^{-1} the ESI generated ion signal decreased by

a factor of 30, while the ESSI generated ion signal only decreased by a factor of 2. Moreover, ESSI always yielded higher signal intensities than ESI. This clearly shows that it is quite useful to couple ESSI-MS with an HPLC, especially in the high flow regime.

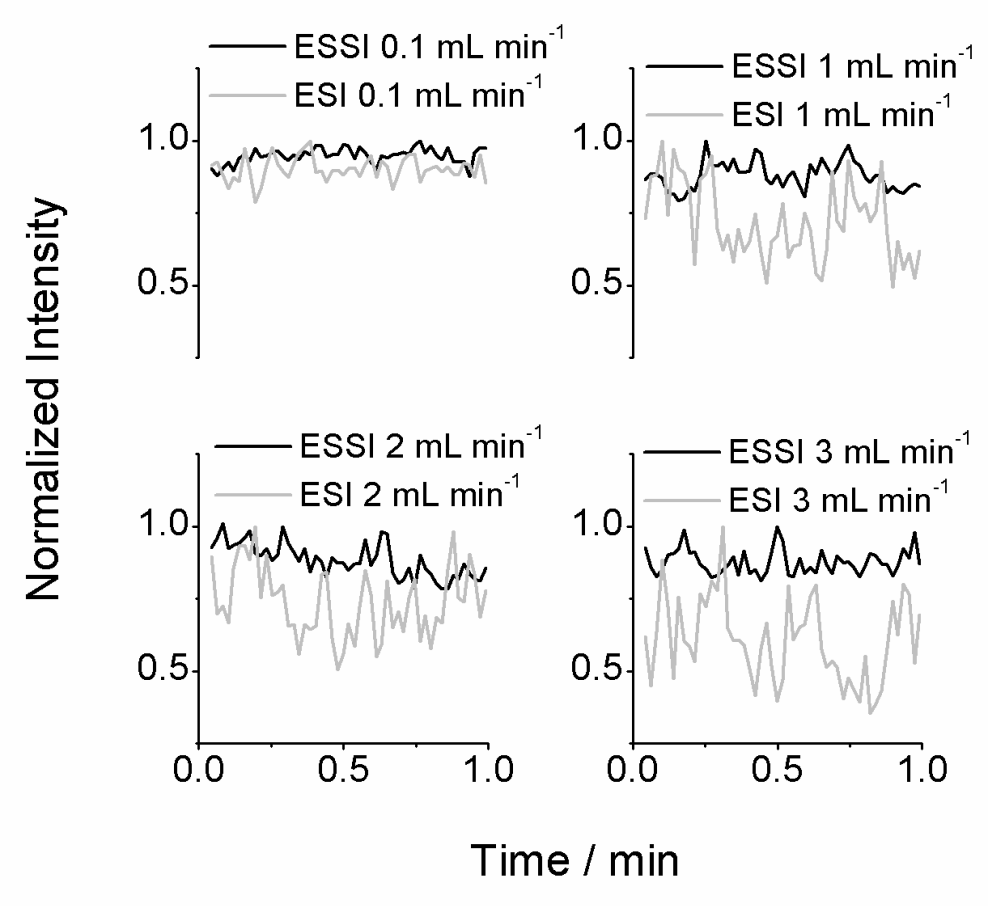

Figure 7.3: Normalized signal intensity fluctuations observed with the ESI and the ESSI interface, using four different sample flow rates (0.1, 1.0, 2.0 and 3.0 mL min^{-1}) measured over a period of one minute.

Using ESSI, quite reasonable signal intensities can be achieved even at a spray distance of 6 cm. At sample flow rates from 0.1, 1.0 and 2.0 mL min^{-1} the signal intensities were within a factor of two of the ESI measurements performed at a distance of 1 cm. This indicates quite a sharp spray plume, which has also been described by Takats *et al.*[64]

The spray stability of ESI and ESSI at four different sample flow rates (0.1, 1.0, 2.0 and 3.0 mL min^{-1}) was also studied. The signal intensities obtained were normalized and are presented in **fig. 7.3**. For ESI, an increase of the sample flow rate leads to a strong decrease in spray stability. In contrast, the spray stability of ESSI is only slightly affected by higher sample flow rates. The very high

nebulization gas flow rate seems to provide efficient and stable solvent nebulization, even at high sample flow rates. This result shows that a stable coupling of our ESI source with flow rates >> 0.1 mL min^{-1} is difficult, while coupling with ESSI still provides stable signals at higher sample flow rates. Of course, when using high sample flow rates with an ESI source, these instabilities can be compensated for by post column splitting. Splitting the sample flow does have disadvantages, including increased dispersion and additional sources of error for quantitative measurements. Using post column splitting usually also results in a larger dead volume, since adjustment of the sample flow rate using post column splitting is usually accomplished by using two capillaries with different back pressures or a restriction valve.[164] It is known that the increased dead volume also increases the dispersion. Therefore, if high efficiency columns (like in ultra-high performance LC) are used, the connection tubes should either be reduced to the absolute minimum in length (small dead volume) or, better even, completely eliminated.[165] ESSI allows a simple and stable connection with sample flow rates up to 3.0 mL min^{-1} without any further treatment of the sample flow after the HPLC outlet. Our data suggests that ESSI is a very good choice for interfacing conventional HPLC with MS.

As a further demonstration of the successful use of LC-ESSI-MS, a separation of five small peptides using a C4 column and a solvent gradient is reported. The baseline separation of all five analytes within 13 min was possible using a 1.0 mL min^{-1} solvent flow rate. Note that to work in optimal ESI conditions, post column splitting was used (~100 µl min^{-1}).

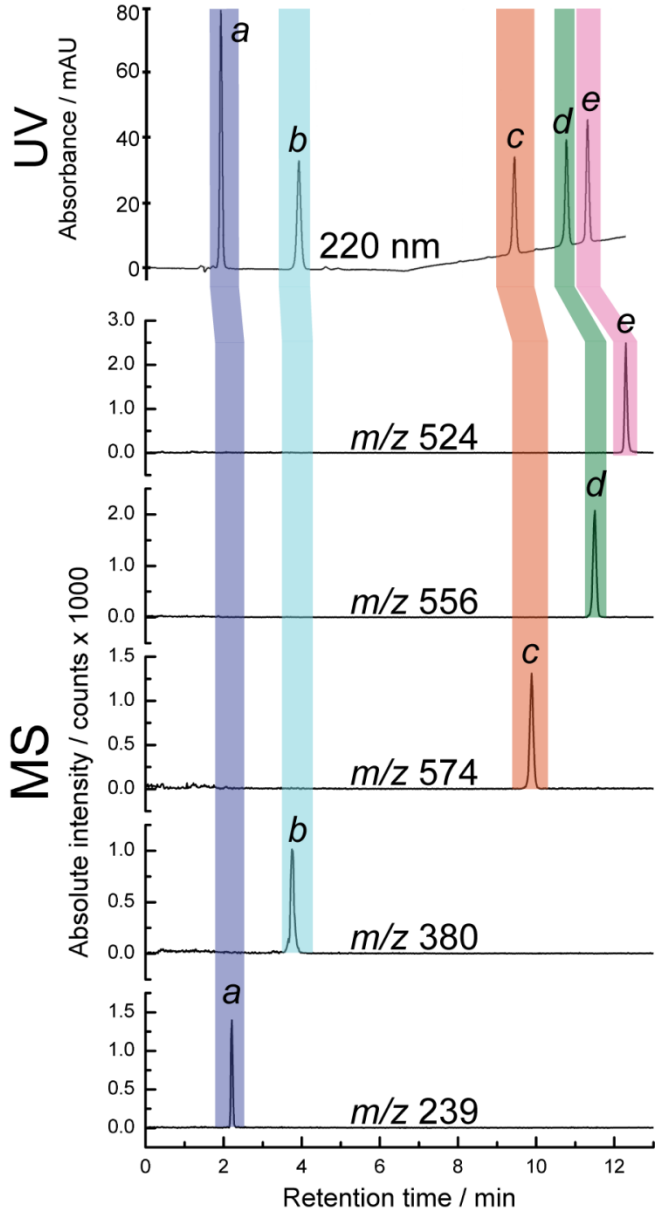

Figure 7.4: Separations of five peptides with a concentration of 10 µg mL^{-1}. Injection volume, 20 µL. Peptides: Gly-Tyr (a), Val-Tyr-Val (b), Methionine Enkepahlin Acetate (c), Leucine Enkepahlin (d), Angiotensim II acetate (e). Concentration: a, 42 µM; b, 26 µM; c, 17 µM; d, 18 µM; e, 10 µM .

Fig. 7.4 presents the UV and MS chromatograms obtained from the analysis of the standard peptide mixture (Gly-Tyr, 42 µM; Val-Tyr-Val, 26 µM; Met-Enkephalin, 17 µM; Leu-Enkephalin, 18 µM; Angiotensin II, 10 µM). The offset in the retention time between the UV and the MS traces is due to different dead volumes required to reach the respective detectors. Very sharp and intense signals were observed when the ESSI interface with a solvent flow of 1.0 mL min^{-1} was used.

When comparing the ESI-MS and ESSI-MS spectra some major differences can be seen (*cf.* **fig. 7.5**). With ESSI, the peptide Val-Tyr-Val forms much more of the singly charged peptide dimer [2M+H$^+$] compared to ESI. The same was observed for leucine enkephalin. Conversely, angiotensin II acetate shows the most intense signal as doubly charged peptide in both ESI and ESSI. However, using ESSI, a higher singly charged peptide signal compared to the ESI experiment was observed. These results let us conclude that the initial droplet size generated using ESSI must be different compared to ESI. The reason for this could be the higher temperature of the used desolvation gas (nitrogen, 523 K) in ESI, or simply the much higher sample flow rate used in ESSI (1.0 mL min^{-1} compared to < 100 uL min^{-1}). It has been reported that ESSI should result in only one dominant charge state when analyzing proteins.[62, 64] Since only small peptides were separated here (highest MW = 1046 Da), the use of ESSI only had the effect of decreasing the intensity of the doubly charged species; species with three or more charges were not observed. Cluster formation was also observed, as expected from previous SSI experiments.[58] We think that this clustering in ESSI is a sign of very efficient nebulization. In order to test the ESSI interface for high flow (1 ml min-^{1}) LC methods, we performed a 6-point calibration for the peptide Val-Tyr-Val and Met-Enkephalin. Using ESI the same calibration was done by post column split flow (~100 µL min^{-1}). The calibration was accomplished by adding up all signal intensities that were related to the peptide (singly charged monomer, singly charged dimer etc.).

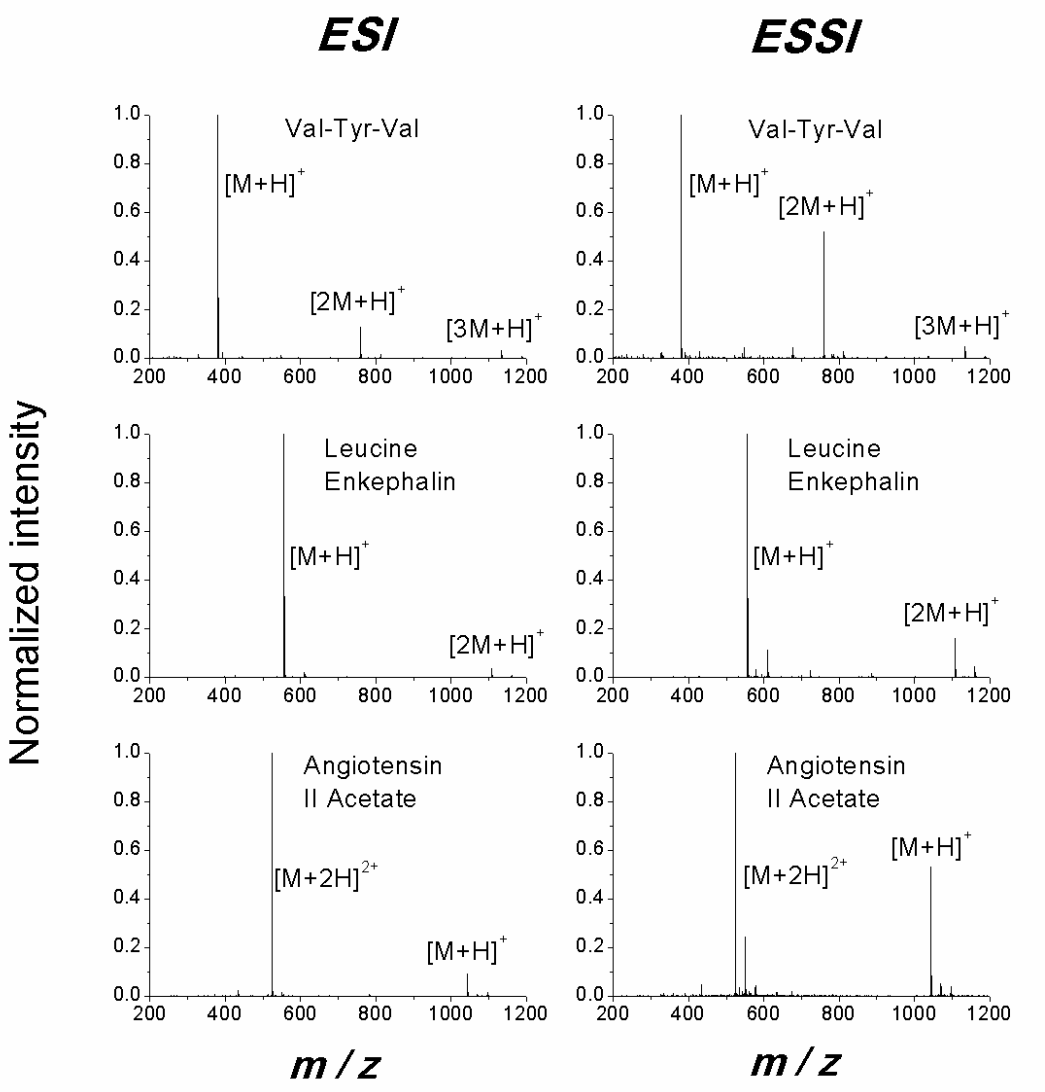

Figure 7.5: Mass spectra obtained from the peptieds Val-Tyr-Val (42µM), Leucine Enkephaline (17 µM), and Angiotensin II acetate (10 µM), using the ESI and the EESI interface.

Injecting 6 different concentration levels for Val-Tyr-Val (130, 26, 13, 2.6, 1.3 and 0.26 µM) and for Met-Enkephalin (87, 17, 8.7, 1.7, 0.87, 0.17 µM) resulted in the calibration curves shown in **fig. 7.6**. The linearity observed in the calibration curves generated by using the ESSI interface was significantly better over the entire concentration range compared to the curves generated using the ESI interface. Coefficients of determinations (r^2) of 0.959 and 0.998 were observed for the peptide Val-Tyr-Val and Met-Enkephalin using ESSI, whereas lower values of 0.759 and 0.837 were obtained by simply placing a line of best fit through all six calibration points obtained for the same two peptides generated by an ESI source. It can, however, be pointed out that ESI shows good linearity up

to a concentration of 25 µM. Above this concentration, the ionization efficiency of the ESI interface is probably not sufficient to fully ionize the increasing amount of analyte. Using only the first five points of the Val-Tyr-Val calibration for the

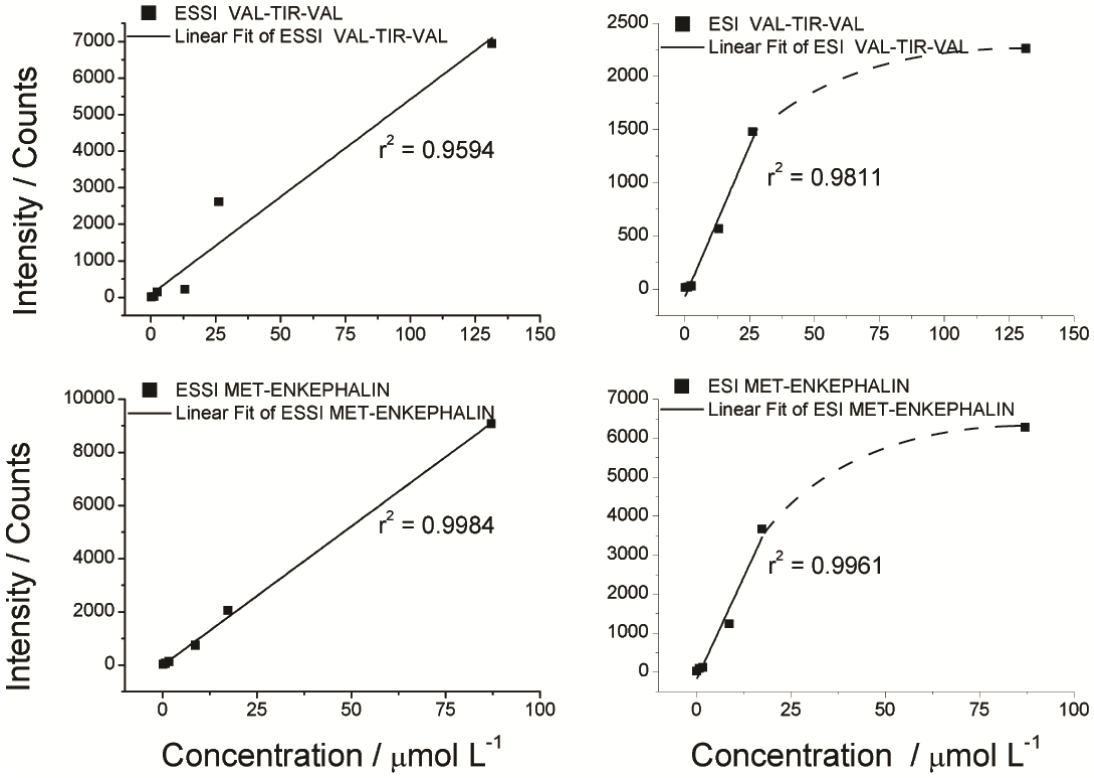

Figure 7.6: Calibration plot for the peptides Val-Tyr-Val (Concentrations: 130, 26, 13, 2.6, 1.3, 0.26 µM) and Met-Enkephalin (Concentrations: 87, 17, 8.7, 1.7, 0.87, 0.17 µM) comparing ESI with ESSI as an ion source for the LC. ESI was performed using post column splitting, whereas ESSI was directly coupled to the LC system.

ESI interface (r^2 = 0.9811), a linear extrapolation to a concentration of 130 µM would result in a hypothetical intensity of 7300, which is similar to what was observed for ESSI. It is common to find nebulization gas flow rates in publications about high-flow interfaces for HPLC-MS. However, what really counts when comparing different interfaces is the nebulization gas velocity, not the volume flow. Therefore, we decided to explore the linear nebulization gas flow velocity in more detail. Many different diameters of spray and nebulization capillaries are reported in the literature.[64, 156-158] The sample capillary of the ESSI source is generally positioned 0.1 to 0.2 mm outside of the nebulization capillary.[64] Therefore, the calculated nebulization gas velocities in this work are slower at the tip of the sample capillary, since as soon as the nitrogen leaves the capillary end, a continuous deceleration of the nebulization gas takes place. In

their review, Covey *et al.*[166] report gas velocities from 100 to 300 m s^{-1} for the majority of the nebulizers. Kovacs *et al.*[62], on the other hand, report nebulization gas velocities up to 1000 m s^{-1} (Mach 3) for SSI. The nebulization gas velocity at the outlet of the sample capillary in this work is thought to be in this range. As a simple approximation to be able to compare different ESI interfaces, the gas flow velocity is obtained by multiplying the measured nitrogen flow rate with the area between the inner and the outer capillary. Since, the used ESI interfaces are very similar in their main design a comparison using the easy calculable nebulizing gas velocity seems to be very reasonable. For our ESSI setup, a nebulization gas flow of 5.5 L min^{-1} results in a nebulization gas velocity of 2900 m s^{-1}. For the commercial ESI interface a nebulization gas flow of 5.5 L min^{-1} would result in a nebulization gas velocity of 850 m s^{-1}. The gas flow velocity of the setup proposed by Hopfgartner *et al.*[156] was calculated to be around 500 m s^{-1}, the one from Hirabayashi *et al*.[57] around 180 m s^{-1}, and from Takats *et al.*[64] around 1590 m s^{-1}. Hiraoka *et al.*[157] observed a rather stable ion signal intensity up to a sample flow rate of 2.3 mL min^{-1}. Higher sample flow rates resulted in a strong decrease of the ion signal intensity, whereas in the work presented here, a slight and continuous decrease of the ion intensity towards higher sample flow rates could be observed. The 2.8 atmosphere back pressure described in their publication should result in a nebulization gas flow rate of roughly 1 L min^{-1}, which for their setup would result in a nebulization gas velocity of 80 m s^{-1}. This is 36 times slower than the nebulization velocity used in our work, which for our interface would lead to poor ion signal stability.

The resulting higher acceleration of the sample helps handling higher sample flow rates, which has been shown in the present work. Due to the high nebulization gas velocity using ESSI the generated droplets are very small. This improves the ionization efficiency, since it is easier to evaporate solvent from smaller than from larger droplets. A key recommendation is therefore to optimize the nebulization gas velocity (rather than simply the gas flow) in the design of new high flow ion sources. A well-designed ion source will improve stability, sensitivity, and could reduce nitrogen gas consumption.

8.5 Conclusions

Electrosonic spray ionization was applied to the ionization of a HPLC effluent with sample flow rates up to 3.0 mL min^{-1}, and was compared to pneumatically assisted ESI. Using ESSI as an interface offers an easy way to couple of LC with MS while maintaining high flow rates. Moreover, with ESSI, good spray stabilities can be achieved even when using high sample flow rates. A nebulizer gas flow rate of 5.5 L min^{-1} was found to be optimal for all sample flow rates. Very good coefficients of determination for the calibration of Val-Tyr-Val and Met-Enkephalin were found for ESSI. The main reason for the superior performance of ESSI is thought to be a decrease in the ionization efficiency of the ESI at higher rates of sample delivered as well as higher concentrations (c.f. fig. 5). ESSI can also be used with standard LC columns, which feature analytical ruggedness, high separation efficiency and can also be used with large injection volumes. ESI is better suited to operate with lower sample flow rates, which is in the flow regime of micro/nano LC systems that are more expensive and usually more difficult to handle than a common LC-system. A standard HPLC-ESI-MS interface requires flow splitting, in which case diffusion can become problematic. Since modern ultra-high performance LC systems work with very low void volumes (< 100 µL), high sample flow rates (up to 2.0 mL min^{-1} with backpressure of > 1000 bar) and small diameter columns (very short separation time), they could be coupled directly with the ESSI interface without generating bigger void volume by post column splitting. When using UHPLC rather high sample flow rates are common, which reduce analysis time[162] and the ESSI source could be a good alternative for a high flow MS interface.

At all sample flow rates, ESSI showed higher signal intensities than ESI, even though no heating of the nebulizer gas was used, which could help to preserve to ionize thermally labile substances. Nebulization of thermally unstable molecules using LC with high sample flow rates for separation could benefit strongly from the interface presented here. Furthermore, the ESSI interface provides a higher linear range due to very efficient ionization, well into the mM range.

Chapter 9

Conclusions and Outlook

This dissertation tried to answer several fundamental questions related to the reaction mechanism, the degradation efficiency and the by-product generation of contaminated air passing through a commercially available plasma air purifier.

9.1 Chapter 3

This chapter showed that the degradation efficiencies of the PAP studying volatile organic compounds are less that 11% for all measured VOCs and are not comparable to model reactors which incorporate catalytic material that have degradation efficiencies of more than 90%. Best degradation efficiency was accomplished for cyclohexene (11%) and worst for benzene (<1%). As assumed, oxidative processes involving ozone and radicals play the dominant role in PAP degradation processes as adipaldehyde was identified to be formed from cyclohexene as a degradation product. Probably even more important degradation processes that seem to occur in the PAP are tropospheric removal processes that involve radicals such as ·OH.

Model reactors incorporating catalytic material usually deal with much lower air velocities compared to the PAP. Although the PAP could handle air velocities normally used in heating and ventilation systems, its rather low degradation efficiency is not suitable for cleaning air contaminated with VOCs.

9.2 Chapter 4

Kinetic studies showed that ozonolysis cannot be the dominating process of cyclohexene degradation in the PAP. The measured amounts of 300 ppb ozone produced in the PAP only accounts for the degradation of 0.5% of the introduced cyclohexene, whereas in **Chapter 3** a degradation of 11% of cyclohexene was measured. To circumvent offline sampling, VOC sensors based on resistance measurements were used to monitor different VOC concentrations in the PAP. Qualitative results showed very promising data. Unfortunately, it was not possible to quantitatively measure the degradation efficiency of the PAP, since the sensors have a cross reactivity with ozone. This chapter showed that a better analytical method is needed in order to be able draw conclusions about the fate of contaminants passing the PAP.

9.3 Chapter 5

This chapter presented a newly designed ionization source, which was designed during this thesis. This source is based on a discharge plasma and was adapted from an already existing plasma ionization source.[55] It is much smaller and pen-like compared to similar sources, therefore it is referred to as the miniaturized flowing atmospheric pressure afterglow (miniFAPA) ionization source. The implementation of the miniFAPA ionization source in capillary electrophoresis-mass spectrometry (CE-MS) offers several advantages. As the outer electrode is grounded, safer handling and adjustment is possible and there is no disturbance of the electric field in front of the mass spectrometer. The downscaling of the ionization source enables facile positioning and rearrangement. The disassembly of the miniFAPA ionization source is very fast and easy, allowing cleaning within minutes in case of contamination. The plasma torch of the miniFAPA ionization source is very stable allowing high nebulization flow rates.

The outlet of the CE capillary (~ 10 cm) was coated with silver paint, which was incorporated in the stainless steel T-junction. The enhanced stiffness as well as the possibility to ground the CE capillary behind the T-junction allowed facile use of nebulization gas.

Limits of detection for the miniFAPA-CE-MS setup were achieved in the femtomol range. These results clearly showed that the source is ideal for coupling separation methods with the MS. It can also desorb analytes from a surface or directly ionize a part of the exhaust in the PAP, which is shown in **Chapter 6**.

9.4 Chapter 6

Analyzing the exhaust of the PAP after introduction of different amines showed very interesting results. A breakdown of the amines to small non-toxic molecules as proposed by the manufacture was not observed. Quite the opposite was true as higher molecular weight products were detected. Probably due to oligomerization reactions of the amines in the PAP. Primary amines react differently than secondary amines in the PAP. Extensive studies showed that the observed products are ionic clusters of positively charged amine molecules with

negatively charged nitrate molecules. Moreover, it could be seen that most products in the PAP are generated from reactions with OH radicals. Patterns in the mass spectra with Δm = 14 were observed and can be explained by OH radicals attacking the amine groups, resulting in a loss of CH_2 (m/z = 14). However, a lack in resolution of the mass spectrometer used allowed no confirmation of this assumption. Furthermore, it was not known if the by-products formed in the PAP are toxic and since a formation of toxic by-products would be a problem, it is not recommended to use the PAP in its current state as air purifier for amine exhaust gases.

The presented interface offers a direct coupling of the exhaust of a PAP with a mass spectrometer. This approach helps to overcome sampling issues and would therefore be an approach worth using to study and compare PAPs similar to the one presented in this work.

9.5 Chapter 7

Low molecular weight molecules, high molecular weight proteins and bioparticles experienced a decrease in amount when passing through the switched on PAP. Investigations of methyltriclosane with the PAP switched off compared to switched on showed a reduction of 17% of the initial amount. A mass balance showed that nearly the same amount of methyltriclosane is being deposited on the copper electrodes, independent of the PAP. The decrease of methyltriclosane was caused by precipitation rather than a chemical degradation processes.

High amounts of bovine serum albumin (BSA) were found to be deposited on the copper electrodes. Furthermore, olygomerized BSA was found in the form of a white, water-insoluble solid found on the copper electrodes. However, only a small amount of the BSA was found to be oligomerized and thus the main reduction observed for BSA is thought to be due to deposition as well.

Reduction in the numbers of aerosolized *B. subtilis, B. anthracis and L. pneumophila* showed that the switched on PAP is capable of reducing the numbers of aerolized bacteria and spores. The PAP and the wind tunnel were wiped with sterile swabs to collect spores (*B. subtilis, B. anthracis*). All surfaces tested were found to be contaminated with viable spores, regardless of whether

the surfaces were located inside or outside the PAP. These results showed that the PAP studied decontaminate surfaces insufficiently. Again, it seems that the observed decrease of the switched on PAP is rather due to electrostatic precipitation than due to degradation to smaller molecules.

During this study an interesting trend was observed: the larger the molecule the higher the measured deposition efficiency of the PAP. However, the results observed in this chapter suggested that non-volatile molecules are mainly deposited on the copper electrodes of the PAP due to precipitation.

9.6 Chapter 8

The performance of electrosonic spray ionization (ESSI) was compared to electrospray ionization (ESI) by interfacing liquid chromatography (LC) with MS. Especially for high flow rate applications, ESSI showed superior stability and nebulization efficiency. This is a huge advantage when interfacing ultra-high performance liquid chromatography with MS, as rather high sample flow rates are used. Using ESSI helps to circumvent post column splitting which would cause an enhanced dead volume, enhanced diffusion effects, and would bias the chromatographic separation leading to worse resolution. The most efficient ionization was achieved with a nebulizer gas flow rate of 5.5 L min^{-1}, resulting in a nebulization gas velocity of 2900 m s^{-1}.

The same ionization source was used in our bench test setup system to efficiently nebulize the studied compounds. The only difference compared to the ESSI source used in **Chapter 8** was that no high voltage was applied to the sample solution. Reproducibility of the SSI source to nebulize the studied compounds was proven to be very good (*c.f.* **Chapter 7**, phenanthrene measurements).

9.7 Final Conclusions and Outlook

The production of higher molecular weight products in **Chapter 6** can be compared to the work of Kim *et al.*[20] They found a remarkably high aerosol production in their work using a pulsed plasma air purifier. Furthermore, their PAP showed a very low conversion rate compared to the other non-thermal plasma reactors they studied. Enhanced benzene removal correlated with the

enhanced formation of water clusters under humid conditions. The following two reaction pathways could explain how these small aerosols and clusters of water could be formed

$$A^- + nH_2O \rightarrow A^-(H_2O)_n \quad (1)$$

$$B^+ + nH_2O \rightarrow B^+(H_2O)_n \quad (2)$$

Where A^- are negative ions such as O^-, O_2^-, O_3^-, OH^-, NO_2^- and CO_3^-, B^+ are positive ions which are in principle constitutes of proton hydrates.[20] These reactions could explain the missing cyclohexene when calculating the mass balance in **Chapter 3**. It seems that higher molecular weight products are especially produced from volatile compounds. Non-volatile compounds on the other hand seem to deposit mainly on the copper electrodes in most cases. Both processes result in a decrease of transmitted substances. Conducting a mass balance is crucial in order to prove if such a system really works. Furthermore, it must be possible to exclude any formation of toxic by-products.

Morvovà *et al.*[34] observed low amounts of a white water insoluble powder, which were later identified as polymerized amino acids. Studying BSA, comparable observations were made. Using high-mass MALDI, it was possible to identify the water insoluble white solid as polymerized BSA. This polymerization must have occurred in the PAP. However, less than 1% of BSA was found to be polymerized. Polymerization to non-volatile molecules could present an interesting alternative to the approach of complete decomposition.

As already presented in the introduction, there are a lot of different non-thermal plasmas-based air purifying systems. One way to compare such systems is to compare their specific input energy densities. Formula (3) shows how these specific input energy densities are calculated. The higher the flow rate of a PAP the lower the specific input energies. Kraus *et al.*[167] describe how to calculate the discharge power for a DBD reactor. They use a voltage-charge Lissajous figure instead of current probe, as individual microdischarges make it difficult to measure the power with a current probe. Such problems are not observed when using an alternating current PAP. To get a rough idea where the PAP stands in

terms of specific input energies, the discharge power was measured with a current probe.

$$\text{Specific input energy [J } L^{-1}] = \frac{\text{discharge power [J s}^{-1}]}{\text{gas flow rate [L min}^{-1}]} \text{ x } 60 \qquad (3)$$

Table 9.1: Specific input energy of the PAP studied in this thesis. The higher the voltage applied the higher the specific input energy.

Voltage [V]	Discharge consumption [J s^{-1}]	Flow rate [L min^{-1}]	Specific input energy [J L^{-1}]
6.0	9.36	320	1.75
6.5	9.40	320	1.76
7.0	11.75	320	2.20
7.5	14.10	320	2.64
8.0	18.80	320	3.53
8.5	25.85	320	4.85
9.0	32.42	320	6.08

T**able 9.1** lists the power consumption as well as the specific input energy for different voltages. A further increase in the specific input energy rapidly decreased the particle number concentration. This was thought to be an indication of enhanced decomposition at higher specific input energies.[21] Subrahmanyam *et al.*[29] observed the complete destruction of 250 ppm isopropanol using a DBD reactor incorporating a MnO_X/sintered metal fiber (SMF) catalyst with a specific input energy of 235 J L^{-1}. They achieved complete oxidation at a specific input energy of 760 J L^{-1}. Ayrault *et al.*[33] studied 180 ppm 2-heptanone in a DBD with a platinum-based catalyst supported on an alumina wash coated honeycomb monolith. A specific input energy of 200 J L^{-1} showed a degradation of 97%. However, without a catalyst, their reactor showed a degradation less than 50%, even at a specific input energy of 500 J L^{-1}. Magureanu *et al.*[27] showed that they could degrade >95% of trichloroethylene at concentrations of 150-200 ppm using a DBD reactor with a MnOx/SMF catalyst at a specific input energy of 150 J L^{-1}. On the other hand, without using a catalyst a degradation of 58% with a specific input energy of 550 J L^{-1} was

observed. The small conversion rates of the volatile organic compounds measured in **Chapter 3** are not surprising, when comparing the specific input energies used in the PAP to other existing systems. However, these model reactors were able to treat < 10 L min^{-1} and they are not suitable to incorporate in a heating ventilation and air conditioning systems. The PAP studied in this thesis, on the other hand, can deal with up to 3200 L min^{-1}. Even at the higher air flow rates the PAP showed high trapping efficiencies (only having an SIE of ~5 J L^{-1}). Unfortunately, the PAP does not work as intended (i.e. degrading all contaminants to small fragments). Instead, a major source of the degradation that is observed is due to deposition onto the copper electrodes, where viable bioparticles are not destroyed or decontaminated.

In its current state, the PAP studied in this thesis cannot be recommended for use as an all-round air purification system. The manufacture claims that all bioparticles are degraded to small non-toxic compounds could not be confirmed. However, a substantial decrease of the bioparticles studied was observed. This decrease was mainly due to electrostatic precipitation.

We believe that future plasma based air purifying systems will use catalytic materials. Although such materials need to be replaced from time to time, these materials will reduce the energy consumption and increases the degradation efficiency enormously. Especially in recent years when energy saving issues have grown in importance, such systems need to be efficient in order to minimize power consumption. Another interesting approach could be to produce higher weight particles in a first system (similar to the PAP studied in this thesis), followed by an electrostatic precipitator that would trap all particles generated in a second stage. However, the trapped air contaminants would have to be collected as solid waste, which would require regular maintenance.

Studying degradation processes in a plasma-based air purification systems is challenging. Due to the high flow rate of the ventilation systems used, only a fraction of the exhaust can be studied online. Therefore, obtaining a mass balance is of paramount importance in order to estimate the amount of degradation. Otherwise wrong conclusions might be drawn. A decrease in the amount of the compounds studied does not necessarily mean that the system

fragments everything to small molecules. A decrease can also be observed because deposition in the air purification system occurs. In the worst case, compounds passing through the PAP could be altered in such a way that even more toxic compounds are formed in the plasma. Interfacing the exhaust of an air purification system with a mass spectrometer is a novel approach that gives lots of new insights into the chemical processes occurring in the PAP. Coupling the PAP with a high-resolution mass spectrometer might help to better understand the processes, which led to the congested mass spectra presented in **Chapter 6,** and could prove that CH_2 abstraction from amines is observed. The lack in resolution of the mass spectrometer used did not allow confirmation of this hypothesis. Moreover, the online study about the molecular processes in the PAP should be extended to other substance classes such as alcohols, ketones and ethers. It would be very interesting to see how such compounds react, and whether they are decomposed in the PAP. Online analysis would be a huge advantage compared to the common offline sampling methods used to study PAPs in literature. It is common practice to measure degradation efficiencies as well as degradation pathways of a PAP by using passive sorbent material. Although the overall cleaning efficiency can easily be evaluated using adsorption tubes, it is difficult to detect the degradation products generated. Some reactive products formed may not be adsorbed at all, while others could react with the sorption material in the tubes, which would therefore render subsequent desorption of such compounds impossible.

Most researchers characterize the degradation efficiencies in various PAPs designs by studying volatile organic compounds. However, only little is known about the chemistry of non-volatile compounds in such systems. It is possible that the reactors in literature are not capable of fully degrading non-volatile compounds, or that researchers are struggling to find appropriate methods that are suitable to study the fate of non-volatile compounds in their plasma reactors. Whatever the reason for this observation, it would definitely be very interesting to study non-volatile compounds in such systems. In this context, it would be important to design an interface capable of studying non-volatile compounds in an online fashion by interfacing the PAP exhaust with a mass spectrometer. Such a system would need to incorporate a special ionization

source such as a secondary electrospray ionization source or a plasma based ionization source**. Chapters 4** and **6** present concepts for such interfaces, using the miniFAPA ionization source. In particular, the miniFAPA ionization source was capable of ionizing small peptides, in an investigation of processes in the miniPAP when using thermospray for nebulization.

Considering that the PAP studied here requires only rather low specific input energies, it would be very interesting to increase this input energy to levels which are also used in other systems described in the literature. Such a study would show exactly which energies are necessary to get full degradation of the studied compounds. However, a complete redesign of the PAP would be inevitable for such a study, as voltages higher than 9.0 kV cannot be used due arcing between the electrodes, which resulted in electrical breakdown. If a redesign would be considered, the question could arise why not to use a dielectric barrier discharge (DBD) plasma instead of a corona plasma reactor. If the goal of the plasma based air purifier is to fully oxidize all flue gasses, a DBD reactor would be more useful. On the other hand, corona plasma reactors seem more suitable as precipitators. A combination of both technologies could become an ideal all-round air purification system in the future.

References

1. Atkinson, R.; Carter, W. P. L., Kinetics and mechanisms of the gas-phase reaction of ozone with organic-compounds under atmospheric conditions. *Chem. Rev.* **1984,** *84*, (5), 437-470.

2. Hu, G. P.; Ran, P. X., Indoor air pollution as a lung health hazard: focus on populous countries. *Curr. Opin. Pulm. Med.* **2009,** *15*, (2), 158-164.

3. Jones, A. P., Indoor air quality and health. *Atmos. Environ.* **1999,** *33*, (28), 4535-4564.

4. Zuskin, E.; Schachter, E.; Mustajbegovic, J.; Pucarin-Cvetkovic, J.; Doko-Jelinic, J.; Mucic-Pucic, B., Indoor air pollution and effects on human health. *Period. Biol.* **2009,** *111*, (1), 37-40.

5. Ingrosso, G., Free radical chemistry and its concern with indoor air quality: an open problem. *Microchem J.* **2002,** *73*, (1-2), 221-236.

6. Sarwar, G.; Corsi, R.; Kimura, Y.; Allen, D.; Weschler, C. J., Hydroxyl radicals in indoor environments. *Atmos. Environ.* **2002,** *36*, (24), 3973-3988.

7. Sessa, R.; Di Pietro, M.; Schiavoni, G.; Santino, I.; Altieri, A.; Pinelli, S.; Del Piano, M., Microbiological indoor air quality in healthy buildings. *Microbiologica* **2002,** *25*, (1), 51-56.

8. Spengler, J. D.; Sexton, K., Indoor air-pollution - a public-health perspective. *Science* **1983,** *221*, (4605), 9-17.

9. Lazaridis, M., *Indoor Air Pollution*. Springer: p 255-304.

10. Rumchev, K.; Brown, H.; Spickett, J., Volatile organic compounds: Do they present a risk to our health? *Rev. Environ. Health* **2007,** *22*, (1), 39-55.

11. Escombe, A. R.; Oeser, C. C.; Gilman, R. H.; Navincopa, M.; Ticona, E.; Pan, W.; Martinez, C.; Chacaltana, J.; Rodriguez, R.; Moore, D. A. J.; Friedland, J. S.; Evans, C. A., Natural ventilation for the prevention of airborne contagion. *PLos Med.* **2007,** *4*, (2), 309-317.

12. Eliasson, B.; Kogelschatz, U., Nonequilibrium volume plasma chemical-processing. *IEEE Trans. Plasma Sci.* **1991,** *19*, (6), 1063-1077.

13. Holzer, F.; Roland, U.; Kopinke, F. D., Combination of non-thermal plasma and heterogeneous catalysis for oxidation of volatile organic compounds Part 1. Accessibility of the intra-particle volume. *Appl. Catal., B* **2002,** *38*, (3), 163-181.

14. Roland, U.; Holzer, F.; Kopinke, F. D., Improved oxidation of air pollutants in a non-thermal plasma. *Catal. Today* **2002,** *73*, 315-323.

15. Roland, U.; Holzer, F.; Kopinke, E. D., Combination of non-thermal plasma and heterogeneous catalysis for oxidation of volatile organic compounds Part 2. Ozone decomposition and deactivation of gamma-Al2O3. *Appl. Catal. B-Environ.* **2005,** *58*, (3-4), 217-226.

16. Roland, U.; Holzer, F.; Poppl, A.; Kopinke, F. D., Combination of non-thermal plasma and heterogeneous catalysis for oxidation of volatile organic compounds Part 3. Electron paramagnetic resonance (EPR) studies of plasma-treated porous alumina. *Appl. Catal. B-Environ.* **2005,** *58*, (3-4), 227-234.

17. Hammer, T., Application of plasma technology in environmental techniques. *Contrib. Plasma Phys.* **1999,** *39*, (5), 441-462.

18. Roth, J. R., *Industiral plasma engineering*. Institute of physics publishing Bristol and Philadelphia: 1995; Vol. 1, p 1-538.

19. Kogelschatz, U., Ozone synthesis in gas discharges. *XVI International Conference on Phenomena in Ionized Gases (Invited Papers)* **1983**, 240-250250.

20. Hyun-Ha, K.; Kobara, H.; Ogata, A.; Futamura, S., Comparative assessment of different nonthermal plasma reactors on energy efficiency and aerosol formation from the decomposition of gas-phase benzene. *IEEE Trans. Ind. Appl* **2005,** *41*, (1), 206-214214.

21. Kim, H. H.; Oh, S. M.; Ogata, A.; Futamura, S., Decomposition of gas-phase benzene using plasma-driven catalyst (PDC) reactor packed with Ag/TiO2 catalyst. *Appl. Catal. B-Environ.* **2005,** *56*, (3), 213-220.

22. Holzer, F.; Roland, U.; Kopinke, F. D., Combination of non-thermal plasma and heterogeneous catalysis for oxidation of volatile organic compounds Part 1. Accessibility of the intra-particle volume. *Appl. Catal. B-Environ.* **2002,** *38*, (3), 163-181.

23. Tevault, D. E., Carbon-monoxide production in silent discharge plasma of air and air methane mixtures. *Plasma Chem. Plasma Process.* **1987,** *7*, (2), 231-242.

24. Magureanu, M.; Mandache, N. B.; Eloy, P.; Gaigneaux, E. M.; Parvulescu, V. I., Plasma-assisted catalysis for volatile organic compounds abatement. *Appl. Catal., B* **2005,** *61*, (1-2), 12-20.

25. Subrahmanyam, C.; Magureanu, A.; Renken, A.; Kiwi-Minsker, L., Catalytic abatement of volatile organic compounds assisted by non-thermal plasma - Part 1. A novel dielectric barrier discharge reactor containing catalytic electrode. *Appl. Catal., B* **2006,** *65*, (1-2), 150-156.

26. Subrahmanyam, C.; Renken, A.; Kiwi-Minsker, L., Catalytic abatement of volatile organic compounds assisted by non-thermal plasma - Part II. Optimized catalytic electrode and operating conditions. *Appl. Catal., B* **2006,** *65*, (1-2), 157-162.

27. Magureanu, M.; Mandache, N. B.; Parvulescu, V. I.; Subrahmanyam, C.; Renken, A.; Kiwi-Minsker, L., Improved performance of non-thermal plasma reactor during decomposition of trichloroethylene: Optimization of the reactor geometry and introduction of catalytic electrode. *Appl. Catal., B* **2007,** *74*, (3-4), 270-277.

28. Subrahmanyam, C.; Renken, A.; Kiwi-Minsker, L., Novel catalytic non-thermal plasma reactor for the abatement of VOCs. *Chem. Eng. J.* **2007,** *134*, (1-3), 78-83.

29. Subrahmanyam, C.; Renken, A.; Kiwi-Minsker, L., Novel catalytic dielectric barrier discharge reactor for gas-phase abatement of isopropanol. *Plasma Chem. Plasma Process.* **2007,** *27*, (1), 13-22.

30. Futamura, S.; Zhang, A. H.; Prieto, G.; Yamamoto, T., Factors and intermediates governing byproduct distribution for decomposition of butane in nonthermal plasma. *IEEE Trans. Ind. Appl* **1996,** *34*, (5), 967-974.

31. Futamura, S.; Einaga, H.; Kabashima, H.; Hwan, L. Y., Synergistic effect of silent discharge plasma and catalysts on benzene decomposition. *Catal. Today* **2004,** *89*, (1-2), 89-95.

32. Mok, Y. S.; Koh, D. J.; Shin, D. N.; Kim, K. T., Reduction of nitrogen oxides from simulated exhaust gas by using plasma-catalytic process. *Fuel Process. Technol.* **2004,** *86*, (3), 303-317.

33. Ayrault, C.; Barrault, J.; Blin-Simiand, N.; Jorand, F.; Pasquiers, S.; Rousseau, A.; Tatibouet, J. M., Oxidation of 2-heptanone in air by a DBD-type plasma generated within a honeycomb monolith supported Pt-based catalyst. *Catal. Today* **2004,** *89*, (1-2), 75-81.

34. Morvova, M.; Hanic, F.; Morva, I., Plasma technologies for reducing CO2 emissions from combustion exhaust with toxic admixtures to utilisable products. *J. Therm. Anal.* **2000,** *61*, (1), 273-287.

35. Oda, T., Non-thermal plasma processing for environmental protection: decomposition of dilute VOCs in air. *J. Electrost.* **2003,** *57*, (3–4), 293-311.

36. Eliasson, B.; Kogelschatz, U., Modeling and applications of silent discharge plasmas. *IEEE Trans. Plasma Sci.* **1991,** *19*, (2), 309-323.

37. Goldstein, E., Berl. Ber. **1886,** *39*, 691.

38. Wien, W., Verhanal. Phys. Ges. **1898,** *17*.

39. Gross, J. H., *Mass spectrometry: A textbook*. Springer: Berlin, 2004.

40. Hoffmann, E.; Stroobant, V., *Mass spectrometry: Principles and applications*. John Wiley & Sons Ltd: Hoboken, NJ, 2007.

41. Bleakney, W., A new method of positive ray analysis and its application to the measurement of ionization potentials in mercury vapor. *Phys. Rev.* **1929,** *34*, (1), 157-160.

42. Nier, A. O., A mass spectrometer for isotope and gas analysis. *Rev. Sci. Instrum.* **1947,** *18*, (6), 398-411.

43. Carroll, D. I.; Dzidic, I.; Stillwell, R. N.; Haegele, K. D.; Horning, E. C., Atmospheric-pressure ionization mass-spectrometry - Corona discharge ion-source for use in liquid chromatography mass spectrometer-computer analytical system. *Anal. Chem.* **1975,** *47*, (14), 2369-2373.

44. Harrison, W. W.; Hang, W., Powering the analytical glow discharge. *Fresenius J. Anal. Chem.* **1996,** *355*, (7-8), 803-807.

45. Bogaerts, A.; Gijbels, R., Fundamental aspects and applications of glow discharge spectrometric techniques. *Spectroc. Acta Pt. B-Atom. Spectr.* **1998,** *53*, (1), 1-42.

46. Hang, W.; Yan, X. M.; Wayne, D. M.; Olivares, J. A.; Harrison, W. W.; Majidi, V., Glow discharge source interfacing to mass analyzers: Theoretical and practical considerations. *Anal. Chem.* **1999,** *71*, (15), 3231-3237.

47. Karas, M.; Bachmann, D.; Bahr, U.; Hillenkamp, F., Matrix-assisted ultraviolet-laser desorption of nonvolatile compounds. *Int. J. Mass Spectrom. Ion Process.* **1987,** *78*, 53-68.

48. Karas, M.; Hillenkamp, F., Laser desorption ionization of proteins with molecular masses exceeding 10000 daltons. *Anal. Chem.* **1988,** *60*, (20), 2299-2301.

49. Hillenkamp, F.; Karas, M.; Ingendoh, A.; Stahl, B., *Matrix assisted UV-laser desorption ionization - A new approach to mass-spectrometry of large biomolecules*. Elsevier Science Publ B V: Amsterdam, 1990; p 49-60.

50. Fenn, J. B.; Mann, M.; Meng, C. K.; Wong, S. F.; Whitehouse, C. M., Electrospray ionization for mass-spectrometry of large biomolecules. *Science* **1989,** *246*, (4926), 64-71.

51. Mann, M.; Meng, C. K.; Fenn, J. B., Interpreting mass-spectra of multiply charged ions. *Anal. Chem.* **1989,** *61*, (15), 1702-1708.

52. Andrade, F. J.; Shelley, J. T.; Wetzel, W. C.; Webb, M. R.; Gamez, G.; Ray, S. J.; Hieftje, G. M., Atmospheric pressure chemical ionization source. 1. Ionization of compounds in the gas phase. *Anal. Chem.* **2008,** *80*, (8), 2646-2653.

53. Andrade, F. J.; Shelley, J. T.; Wetzel, W. C.; Webb, M. R.; Gamez, G.; Ray, S. J.; Hieftje, G. M., Atmospheric pressure chemical ionization source. 2. Desorption-ionization for the direct analysis of solid compounds. *Anal. Chem.* **2008,** *80*, (8), 2654-2663.

54. Jecklin, M. C.; Gamez, G.; Touboul, D.; Zenobi, R., Atmospheric pressure glow discharge desorption mass spectrometry for rapid screening of pesticides in food. *Rapid Commun. Mass Spectrom.* **2008,** *22*, (18), 2791-2798.

55. Andrade, F. J.; Wetzel, W. C.; Chan, G. C. Y.; Webb, M. R.; Gamez, G.; Ray, S. J.; Hieftje, G. M., A new, versatile, direct-current helium atmospheric-pressure glow discharge. *J. Anal. At. Spectrom.* **2006,** *21*, (11), 1175-1184.

56. Harper, J. D.; Charipar, N. A.; Mulligan, C. C.; Zhang, X. R.; Cooks, R. G.; Ouyang, Z., Low-Temperature Plasma Probe for Ambient Desorption Ionization. *Anal. Chem.* **2008,** *80*, (23), 9097-9104.

57. Hirabayashi, A.; Sakairi, M.; Koizumi, H., Sonic spray ionization method for atmospheric-pressure ionization mass-spectrometry. *Anal. Chem.* **1994,** *66*, (24), 4557-4559.

58. Takats, Z.; Nanita, S. C.; Cooks, R. G.; Schlosser, G.; Vekey, K., Amino acid clusters formed by sonic spray ionization. *Anal. Chem.* **2003,** *75*, (6), 1514-1523.

59. Iribarne, J. V.; Thomson, B. A., Evaporation of small ions from charged droplets. *J. Chem. Phys.* **1976,** *64*, (6), 2287-2294.

60. Dole, M.; Mack, L. L.; Hines, R. L., Molecular beams of macroions. *J. Chem. Phys.* **1968,** *49*, (5), 2240-&.

61. Dams, R.; Benijts, T.; Gunther, W.; Lambert, W.; De Leenheer, A., Sonic spray ionization technology: Performance study and application to a LC/MS analysis on a monolithic silica column for heroin impurity profiling. *Anal. Chem.* **2002,** *74*, (13), 3206-3212.

62. Kovacs, Z.; Dinya, Z.; Antus, S., LC-SSI-MS techniques as efficient tools for characterization of nonvolatile phenolic compounds of a special Hungarian wine. *J. Chromatogr. Sci.* **2004,** *42*, (3), 125-129.

63. Arinobu, T.; Hattori, H.; Seno, H.; Ishii, A.; Suzuki, O., Comparison of SSI with APCI as an interface of HPLC-mass spectrometry for analysis of a drug and its metabolites. *J. Am. Soc. Mass Spectrom.* **2002,** *13*, (3), 204-208.

64. Takats, Z.; Wiseman, J. M.; Gologan, B.; Cooks, R. G., Electrosonic spray ionization. A gentle technique for generating folded proteins and protein complexes in the gas phase and for studying ion - Molecule reactions at atmospheric pressure. *Anal. Chem.* **2004,** *76*, (14), 4050-4058.

65. Touboul, D.; Jecklin, M. C.; Zenobi, R., Investigation of deprotonation reactions on globular and denatured proteins at atmospheric pressure by ESSI-MS. *J. Am. Soc. Mass Spectrom.* **2008,** *19*, (4), 455-466.

66. Jecklin, M. C.; Touboul, D.; Bovet, C.; Wortmann, A.; Zenobi, R., Which electrospray-based ionization method best reflects protein-ligand interactions found in solution? A comparison of ESI, nanoESI, and ESSI for the determination of dissociation constants with mass spectrometry. *J. Am. Soc. Mass Spectrom.* **2008,** *19*, (3), 332-343.

67. Bartle, K. D.; Myers, P., History of gas chromatography. *Trac-Trends Anal. Chem.* **2002,** *21*, (9-10), 547-557.

68. Settle, F. A., *Handbook of instrumental techniques for analytical chemistry*. Prentice Hall PTR: Upper Saddle River, New Jersey, **1997**; Vol. 1.

69. Attaway, H.; Gooding, C. H.; Schmidt, M. G., Biodegradation of BTEX vapors in a silicone membrane bioreactor system. *J. Ind. Microbiol. Biotechnol.* **2001,** *26*, (5), 316-325.

70. Kohno, H.; Berezin, A. A.; Chang, J. S.; Tamura, M.; Yamamoto, T.; Shibuya, A.; Hondo, S., Destruction of volatile organic compounds used in a semiconductor industry by a capillary tube discharge reactor. *IEEE Trans. Ind. Appl.* **1998,** *34*, (5), 953-966.

71. Daifullah, A. A. M.; Girgis, B. S., Impact of surface characteristics of activated carbon on adsorption of BTEX. *Colloids Surf., A* **2003,** *214*, 181-/193.

72. Buczynska, A. J.; Krata, A.; Stranger, M.; Godoi, A. F. L.; Kontozova-Deutsch, V.; Bencs, L.; Naveau, I.; Roekens, E.; Van Grieken, R., Atmospheric BTEX-concentrations in an area with intensive street traffic. *Atmos. Environ.* **2009,** *43*, (2), 311-318.

73. Kelly-Wintenberg, K.; Sherman, D. M.; Tsai, P. P. Y.; Ben Gadri, R.; Karakaya, F.; Chen, Z. Y.; Roth, J. R.; Montie, T. C., Air filter sterilization using a one atmosphere uniform glow discharge plasma (the Volfilter). *IEEE Trans. Plasma Sci.* **2000,** *28*, 64-71.

74. Van Durme, J.; Dewulf, J.; Sysmans, W.; Leys, C.; Van Langenhove, H., Abatement and degradation pathways of toluene in indoor air by positive corona discharge. *Chemosphere* **2007,** *68*, (10), 1821-1829.

75. Ohura, T.; Amagai, T.; Senga, Y.; Fusaya, M., Organic air pollutants inside and outside residences in Shimizu, Japan: Levels, sources and risks. *Sci. Total Environ.* **2006,** *366*, (2-3), 485-499.

76. Cheng, W. H., Adsorption characteristics of granular activated carbon and SPME indication of VOCs breakthrough. *Aerosol Air Qual. Res.* **2008,** *8*, (2), 178-187.

77. Indarto, A.; Choi, J. W.; Lee, H.; Song, H. K., Decomposition of greenhouse gases by plasma. *Environ. Chem. Lett.* **2008,** *6*, (4), 215-222.

78. Matysik, S.; Herbarth, O.; Mueller, A., Determination of microbial volatile organic compounds (MVOCs) by passive sampling onto charcoal sorbents. *Chemosphere* **2009,** *76*, (1), 114-119.

79. NIOSH hydrocarbons, armomatic: Method 1501.

80. Li, S. P.; Matthews, J.; Sinha, A., Atmospheric hydroxyl radical production from electronically excited NO2 and H2O. *Science* **2008,** *319*, (5870), 1657-1660.

81. Champion, C., Theoretical cross sections for electron collisions in water: structure of electron tracks. *Phys. Med. Biol.* **2003,** *48*, (14), 2147-2168.

82. Itikawa, Y.; Mason, N., Rotational excitation of molecules by electron collisions. *Phys. Rep.-Rev. Sec. Phys. Lett.* **2005,** *414*, (1), 1-41.

83. Obermeyer, G.; Aschmann, S. M.; Atkinson, R.; Arey, J., Carbonyl atmospheric reaction products of aromatic hydrocarbons in ambient air. *Atmos. Environ.* **2009,** *43*, (24), 3736-3744.

84. Atkinson, R., Atmospheric chemistry of VOCs and NOx. *Atmos. Environ.* **2000,** *34*, (12-14), 2063-2101.

85. Aschmann, S. M.; Tuazon, E. C.; Arey, J.; Atkinson, R., Products of the gas-phase reaction of O-3 with cyclohexene. *J. Phys. Chem. A* **2003,** *107*, (13), 2247-2255.

86. Hatakeyama, S.; Tanonaka, T.; Weng, J. H.; Bandow, H.; Takagi, H.; Akimoto, H., Ozone cyclohexene reaction in air - quantitative-analysis of particulate products and the reaction-mechanism. *Environ. Sci. Technol.* **1985,** *19*, (10), 935-942.

87. Grosjean, D.; Grosjean, E.; Seinfeld, J. H., Atmospheric chemistry of 1-octene, 1-decene and cyclohexene. *Environ. Sci. Technol.* **1996,** *30*, 1038-1047.

88. Jenkin, M. E.; Watson, L. A.; Utembe, S. R.; Shallcross, D. E., A Common Representative Intermediates (CRI) mechanism for VOC degradation. Part 1: Gas phase mechanism development. *Atmos. Environ.* **2008,** *42*, (31), 7185-7195.

89. NIST http://webbook.nist.gov/chemistry/.

90. Ouyang, Z.; Noll, R. J.; Cooks, R. G., Handheld Miniature Ion Trap Mass Spectrometers. *Anal. Chem.* **2009,** *81*, (7), 2421-2425.

91. NIST_Database, <http://www.nist.gov/srd/nist1a.htm>. **2009**.

92. Olivares, J. A.; Nguyen, N. T.; Yonker, C. R.; Smith, R. D., Oline mass-spectrometric detection for capillary zone electrophoresis. *Anal. Chem.* **1987,** *59*, (8), 1230-1232.

93. Lu, Q. H.; Bird, S. M.; Barnes, R. M., Interface for capillary electrophoresis and inductively-coupled plasma-mass spectrometry. *Anal. Chem.* **1995,** *67*, (17), 2949-2956.

94. Olesik, J. W.; Kinzer, J. A.; Olesik, S. V., Capillary electrophoresis inductively-coupled plasma spectrometry for rapid elemental speciation. *Anal. Chem.* **1995,** *67*, (1), 1-12.

95. Tanaka, Y.; Otsuka, K.; Terabe, S., Evaluation of an atmospheric pressure chemical ionization interface for capillary electrophoresis-mass spectrometry. *J. Pharm. Biomed. Anal.* **2003,** *30*, (6), 1889-1895.

96. Mol, R.; de Jong, G. J.; Somsen, G. W., On-line capillary electrophoresis-mass spectrometry using dopant-assisted atmospheric pressure photoionization: Setup and system performance. *Electrophoresis* **2005,** *26*, (1), 146-154.

97. Kolch, W.; Neususs, C.; Peizing, M.; Mischak, H., Capillary electrophoresis - Mass spectrometry as a powerful tool in clinical diagnosis and biomarker discovery. *Mass Spectrom. Rev.* **2005,** *24*, (6), 959-977.

98. Ohnesorge, J.; Neususs, C.; Watzig, H., Quantitation in capillary electrophoresis-mass spectrometry. *Electrophoresis* **2005,** *26*, (21), 3973-3987.

99. Simpson, D. C.; Smith, R. D., Combining capillary electrophoresis with mass spectrometry for applications in proteomics. *Electrophoresis* **2005,** *26*, (7-8), 1291-1305.

100. Smyth, W. F., Recent applications of capillary electrophoresis-electrospray ionisation-mass spectrometry in drug analysis. *Electrophoresis* **2005,** *26*, (7-8), 1334-1357.

101. Klampfl, C. W., Recent advances in the application of capillary electrophoresis with mass spectrometric detection. *Electrophoresis* **2006,** *27*, (1), 3-34.

102. Monton, M. R. N.; Soga, T., Metabolome analysis by capillary electrophoresis-mass spectrometry. *J. Chromatogr. A* **2007,** *1168*, (1-2), 237-246.

103. Scriba, G. K. E., Nonaqueous capillary electrophoresis-mass spectrometry. *J. Chromatogr. A* **2007,** *1159*, (1-2), 28-41.

104. Zamfir, A. D., Recent advances in sheathless interfacing of capillary electrophoresis and electrospray ionization mass spectrometry. *J. Chromatogr. A* **2007,** *1159*, (1-2), 2-13.

105. Gaspar, A.; Englmann, M.; Fekete, A.; Harir, M.; Schmitt-Kopplin, P., Trends in CE-MS 2005-2006. *Electrophoresis* **2008,** *29*, (1), 66-79.

106. Herrero, M.; Ibanez, E.; Cifuentes, A., Capillary electrophoresis-electrospray-mass spectrometry in peptide analysis and peptidomics. *Electrophoresis* **2008,** *29*, (10), 2148-2160.

107. Maxwell, E. J.; Chen, D. D. Y., Twenty years of interface development for capillary electrophoresis-electrospray ionization-mass spectrometry. *Anal. Chim. Acta* **2008,** *627*, (1), 25-33.

108. Nesbitt, C. A.; Zhang, H. X.; Yeung, K. K. C., Recent applications of capillary electrophoresis-mass spectrometry (CE-MS): CE performing functions beyond separation. *Anal. Chim. Acta* **2008,** *627*, (1), 3-24.

109. Klampfl, C. W., CE with MS detection: A rapidly developing hyphenated technique. *Electrophoresis* **2009,** *30*, S83-S91.

110. Mischak, H.; Coon, J. J.; Novak, J.; Weissinger, E. M.; Schanstra, J. P.; Dominiczak, A. F., Capillary electrophoresis-mass spectrometry as a powerful tool in biomarker discovery and clinical diagnosis: An update of recen developments. *Mass Spectrom. Rev.* **2009,** *28*, (5), 703-724.

111. Pantuckova, P.; Gebauer, P.; Bocek, P.; Krivankova, L., Electrolyte systems for on-line CE-MS: Detection requirements and separation possibilities. *Electrophoresis* **2009,** *30*, (1), 203-214.

112. Ramautar, R.; Somsen, G. W.; de Jong, G. J., CE-MS in metabolomics. *Electrophoresis* **2009,** *30*, (1), 276-291.

113. Staub, A.; Schappler, J.; Rudaz, S.; Veuthey, J. L., CE-TOF/MS: Fundamental concepts, instrumental considerations and applications. *Electrophoresis* **2009,** *30*, (10), 1610-1623.

114. Jecklin, M. C.; Gamez, G.; Zenobi, R., Fast polymer fingerprinting using flowing afterglow atmospheric pressure glow discharge mass spectrometry. *Analyst* **2009,** *134*, (8), 1629-1636.

115. Gibson, G. T. T.; Mugo, S. M.; Oleschuk, R. D., Nanoelectrospray emitters: Trends and perspective. *Mass Spectrom. Rev.* **2009,** *28*, (6), 918-936.

116. Wu, Y. T.; Chen, Y. C., Sheathless capillary electrophoresis/electrospray ionization mass spectrometry using a pulled bare fused-silica capillary as the electrospray emitter. *Anal. Chem.* **2005,** *77*, (7), 2071-2077.

117. Edwards, J. L.; Chisolm, C. N.; Shackman, J. G.; Kennedy, R. T., Negative mode sheathless capillary electrophoresis electrospray ionization-mass spectrometry for metabolite analysis of prokaryotes. *J. Chromatogr. A* **2006,** *1106*, (1-2), 80-88.

118. Janini, G. M.; Zhou, M.; Yu, L. R.; Blonder, J.; Gignac, M.; Conrads, T. P.; Issaq, H. J.; Veenstra, T. D., On-column sample enrichment for capillary electrophoresis sheathless electrospray ionization mass spectrometry: Evaluation for peptide analysis and protein identification. *Anal. Chem.* **2003,** *75*, (21), 5984-5993.

119. Shamsi, S. A.; Miller, B. E., Capillary electrophoresis-mass spectrometry: Recent advances to the analysis of small achiral and chiral solutes. *Electrophoresis* **2004,** *25*, (23-24), 3927-3961.

120. Hayen, H.; Michels, A.; Franzke, J., Dielectric Barrier Discharge Ionization for Liquid Chromatography/Mass Spectrometry. *Anal. Chem.* **2009,** *81*, (24), 10239-10245.

121. Nilsson, S. L.; Andersson, C.; Sjoberg, P. J. R.; Bylund, D.; Petersson, P.; Jornten-Karlsson, M.; Markides, K. E., Phosphate buffers in capillary electrophoresis/mass spectrometry using atmospheric pressure photoionization and electrospray ionization. *Rapid Commun. Mass Spectrom.* **2003,** *17*, (20), 2267-2272.

122. Ouyang, Z.; Cooks, R. G., Miniature Mass Spectrometers. In *Annual Review of Analytical Chemistry*, Annual Reviews: Palo Alto, 2009; Vol. 2, pp 187-214.

123. Mentese, S.; Arisoy, M.; Rad, A. Y.; Gullu, G., Bacteria and Fungi Levels in Various Indoor and Outdoor Environments in Ankara, Turkey. *Clean-Soil Air Water* **2009,** *37*, (6), 487-493.

124. Hall, J. V.; Winer, A. M.; Kleinman, M. T.; Lurmann, F. W.; Brajer, V.; Colome, S. D., Valuing the health benefits of clean-air. *Science* **1992,** *255*, (5046), 812-817.

125. Lazaridis, M., *Indoor Air Pollution*. Springer, Po Box 17, 3300 Aa Dordrecht, Netherlands: 2011; Vol. 19, p 255-304.

126. Gao, D.; Yang, X. C.; Zhou, F.; Wu, Y. A., Experimental study on indoor air cleaning technique of nano-titania catalysis under plasma discharge. *Plasma Sci. Technol.* **2008,** *10*, (2), 216-220.

127. Schmid, S.; Jecklin, M. C.; Zenobi, R., Degradation of volatile organic compounds in a non-thermal plasma air purifier. *Chemosphere* **2010,** *79*, (2), 124-130.

128. Jecklin, M. C.; Schmid, S.; Urban, P. L.; Amantonico, A.; Zenobi, R., Miniature flowing atmospheric-pressure afterglow ion source for facile interfacing of CE with MS. *Electrophoresis* **2010,** *31*, (21), 3597-3605.

129. Harshbarger, W. R.; Porter, R. A.; Miller, T. A.; Norton, P., Study of optical emission from an rf plasma during semiconductor etching. *Appl. Spectrosc.* **1977,** *31*, (3), 201-207.

130. Heimann, G.; Warneck, P., OH radical induced oxidation of 2,3.dimethyylbutane in air. *J. Phys. Chem. A* **1992,** *96*, (21), 8403-8409.

131. Aschmann, S. M.; Arey, J.; Atkinson, R., Atmospheric chemistry of three C-10 alkanes. *J. Phys. Chem. A* **2001,** *105*, (32), 7598-7606.

132. Lim, Y. B.; Ziemann, P. J., Chemistry of Secondary Organic Aerosol Formation from OH Radical-Initiated Reactions of Linear, Branched, and Cyclic Alkanes in the Presence of NOx. *Aerosol Sci. Technol.* **2009,** *43*, (6), 604-619.

133. Kalberer, M.; Paulsen, D.; Sax, M.; Steinbacher, M.; Dommen, J.; Prevot, A. S. H.; Fisseha, R.; Weingartner, E.; Frankevich, V.; Zenobi, R.; Baltensperger, U., Identification of polymers as major components of atmospheric organic aerosols. *Science* **2004,** *303*, (5664), 1659-1662.

134. Burlica, R.; Kirkpatrick, M. J.; Locke, B. R., Formation of reactive species in gliding arc discharges with liquid water. *J. Electrost.* **2006,** *64*, (1), 35-43.

135. Huang, L. P.; Yang, S.; Liu, S. J.; Wang, Q. H.; Zhu, Y. Z., Removal of NO2 Produced by Corona Discharge in Indoor Air Cleaning. *J. Adv. Oxid. Technol.* **2009,** *12*, (2), 238-241.

136. Atkinson, R., Gas-phase tropospheric chemistry of volatile organic compounds .1. Alkanes and alkenes. *J. Phys. Chem. Ref. Data* **1997,** *26*, (2), 215-290.

137. Kohno, H.; Berezin, A. A.; Chang, J. S.; Tamura, M.; Yamamoto, T.; Shibuya, A.; Hondo, S., Destruction of volatile organic compounds used in a semiconductor industry by a capillary tube discharge reactor. *IEEE Trans. Ind. Appl.* **1998,** *34*, (5), 953-966.

138. Roland, U.; Holzer, F.; Kopinke, F. D., Improved oxidation of air pollutants in a non-thermal plasma. *Catal. Today* **2002,** *73*, (3-4), 315-323.

139. Subrahmanyarn, C.; Renken, A.; Kiwi-Minsker, L., Novel catalytic dielectric barrier discharge reactor for gas-phase abatement of isopropanol. *Plasma Chem. Plasma Process.* **2007,** *27*, (1), 13-22.

140. Atlas, R. M., Legionella: from environmental habitats to disease pathology, detection and control. *Environ. Microbiol.* **1999,** *1*, (4), 283-293.

141. Swanson, M. S.; Hammer, B. K., Legionella pneumophila pathogenesis: A fateful journey from amoebae to macrophages. *Annu. Rev. Microbiol.* **2000,** *54*, 567-613.

142. Driks, A., Maximum shields: the assembly and function of the bacterial spore coat. *Trends Microbiol.* **2002,** *10*, (6), 251-254.

143. Sadosky, A. B.; Wiater, L. A.; Shuman, H. A., Identification of leionella-pneumopfila genes required for growth within and killing of human macrophages. *Infect. Immun.* **1993,** *61*, (12), 5361-5373.

144. Segal, G.; Shuman, H. A., Intracellular multiplication and human macrophage killing by Legionella pneumophila are inhibited by conjugal components of IncQ plasmid RSF1010. *Mol. Microbiol.* **1998,** *30*, (1), 197-208.

145. Feeley, J. C.; Gibson, R. J.; Gorman, G. W.; Langford, N. C.; Rasheed, J. K.; Mackel, D. C.; Baine, W. B., Charcoal-yeast extract agar: primary isolation medium for *Legionella pneumophila*. *J. Clin. Microbiol.* **1979,** *10*, (4), 437-441.

146. Sambrook, J.; Fritsch, E. F.; Maniatis, T., *Molecular cloning: a laboratory manual*. 1989; p xxxviii + 1546.

147. Debartolomeis, J.; Cabelli, V. J., Evaluation of an escherichia coli host strain for eneumeration of F male specific bacteriophages. *Appl. Environ. Microbiol.* **1991,** *57*, (5), 1301-1305.

148. Beyer, W.; Pocivalsek, S.; Bohm, R., Polymerase chain reaction-ELISA to detect Bacillus anthracis from soil samples - limitations of present published primers. *J. Appl. Microbiol.* **1999,** *87*, (2), 229-236.

149. Mizuno, A., Electrostatic precipitation. *IEEE Trns. Dielectr. Electr. Insul.* **2000,** *7*, (5), 615-624.

150. Hillamo, R. E.; Kauppinen, E. I., On the performance of the berner low-pressure impactor. *Aerosol Sci. Technol.* **1991,** *14*, (1), 33-47.

151. Issaq, H. J.; Chan, K. C.; Janini, G. M.; Conrads, T. P.; Veenstra, T. D., Multidimensional separation of peptides for effective proteomic analysis. *J. Chromatogr. B* **2005,** *817*, (1), 35-47.

152. Kostiainen, R.; Kauppila, T. J., Effect of eluent on the ionization process in liquid chromatography-mass spectrometry. *J. Chromatogr. A* **2009,** *1216*, (4), 685-699.

153. Whitehouse, C. M.; Dreyer, R. N.; Yamashita, M.; Fenn, J. B., Electrospray interface for liquid chromatographs and mass spectrometers. *Anal. Chem.* **1985,** *57*, (3), 675-679.

154. Bruins, A. P.; Covey, T. R.; Henion, J. D., Ion spray interface for combined liquid chromatography/atmospheric pressure ionization mass-spectrometry. *Anal. Chem.* **1987,** *59*, (22), 2642-2646.

155. Lee, E. D.; Henion, J. D., Thermally assisted electrospray interface for liquid-chromatography mass-spectrometry. *Rapid Commun. Mass Spectrom.* **1992,** *6*, (12), 727-733.

156. Hopfgartner, G.; Wachs, T.; Bean, K.; Henion, J., High-flow ion spray liquid-chromatography mass-spectrometry. *Anal. Chem.* **1993,** *65*, (4), 439-446.

157. Hiraoka, K.; Fukasawa, H.; Matsushita, F.; Aizawa, K., High-flow liquid-chromatography mass-spectrometry interface using a parallel ion-spray. *Rapid Commun. Mass Spectrom.* **1995,** *9*, (14), 1349-1355.

158. Hirabayashi, A.; Sakairi, M.; Koizumi, H., Sonic spray mass-spectrometry. *Anal. Chem.* **1995,** *67*, (17), 2878-2882.

159. Dodd, E. E., The statistics of liquid spray and dust electrification by the hopper and laby method. *J. Appl. Phys.* **1953,** *24*, (1), 73-80.

160. Niessen, W. M. A.; Voyksner, R. D., Current practice of liquid chromatography mass spectrometry - Preface. *J. Chromatogr. A* **1998,** *794*, (1-2), 1-1.

161. M.L., G.; R.M., C., *The encyclopedia of mass spectrometry: Ionization methods*. Elsevier: St. Louis, 2007.

162. Berry, J.; Henderson, J. W.; Joseph, M., The Application Book. *LC GC Eur.* **2009**, 8-42.

163. Touboul, D.; Jecklin, M. C.; Zenobi, R., Ion internal energy distributions validate the charge residue model for small molecule ion formation by spray methods. *Rapid Commun. Mass Spectrom.* **2008,** *22*, (7), 1062-1068.

164. Gangl, E. T.; Annan, M.; Spooner, N.; Vouros, P., Reduction of signal suppression effects in ESI-MS using a nanosplitting device. *Anal. Chem.* **2001,** *73*, (23), 5635-5644.

165. Northrop, D. M.; Scott, R. P. W.; Martire, D. E., Preparation and evaluation of bimodal size-exclusion chromatography column a misture of 2 silicas of different pore diameter. *Anal. Chem.* **1991,** *63*, (14), 1350-1354.

166. Covey, T. R.; Thomson, B. A.; Schneider, B. B., Atmospheric pressure ion sources. *Mass Spectrom. Rev.* **2009,** *28*, (6), 870-897.

167. Kraus, M.; Eliasson, B.; Kogelschatz, U.; Wokaun, A., CO2 reforming of methane by the combination of dielectric-barrier discharges and catalysis. *Phys. Chem. Chem. Phys.* **2001,** *3*, (3), 294-300.

Appendix

A – Abbreviations

3mp	3-methylpyridine
AC	alternating current
APCI	atmospheric pressure chemical ionization
API	atmospheric pressure ionization
APPI	atmospheric pressure photoionization
BGE	background electrolyte
BL2	biosafety level 2
BL3	biosafety level 3
BSA	bovine serum albumin
BTEX	benzene, toluene, ethylbenzene and the xylene isomers
CE	capillary electrophoresis
cha	chloraniline
CS_2	carbon disulfide
CsI	cesium iodide
CZE	capillary zone electrophoresis
DBD	dielectric-barrier discharge
DC	direct current
dmba	N,N-dimethylbenzamide
EDC	electron capture detectors
EI	electron ionization
EOF	electroosmotic flow
ESI	electrospray ionization
ESI	electrospray ionization
ESSI	electrosonic spray ionization

ESSI	electrosonic spray ionization
FA-APGD	flowing afterglow atmospheric pressure glow discharge
FAPA	flowing atmospheric pressure afterglow
FID	flame ionization detector
GC	gas chromatography
HEPA	high efficiency particulate air
HPLC	high performance liquid chromatography
HPLC	high performance liquid chromatography
ICP	inductively coupled plasma
ID	inner diameter
LC	liquid chromatography
LIF	laser-induced fluorescence
LOD	limits of detection
LTP	low temperature plasma
MALDI	matrix-assisted laser desorption/ionization
MCP	microchannel plate
miniFAPA	miniaturized flowing atmospheric pressure afterglow
miniPAP	miniaturized plasma air purifier
MS	mass spectrometry
MSD	mass spectrometric detector
NIST	national Institute of Standards and Technology
NTP	non-thermal plasma
NTP	non-thermal plasma
OD	outer diameter
PAHs	Polycyclic aromatic hydrocarbons
PAP	plasma air purifier
PDC	plasma-driven catalyst
PMMA	poly-(methyl-methacrylate)
PTFE	polytetrafluoroethylene
PVC	polyvinyl chloride
pyr	pyridine
QTOF	quadrupole time-of-flight
SMF	sintered metal fibers

SSI	sonic spray ionization
TCE	trichloroethylene
TDC	thermal conductive detector
TFA	trifluoroacetic acid
TIC	total ion current
tmp	tripropylamine
TOF	time-of-flight
UHPLC	ultra-high performance liquid chromatography
UV	ultraviolet
VIS	visual
VOC	volatile organic compounds

B – Variables and Units

Pa	Pascal
$\boldsymbol{v_p}$	electrophoretic migration velocity
μ_p	electrophoretic mobility
$\boldsymbol{E}$	electric field
$\boldsymbol{q}$	charge
EOF	electroosmotic flow
MW	molecular weight
$[\boldsymbol{A_0}]$	concentration of component A at time = 0
$[\boldsymbol{B_0}]$	concentration of component B at time = 0
$[\boldsymbol{A}]_t$	concentration of component A after a given time
k(T)	rate constant
t	time
$\boldsymbol{m/z}$	mass-to-charge ratio